POLYMER/METAL OXIDE MODIFIED CLAY

NANOFIBROUS MEMBRANES FOR DECONTAMINATION

THESIS SUBMITTED TO
DELHI TECHNOLOGICAL UNIVERSITY
FOR THE AWARD OF THE DEGREE OF

DOCTOR OF PHILOSOPHY

Submitted by
PRIYA BANSAL
(Reg. No. 2K16/Ph.D/AC/06)

Under the Supervision of
PROFESSOR ROLI PURWAR

DEPARTMENT OF APPLIED CHEMISTRY
DELHI TECHNOLOGICAL UNIVERSITY
SHAHBAD DAULATPUR, BAWANA ROAD, DELHI-110042,
INDIA
OCTOBER 2021

DELHI TECHNOLOGICAL UNIVERSITY
(Formerly Delhi College of Engineering)

Department of Applied Chemistry
Shahbad Daulatpur, Bawana Road, Delhi – 110042, India

DECLARATION

This is to certify that the work presented in this thesis entitled **"Polymer/metal oxide modified clay nanofibrous membranes for decontamination"** is original and has been carried out by me for the degree of **Doctor of Philosophy** under the supervision of Dr. Roli Purwar, Professor, Department of Applied Chemistry. This thesis is a contribution of my original research work. Wherever research contributions of others are involved, every effort has been made to clearly indicate the same. To the best of my knowledge, this research work has not been submitted in part or full for the award of any degree or diploma of Delhi Technological University or any other University/Institutions.

<div align="right">

Priya Bansal
Research Scholar
(Reg. No. 2K16/Ph.D./AC/06)

</div>

Date:

Time:

CERTIFICATE

This is to certify that the PhD thesis entitled **"Polymer/metal oxide modified clay nanofibrous membranes for decontamination"** submitted to the Delhi Technological University, Delhi-110042, in fulfilment of the requirement for the award of the degree of Doctor of Philosophy by the candidate **Ms. Priya Bansal** (Reg. No. 2K16/Ph.D./AC/06) under the supervision of **Dr. Roli Purwar**, Professor, Department of Applied Chemistry. It is further certified that the work embodied in this thesis has neither partially nor fully submitted to any other university or institution for the award of any degree or diploma.

(Prof. Roli Purwar)
Supervisor
Department of Applied Chemistry
Delhi Technological University
Delhi

Head of Department
Department of Applied Chemistry
Delhi Technological University
Delhi

Dedicated to my beloved Family

ACKNOWLEDGEMENT

Lastly, I would acknowledge my colleagues, friends, technical, non-technical staff and administration of Delhi technological University for their direct and indirect contribution in the completion of this research work.

At the end, I pray to the Almighty to provide me the calmness to accept the future challenges of life.

Date:

Time:

(Priya Bansal)

ABSTRACT

This research focusses on the development of polyacrylonitrile/zinc oxide modified montmorillonite nanofibrous membranes for the efficient capture of particulate matter from atmosphere as well as decontamination of hexavalent chromium ions from water sources. Montmorillonite clay has been modified with zinc oxide nanoparticles, termed as zinc oxide modified montmorillonite, using three different raw materials namely zinc oxide nanoparticle, zinc nitrate and aloe vera gel. The particle size of zinc oxide modified montmorillonite varies from 16 nm to 48 nm. The surface morphology showed the presence of cuboidal shaped zinc oxide nanoparticles over the surface of the flaky shaped montmorillonite. The modification of montmorillonite to zinc oxide modified montmorillonite enhanced the thermal stability of montmorillonite.

Polyacrylonitrile/Montmorillonite nanofibrous nanocomposites were fabricated using electrospinning technique with variation in concentration of montmorillonite from 0.25% to 1.00%. The electrospinning process developed PAN/Mt nanofibrous nanocomposites having reduced fiber diameters and high surface roughness as observed in Field Emission Scanning Electron Microscopy. The nanocomposite nanofibers were characterized by X-ray diffraction and Thermogravimetric analyzer for intercalation and thermal stability respectively.

Electrospun polyacrylonitrile/zinc oxide modified montmorillonite nanofibrous nanocomposites with varying concentrations of zinc oxide modified montmorillonite ranging from 0.25% to 1.00% (w/w) were prepared to be used as filtration membranes. The addition of zinc oxide modified montmorillonite to polyacrylonitrile dope solution affects its viscosity and ionic conductivity. The surface morphology of the nanofibrous membranes was studied using field emission scanning electron microscopy. The average diameter of polycrylonitrile nanofibers and its nanocomposites was found to be between 247 nm to 468 nm. The addition

of zinc oxide modified montmorillonite enhanced the thermal stability of polyacrylonitrile nanofibrous membranes from 188 °C to 310 °C.

Ultrafine particulate matter and airborne microorganisms present in atmosphere are responsible for affecting the human health and the global climate. The development of bifunctional membranes which can simultaneously filter the particulate matter and inhibit the growth of microorganisms is the need of the hour. Polyacrylonitrile/montmorillonite nanofibrous nanocomposites were tested for their water vapor transmission rate, air permeability, burst strength and tensile strength. The filtration efficiency of 0.75% Polyacrylonitrile/montmorillonite nanofibrous nanocomposite was found to be 98.7% for PM2.5 particles present in air with a pressure drop of 46.8 Pa. An increase in porosity, air permeability and water vapor transmission rate of the nanofibrous membranes was observed with an increase in concentration of zinc oxide modified montmorillonite in polyacrylonitrile nanofibers upto 0.75%. The filtration efficiency of the nanofibrous membranes was evaluated using environment particle air monitor instrument. Polyacrylonitrile/zinc oxide modified montmorillonite nanofibrous membranes having 0.75% w/w zinc oxide modified montmorillonite exhibited filtration efficiency of 99.9% and a pressure drop of 26.72 Pa. The antimicrobial property of PAN/ZnO-Mt nanofibrous membranes was studied against *S. aureus* and *E. coli* bacterial strains showing 99.58% and 99.71% antibacterial activity respectively.

The efficient adsorption of hexavalent chromium ions from wastewater using montmorillonite, zinc oxide modified montmorillonite, polyacrylonitrile /montmorillonite and polyacrylonitrile/zinc oxide nanoparticle modified montmorillonite nanofibrous nanocomposites as adsorbents has been studied. The effect of pH, concentration, time and amount of adsorbent on the removal of hexavalent chromium ions from water were investigated. Adsorption of hexavalent chromium ions over the adsorbents follows pseudo-

second-order kinetics, Langmuir and Freundlich isotherm. Polyacrylonitrile/zinc oxide nanoparticle modified montmorillonite and polyacrylonitrile /montmorillonite nanofibrous nanocomposites were found to be more effective adsorbents for Cr (VI) ions compared to zinc oxide modified montmorillonite and montmorillonite.

OVERVIEW OF THESIS

The entire thesis has been summarized in nine chapters. The chapter 1 of the thesis briefly introduces the past and the current scientific importance of this research work and focuses on the objectives of the thesis. The detailed scientific literature related to the polymeric nanofibrous membranes used for particulate matter filtration and decontamination of heavy metal ions from wastewater has been summarized in chapter 2. The chapter 3 of the thesis discusses the experimental methods used while carrying out the research work describing the source of the materials used, experimental procedures, name and parameters of various characterization techniques used to achieve the objective of the research work. The preparation and characterization of zinc oxide modified montmorillonite has been discussed in chapter 4. This chapter discusses the preparation of zinc oxide modified montmorillonite using three different raw materials and further its characterization using different techniques. The chapter 5 gives an insight about the preparation and characterization of polyacrylonitrile/montmorillonite and polyacrylonitrile/zinc oxide modified montmorillonite nanofibrous nanocomposites using electrospinning technique. The chapter 6 deals with the application of the developed nanofibrous nanocomposites in particulate matter filtration. The antibacterial properties of these nanofibrous nanocomposites have also been discussed in this chapter. The decontamination of heavy metal ion, chromium (VI) using montmorillonite, zinc oxide modified montmorillonite and the developed nanofibrous nanocomposites has been described in chapter 7 of the thesis. The chapter 8 summarizes the entire research work and also focusses on the future prospects of this research. The literature referred to carry out this entire research has been summarized in chapter 9 of the thesis.

TABLE OF CONTENTS

Contents	Page No.

LIST OF FIGURES

LIST OF TABLES

LIST OF ABBREVIATIONS

Mt   Montmorillonite

PAN   Polyacrylonitrile

ZnO-Mt   Zinc oxide modified montmorillonite

PM   Particulate Matter

DMF   N,N-dimethyl formamide

PAN/Mt   Polyacrylonitrile/montmorillonite

PAN/ZnO-Mt   Polyacrylonitrile/zinc oxide modified montmorillonite

WVTR   Water vapor transmission rate

AATCC   American Association of Textile Chemists and Colorists

ASTM   American society for testing and materials

BET   Brunauer-Emmett-Teller

NAD   Nicotinamide adenine dinucleotide

NADH   Nicotinamide adenine dinucleotide hydrogen

CHAPTER 1

INTRODUCTION AND OBJECTIVES OF RESEARCH

1.1 Introduction

The presence of particulate matter (PM) in the atmosphere is amongst one of the serious environmental issues being faced by majority of the population in the world which in turn is having adverse effects on the human health and the global climate further disturbing the ecological balance [1]. The emerging industrialization and increased use of automobiles has led to an increase in the concentration of toxic pollutants in the atmosphere. PM is generally a mixture of water droplets present in air, dust, smaller organic and inorganic particles generated through vehicular emissions and incomplete burning of fossil fuels [2]. PM particles are classified based on their size as PM0.1 (ultrafine particles), PM2.5 (fine particles) and PM10 (thoracic particles) having an aerodynamic diameter less than 0.1 μm, 2.5 μm and 10 μm [3]. The smaller size of the fine particles makes it easier for them to enter the lungs causing serious health problems [4] while the thoracic particles are capable of being blocked by nasal passage [5]. The particles having diameter greater than 10 μm are easier to eradicate by utilizing air cleaners such as scrubbers, sedimentation tanks and cyclones which are not effective for particles of diameter lesser than 10 μm while it is difficult to filter the fine and ultrafine particles from the atmosphere [6]. PM has become a hazard for the human health because of its smaller size which is responsible for its easier penetration into the respiratory tract and blood vessels leading to respiratory and cardiovascular problems [7, 8].

In addition to PM, the presence of airborne microorganisms such as bacteria, viruses, fungi in the atmosphere are also responsible for adversely affecting the human health. These can result in contagious infectious diseases, allergies and respiratory problems and so on [9, 10]. The most extensively used technology for the eradication of these airborne microorganisms is the utilization of antimicrobial air filters [9, 11–13].

The presence of heavy metal ions such as Cd (II), Pb (II), Hg (II), Cu (II), Cr (VI) etc is also toxic to the environment and human health even at a very low concentration. The non-biodegradable toxic metal ions like chromium (Cr) released from industries mainly in its hexavalent state are injurious to human health and aquatic environment when their tolerance limit exceeds in water bodies. Hexavalent chromium ion is one amongst the highly toxic metal ions because of its carcinogenicity, mutagenicity, tetragenicity in living organisms and is hundred times more toxic than its trivalent state. According to the regulations of USEPA (U.S. Environmental Protection Agency), the maximum concentration of chromium must be lower than 100 μg/L while World Health Organization suggests it to be 50 μg/L [14].

Electrospinning is a simple and convenient approach utilizing electrostatic forces to spin fibers having diameters in submicron range. The apparatus consists of three major components namely a capillary syringe containing polymer solution, vertical or horizontal rotating collector plate or drum and high voltage electric source. A polymer solution is prepared in a suitable solvent for electrospinning and fed into the syringe. The syringe is then connected to a high voltage source providing it the electric field which generates an electric charge over it. A charged jet is produced from the syringe when the surface tension is overcome by the repulsive electric forces leading to solvent evaporation and the fibers spun are collected at the rotating collector plate [15].

2

The electrospun fibrous membranes have emerged as a promising material for efficient filtration of PM particles [16]. The nanofibrous membranes produced using electrospinning have diameters ranging from 40 to 2000 nm, higher surface-to-volume ratio, good network connectivity, tunable geometries and controllable structure. These properties of the nanofibrous membranes make them promising filtration materials [16]. Various electrospun nanofibrous membranes have been developed for air filtration applications using polyacrylonitrile [8, 17–22], polyamide [23, 24], polybenzimidazole [25], polyurethane/chitosan [9], polyvinyl alcohol/cellulose nanocrystals [26], polyimide/metal organic frameworks [27], cellulose based nanofibers [28], copper oxide/ polyacrylonitrile [29], and so on. Nanoparticles have also been doped to nanofibers for improvement in specific surface area [29]. At present, most of the research focusses on development of composite polymeric membranes for filtration of PM as a polymer solution comprising a single constituent does not exhibit efficient filtration whereas modified polymeric solutions enhance the properties of membranes improving the filtration performance of the membranes.

Adsorption is one of the majorly used practices for the elimination of heavy metal ions and dyes from wastewater. Adsorption is being preferred over various methods such as liquid- liquid extraction, membrane filtration, ion exchange, coagulation, electrolysis, precipitation due to its higher energy saving, efficiency, broad operational range of pH and temperature, easy recycling of adsorbent and selectivity at lower contaminant concentration [30, 31]. Various hydrogels [32–35], biopolymers [36–38], microspheres [39] and nanofibrous membranes [40, 41] have found application in adsorption of metal ions.

Montmorillonite (Mt) is a phyllosilicate mineral with nanolayered structure. The crystal structure of Mt is comprised of stacked layers of an octahedral alumina (O-Al(Mg)-O) layer fused between two tetrahedral silica (O-Si-O) layers [42]. The stacked layers are held together by van der Waals and electrostatic forces which can be easily overcome by physical and chemical methods, resulting in excellent sorption ability, cation exchange capacity, high surface area and catalytic properties of Mt. The Mt nanolayers formed on exfoliation resulting due to dissociation of Mt aggregates to Mt particles in aqueous dispersion, have higher aspect ratios and larger surface area which on addition to the polymeric membrane results in Mt/polymer nanocomposites with enhanced barrier, mechanical and thermal properties [14, 42].

Adsorption of metal ions using Mt clay and their modified forms have been widely studied in the last two decades. The bonding between the two silica sheets is very weak, which permits water and exchangeable ions to enter. The efficiency to exchange cations, high swelling ability, mechanical & chemical stability and dispersion properties make them suitable adsorbent for metal ion removal. The adsorption efficiency of the clay can be improved by modifying them with organic materials and nanoparticles through intercalation, pillaring, acid/base activation and organofunctionalization [62, 63].

Zinc oxide (ZnO) nanoparticles having varying morphologies show unique properties such as photocatalytic[43–46], photoluminescence [47], optical [45, 48], antimicrobial activity [49–52], anticancer drug delivery [53, 54]. The efficiency of ZnO nanoparticles can be enhanced by addition of transition metals (such as Mn, Fe, Cu) and biomolecules which has expanded its use in biosensors, antimicrobial agents, antioxidants, water disinfectants, drug delivery systems and bio imaging materials [55, 56]. The metal

oxide nanoparticles especially ZnO supported Mt provide reactive absorbance with high surface area, improved chemical reactivity and display added physicochemical functions of both the metal oxide nanoparticles and Mt [46, 57]. ZnO/clay nanocomposites have been studied as good adsorbents for metal ion removal [58] and can photocatalytically degrade cationic and anionic dyes [59], pharmaceuticals present in waste water [60]. The major constraint of the simple clay minerals is the aggregation of the platelet under used condition, reducing its surface area and therefore removal efficiency. Clay/polymer composites have improved the adsorption capacity of bare clay minerals [61].

The polymers having high tensile strength, resistant to chemicals and conductivity have been used by various researchers to spun into fibers using electrospinning and to study their structural and morphological properties. The nanofibers due to their tunable properties and possibility of producing 3D structure have gained much attention. One of the widely used polymer for electrospinning is polyacrylonitrile (PAN) due to its ease to spinnability, commercial availability, stability and good mechanical properties. Acrylonitrile based polymer, PAN has been widely used for electrospinning due to their solubility in various solvents such as dimethylformamide, dimethylsulfone, dimethylsulfoxide and tetramethylsulfide. Dimethylformamide is the best solvent to prepare polyacrylonitrile solutions. The higher carbon percentage and stability to tune the structure of polyacrylonitrile has made it one of the broadly researched polymers having applications in various fields such as filtration, tissue engineering, electronics and energy storage. The intermolecular forces present between the polymer chains are responsible for the high crystalline melting point, i.e., 317°C and its solubility in certain solvents. Surface modification of polyacrylonitrile can be carried out easily due to the

presence of surface-active groups (CN) which are converted to functional groups chemically. Wide literature is available on the use of PAN as a starting material in blends and composites for several applications such as catalysis, photosensors, protective clothing, filtration membranes and electrochemical devices [64].

Although a good amount of research has been carried out using polymeric nanofibrous membranes for filtration of PM2.5 and decontamination of heavy metal ions. Supported clay and its modified forms have been used for the adsorption of heavy metal ions. To the best of our knowledge, polymeric nanofibrous membranes supported with zinc oxide nanoparticle modified clay have been rarely used for the filtration of PM2.5 from atmosphere and decontamination of heavy metal ions present in wastewater. The addition of zinc oxide nanoparticles to the nanofibrous membranes enhances the antibacterial properties of the membranes.

1.2 Research Gap

The supported clay as well as the modified clay has been developed for adsorption of heavy metal ions. Polymeric nanofibrous membranes, composite polymeric nanofibrous membranes have been extensively studied for the filtration of particulate matter as well as decontamination of hexavalent chromium ions. To the best of our knowledge, polymeric nanofibrous membranes supported with montmorillonite and zinc oxide modified montmorillonite have not yet been utilised in filtration applications. The antibacterial properties of zinc oxide, stacked structure of montmorillonite and higher specific surface area of nanofibrous membranes could be used for the development of antibacterial polymeric/zinc oxide modified montmorillonite nanofibrous membranes

which could be a potential candidate to be utilized in efficient capture of particulate matter as well as adsorption of hexavalent chromium ions.

1.3 Motivation of Research

Majority of Indian subcontinent breathes air rich in higher particulate matter. The PM 2.5 is particularly dangerous and can lead to severe health effects due to its larger penetrability into the human respiratory system and eventual growth in human organs and blood. The waste from several industries is also being discharged into soil and water bodies producing serious environmental damages.

Large specific surface area, chemical and mechanical stability, layered structure, and high cation exchange capacity has made clays excellent adsorbent materials as well as useful components of barrier protective materials. The properties of zinc oxide nanoparticles, clay and nanofibers can be utilized to develop zinc oxide nanoparticle supported clay polymeric nanofibrous membranes in the field of decontamination of heavy metal ions and filtration of contaminants from the environment. These nanofibrous membranes can be utilized at industrial level for filtration application.

It has been realized that polyacrylonitrile and its derivatives have been used in various applications such as protective clothing, tissue engineering, energy storage, biomedical and filtration. The wide array of tailor-made properties makes them a perfect choice for several disciplines of science and engineering. Although the potential in this field lies in the development of polyacrylonitrile fibers by incorporation of clay, zinc oxide modified clay which can further be used in sensors, protective clothing, biomedical, decontamination of metal ions from wastewater and carbon-based high-performance fibers. It is expected that in the coming era various

other applications and potential of polyacrylonitrile based nanofibers will be explored by the scientific community.

1.4 Objectives

The broad objective of this research work was to develop antibacterial polyacrylonitrile/ zinc oxide nanoparticles modified montmorillonite electrospun nanofibrous membranes for particulate matter filtration and decontamination of Cr (VI) ions.

1.5 Specific Objectives

To achieve the above broad objective, the specific objectives are as follows:

1. Synthesis of zinc oxide nanoparticle modified montmorillonite and their characterization.

2. Fabrication of polymer/ montmorillonite nanofibrous membranes by electrospinning and their characterization.

3. Fabrication of polymer/ zinc oxide nanoparticles modified montmorillonite nanofibrous membranes by electrospinning and their characterization.

4. To study the particulate matter filtration efficiency, antimicrobial activity and decontamination of hexavalent chromium ions by the electrospun nanofibrous membranes.

CHAPTER 2

LITERATURE REVIEW

2.1 Overview

In this chapter, electrospinning technique has been introduced. Various electrospun nanofibrous membranes used for PM2.5 filtration and adsorption of Cr(VI) metal ions have been briefly discussed. This chapter also includes various polyacrylonitrile nanofibrous and their applications in different fields.

2.2 Electrospinning

Electrospinning is amongst the widely used facile technique for fabrication nanofibers having diameter in the range of 20 to 4000 nm. The technique utilizes high voltage for the production of nanofibers from natural as well as synthetic polymer solutions. The basic set up of electrospinning involves four major components namely, syringe, high voltage source, spinneret and a grounded collector (generally a rotating drum or a vertical plate) (Fig 2.1). The polymer to be electrospun is initially dissolved in a particular solvent to prepare a polymeric solution known as dope solution. The polymer solution could be of natural or synthetic, loaded with nanoparticles, metals, active agents and ceramics. This polymeric solution is then introduced into the syringe to carry out the electrospinning. During the process of electrospinning, the polymeric solution which is held by the surface tension of the solution at the end of the syringe is subjected to high voltage electric field. This electric field induces electric charge over the surface of the liquid. A charged solution jet is produced on the Taylor cone (cone shaped fluid jet) tip when the forces of surface tension overcome the electrical forces as the electric field approaches a critical value. The jet formation between the syringe tip and collector

plate leads to the solvent evaporation, solidifying the polymer which is collected on the collecting plate as an interconnected mat. The electrospinning process is dependent on the process parameters including the voltage, flow rate, type of collector and tip to collector distance, solution parameters such as concentration, viscosity, conductivity, surface tension and molecular weight of the polymer and the ambient experimental conditions such as temperature, humidity etc. The electrospun nanofibrous membranes have smaller diameters, higher porosity, surface area to volume ratio, interconnected porous structure, tuneable network geometry and good internal connectivity which make them suitable to be used in energy storage, tissue engineering, sensors, protective clothing and filtration applications [15].
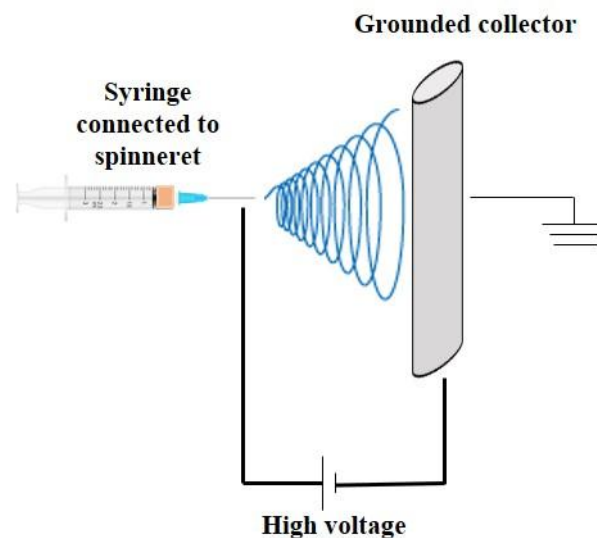
Fig 2.1: Electrospinning set up

2.3 Electrospun nanofibrous membranes for air filtration

The rapidly growing industrialization and urbanization has led to an increase in levels of atmospheric pollution worldwide. During the past years, two types of materials has been used for air purification namely porous films and fibrous filters [13]. The porous

films work on the principle of size-exclusion for the removal of particles. For efficient filtration, smaller surface pores are required for attachment of the filtered particles, which result in an increase in the pressure and reduction in the surface porosity [65]. On the other hand, the fibrous filters are composed of fibers of controllable interconnected pre structure with easy processability [66]. The fibrous filters capture PM via diffusion, interception and impaction. The fibrous membranes are considered to be better in terms of filtration capacity as compared to porous films. Thus, the electrospun nanofibrous membranes can be utilized as high-performance filter membranes due to their smaller diameters, larger surface area to volume ratio, good internal connectivity, tuneable network geometry and controllable morphology [13].

Based on the classical filtration theory, the filtration using fibrous materials has been divided into five mechanisms for trapping of particulate matter, namely, interception, Brownian diffusion, inertial impaction, electrostatic effect and gravitational effect [16, 67]. As the filtration occurs, the particulate matter when closer to the fibers generally deviates from the gas flow streamlines [6]. This deviation affects the performance of the fibrous material as a filter media. The deviation occurs via the following five mechanisms. The interception of PM occurs when the van der Waals interaction results on contacting the surface of the fibrous membrane assuming that PM follows a flow line and no deviation occurs. The capture of PM usually occurs through the interception mechanism for particle size of 0.1 to 1 μm [67,68]. As the particle size decreases, Brownian motion is favoured. The collision of PM with fibers results in deposition. During the Brownian motion, PM deviates randomly from its original flow and gets captured when this deviation is larger enough to impact the fiber and the PM. Brownian diffusion is generally exhibited for particles with size lower than 0.1 μm [68-70]. The

capture of particles with size 0.3 to 1µm is governed by inertial impaction. As the air flow turns, PM gets detached from the air flow line under the influence of inertia, further impinging and depositing over the fibrous membrane [67, 68]. When both the particles and the fibrous membranes are charged, electrostatic attraction comes into account. The electrostatic attraction results in a change of the track of PM in comparison to the air stream, resulting in deposition over the fibrous membrane. The electrostatic attraction is responsible for the firm adherence of PM over fibrous filter [71,72]. The gravitational effect is the least significant as the gravitational force has minimum contribution for majority of the particle size. Thus, different mechanisms favour the process of filtration for varying particle sizes [16].

The physical properties of air filtration materials and also its basic structure governs the filtration process having significant effects on the performance of the membranes as filters [16]. The nanofiber diameter and its distribution [73,74], surface area and pore size [75, 76], fiber basis weight [77] and packing density [78] are amongst the structural parameters of electrospun nanofiber membranes effecting the filtration performance [16]. Apart from these structural properties other parameters affecting the filtration performance of the fibrous membranes are face velocity [78, 79], particle size [77,80], temperature [81] and humidity [81].

The electrospun nanofibrous membranes have been utilized for the development of high-performance filters due to their excellent adhesion over the surface, high porosity, high specific surface area and low- basis weight with uniform fiber size [16, 82]. Till date, several polymers such as polyacrylonitrile [8, 18, 83], polyvinyl alcohol [75, 84], polyamide [23, 24], polyurethane [9], polysulfone [85], chitosan [11], cellulose acetate

[86], lignin [87] have been utilized to develop electrospun nanofibrous membranes with superior performance as filters.

2.3.1 Electrospun polymeric nanofibrous membranes

According to the Kuwabara model [88], to have a higher filtration efficiency, it is necessary to have smaller fiber diameters. The smaller pores of the fibrous materials are efficient in complete removal of particles having larger size than them due to sieving effect. Thus, the electrospun nanofibrous materials having smaller pore size are efficient in removal of ultrafine particles [88]. High filtration efficiency and lower pressure drop are the essential properties of an efficient electrospun nanofibrous membrane to be utilized in filtration of PM from the atmosphere [16, 88]. Zhang et al. developed electrospun polyvinyl alcohol/ cellulose nanocrystals composite nanofibrous air filters with a lower pressure drop of 91 Pa and PM2.5 filtration efficiency of 99.1%. The addition of cellulose nanocrystals resulted in an increase in the surface charge density of the solution for electrospinning which reduced the diameter of the fibers [26]. The ability to sustain the structural stability on deformation stress is necessary to ensure a reliable porous packing membrane [17]. Anti-deformed composite electrospun membranes of poly(ethylene oxide)@polyacrylonitrile/polysulfone having binary structure exhibited a filtration efficiency of 99.992% for PM2.5 with a lower pressure drop of 95 Pa. These composite membranes had smaller pore size, tensile strength of 8.2 MPa and higher porosity [17]. Zhu et al. reported multifunctional and bio-based air filtration membranes of chitosan/poly(vinyl alcohol) using green electrospinning and UV curing. The addition of silica nanoparticles to these membranes introduced surface roughness and enhanced the filtration efficiency to 98.73% for NaCl aerosols. On addition of silver nanoparticles on the surface of silica nanoparticle supports chitosan/poly(vinyl alcohol), the filtration efficiency for NaCl aerosols increased from

42.97% to 96.6% for NaCl particles as the basis weight increased from 1.48 to 6.2 gm^{-2} [89]. A biodegradable cellulose based air filter, Ag-MOFs@CNF@ZIF-8 having multi-layered structure was fabricated by Ma et al. with enhanced filtration performance for PM2.5 (94.3%), mechanical properties and gas adsorption. The improved PM 2.5 filtration efficiency of these developed filters is due to the presence of MOFs which enhances the interaction between the filter membrane and PM2.5 [28]. Jing et al. fabricated electrospun polyacrylonitrile nanofibers with ionic liquid diethyl ammonium dihydrogen phosphate which could find application in the field of filtration devices of PM2.5 and environmental protection systems. The hydrophilic ionic liquid introduced surface roughness and improved the hydrophilicity of polyacrylonitrile nanofibers. The interlinked nanofibrous structure and the surface chemistry of the nanofibrous membranes is responsible for the higher affinity of the nanofibers for PM2.5 and thus the PM2.5 capture increases for polyacrylonitrile/diethyl ammonium dihydrogen phosphate nanofibers in comparison to polyacrylonitrile nanofibrous membranes [8]. Hao et al. [27] prepared polyimide nanofibrous membranes modified with zeolitic imidazole framework-8 (PI-ZIF) with better thermal and chemical stability showed PM2.5 filtration efficiency of 96.6%, thermal stability upto temperature of 300 °C and pressure drop of 72 Pa. The addition of ZIF-8 to PI improved the capture of PM2.5 due to enhancement of adhesion of PM2.5 over the nanofibrous surface because of presence of surface charge of ZIF-8, rough surface morphology of the nanofibers and the higher adhesion of the ultrathin fibers towards PM2.5. Electrospun polyacrylonitrile nanofibrous air filters have been prepared by varying the concentration of polyacrylonitrile dope solution (11 wt%, 8wt% and 5 wt%) at a constant temperature of 20 °C and varying the relative humidity (30%, 40%, 50% and 60%). The developed bead-on-string air filters were able to capture the solid and oil-based PM present in

atmosphere with a filtration efficiency of 99% and a very low pressure drop of 27 Pa. These ultrafine fibers developed between the beads resulted in better PM2.5 filtration efficiencies and the construction of nanobeads developed open interconnected air flow channels responsible for the lower air flow resistance. These air filters could be utilized in practical applications because of their reusability, excellent performance and mechanical robustness [90]. Polyacrylonitrile/poly(acrylic acid) nanofibrous membranes with weight ratios of 3/7, 4/6, 5/5, 6/4, 7/3 and 10/0 were prepared having mechanical strength from 3.8 to 6.6 MPa comparatively higher than polyacrylonitrile nanofibers. The nanofibers had filtration efficiency>99.92% against NaCl aerosol particles and lower pressure drop of 310 Pa [18]. Polyacrylonitrile/ attapulgite composite nanofibers have been developed by acid activation of attapulgite and its modification with 3-aminopropyltriethoxysilane which were capable of effective capture of PM and heavy metals [20]. The polymeric nanofibrous membranes having application in PM2.5 filtration have been tabulated in Table 2.1.

Table 2.1 Summary of various polymeric nanofibrous membranes for PM2.5 filtration

S. No.	Nanofibrous membrane	PM2.5 filtration efficiency (%)	Pressure drop
1.	Poly(vinyl alcohol)-poly(acrylic acid)-silica nanoparticle-silver nanoparticles (PVA-PAA-SiO2-AgNP), base weight 4.26 gm^{-2} [91]	98.85	150 Pa
2.	Herbal extract incorporated polyvinylpyrrolidone [92]	99.99%	4.75 mmH_2O
3.	Polyacrylonitrile, basis weight 25 gm^{-2} [93]	99.78	172.3 Pa
4.	Polyacrylonitrile [19]	99.26	
5.	Poly(methylmethacrylate)/ polydimethylsiloxane-chitosan [94]	98.23	21 Pa
6.	Polyvinylidene fluoride (PVDF) fibers doped with negative ions powder (NIPs) [65]	99.99	40.5 Pa
7.	Zein/poly(vinyl alcohol) [84]	99.88	

S. No.	Nanofibrous membrane	PM2.5 filtration efficiency (%)	Pressure drop
8.	Multilayered nanofibrous membrane with poly(vinyl) alcohol/chitosan on both sides and middle layer of poly(vinyl) alcohol/biopolymer of N-halamine (PVA /P(ADMH-NVF)) [95]	99.3	183 Pa
9.	Sericin/Poly(vinyl alcohol)/clay [96]		
10.	Polyvinyl chloride/polyurethane [97]	99.5	144 Pa
11.	Hierarchical polysulfone/ TiO_2 nanoparticles [98]	99.997	45.3 Pa
12.	Multilevel nanofibers of silica nanoparticle incorporated PAN [83]	99.989	117 Pa
13.	Hierarchical nanostructured polyetherimide-silica hybrid membranes [99]	99.992	61 Pa
14.	Polyamide-6/polyacrylonitrile/polyamide-6 [100]	99.999	117.5 Pa
15.	Nanosized/porous poly (lactic acid) (PLA-N/PLA-P, double-layer structured) [101]	99.999	93.3 Pa
16.	Poly(m-phenylene isophthalamide)/ polyacrylonitrile composite [102]	99.9	

2.3.2 Antibacterial nanofibrous membranes

The microorganisms present in environment are responsible for deteriorating human health. The microorganisms generally causing infections in human health include *Staphylococcus aureus, Pseudomonas sp., Escherichia coli, Cladosporium sp., Micrococcus sp., Bacillus cereus, Aspergillus sp.* and several viruses. *Pseudomonas aeruginosa* is one of the most dangerous bacterial species which has developed resistance to several antibiotics and is generally associated to nosocomial infection. The pathogens found on air filters include *Penicillium spp., Alternaria spp., Rhizopus spp.,* etc. produce mycotoxins which is more toxic to human health [104].

The deteriorating qualities of purified air as well as water has attracted the attention of researchers towards the development of electrospun nanofibrous membranes having

antimicrobial properties. The microorganisms present in the environment constantly attack the filters effecting their filtration efficiency by formation of biofilms. Thus, there is a need to develop filters with antimicrobial properties [103]. Amidoxime surface functionalised electrospun polyacrylonitrile nanofibrous membranes were reported to be antimicrobial. Further these nanofibrous membranes when treated with silver nitrate solution resulted in formation of highly antimicrobial membranes capable of killing *S. aureus* and *E. coli* within 30 minutes [103]. CS-PVA@SiO2-AgNPs composite nanofibrous membrane prepared by fabrication through UV reduction of silver ions showed significant antibacterial activity against *E. coli* and *B. subtilis* with an increase in the diameter of inhibition zone as the concentration of silver ions increases [89]. A multilayer structured biodegradable Ag-MOFs@CNF@ZIF-8 was fabricated through the process of in-situ generation with high antibacterial activity. The release of silver and zinc ions from MOFs crystal and the presence of stronger interfacial bonding of CNF between the layers of cellulose was responsible for the higher antibacterial activity of the developed filter against *E. coli* bacterial strains [28]. Electrospun composite nanofibrous membranes of polyacrylonitrile-silver prepared by in-situ synthesis of silver nanoparticles in polyacrylonitrile solution were found to be effective against *E. coli* and *S. aureus* bacterial strains [104]. Herbal extract (*S. flaviscens*) incorporated polyvinylpyrrolidone nanofibers have been synthesised with varying concentrations of the herbal extract, 2.04%, 4.07% and 6.11%. The herbal extract incorporated nanofibers showed antibacterial activity of 99.98% against *S. epidermidis* bioaerosols [92]. Zhang et al. [95] developed multilayer electrospun nanofibrous membranes with antibacterial property for air filtration via sequential electrospinning. Initially, N-halamine biopolymer was synthesised through

17

copolymerization between N-vinylformamide and 3-allyl-5,5-dimethylhydantoin which was further combined with poly(vinyl alcohol) and acted as the intermediate layer of the multilevel membrane. On the outer sides of the membrane poly(vinyl alcohol)/ chitosan was assembled. These multi-layered nanofibrous membranes imparted an antibacterial activity against *E. coli* and *S. aureus* bacterial strains due to the existence of N-halamine which damages the surface structure of the bacteria and kills it.

Table 2.2 Summary of various antibacterial polymeric nanofibrous membranes

S. No.	Nanofibrous membrane	Bacterial strains
1.	Poly(vinyl alcohol)-poly(acrylic acid)-silica nanoparticle-silver nanoparticles (PVA-PAA-SiO2-AgNP) [91]	*Escherichia coli* *Bacillus subtilis*
2.	Poly(methylmethacrylate)/polydimethylsiloxane-chitosan [94]	*Escherichia coli* *Staphylococcus aureus*
3.	Sericin/Poly(vinyl alcohol)/clay [96]	*Escherichia coli* *Staphylococcus aureus*
4.	Multilayered fibers of poly(3-hydroxybutyrate-co-3-hydroxyvalerate) film coated with submicron fibers of poly(3-hydroxy alkanoate) and silver nanoparticles [105]	*Listeria monocytogenes* *Salmonella enterica*
5.	Polycaprolactone/chitosan [106]	*Escherichia coli* *Staphylococcus aureus*
6	Silver embedded polycaprolactone [107]	*Staphylococcus aureus*
7.	Poly(vinyl alcohol)-silver mats [108]	*Escherichia coli* *Staphylococcus aureus*
8.	Cross-linked collagen/silver nanoparticles [109]	*Escherichia coli* *Staphylococcus aureus* *P. aeruginosa*
9.	Rice flour-based fibers containing Ag and PVA/β-cyclodextrin [110]	*Escherichia coli* *Staphylococcus aureus*
10.	Poly(vinyl alcohol) nano TiO$_2$ composite [111]	*Staphylococcus aureus* *K. pneumoniae*

2.4 Electrospun nanofibrous membranes for decontamination of Cr (VI) ions

Chromium and its compounds are being extensively used in electroplating, metal processing, metal finishing, metallurgy, leather tanning and various other industries [112]. The waste from these industries is being discharged into soil and water bodies producing serious environmental damages. This wastewater mainly constitutes chromium in its trivalent and hexavalent state. The toxicity of hexavalent chromium is 100 times of its trivalent state, is carcinogenic, tetratogenic and mutagenic to living organisms [113]. United State Environmental Protection Agency (USEPA) has classified Cr in aqueous environment as group A of human carcinogens and its maximum amount in drinking water is regulated to be below 0.10 mgl^{-1}. On the other hand, WHO recommends the maximum amount of total Cr in drinking water to be 0.05 mgl^{-1} [14, 114].

For the decontamination of drinking water, the topmost priority is elimination of chromium from the wastewater. Several techniques such as chemical precipitation, membrane techniques, filtration, ion exchange, electrochemical treatment and reverse osmosis have been utilized for the removal of chromium from wastewater but these techniques are not being widely used because of their high cost, pH-dependence, non-selectivity and use of complex methods. Thus, adsorbent technologies were developed which were economically and technically feasible [112, 115]. Natural materials such as clay minerals, silica, zeolites have been utilised as adsorbents for the heavy metal ion adsorption from wastewater [116]. Electrospun polymeric nanofibrous membranes are also being developed for the heavy metal ion adsorption because of larger specific surface areas, porous structure and tuneable surface functionalities [117].

The higher mechanical, chemical, thermal and corrosion resistance of the polymeric materials make them suitable to be used in purification of water systems [118, 119].

The surface modified electrospun nanofibrous membranes are in great demand for heavy metal ions removal because of their high porosity, controllable surface functionalization and higher specific surface area. The surface functionalized nanofibrous membranes provide effective backbone to anchor the ligands over higher surface area supported fibrous structure [41].

Kummer et al. [115] developed tannin/nylon 6 and chitosan/nylon 6 nanofibrous membranes using Forcespinning method for Cr (VI) ion removal. The adsorption of Cr (VI) was spontaneous, endothermic and a favorable process. Adsorption process best fitted the Elovich kinetic model, pseudo-second-order kinetic model and Langmuir adsorption isotherm with an adsorption capacity of 23.9 mgg^{-1} for chitosan/nylon-6 at pH 3 and 62.7 mgg^{-1} for tannin/nylon-6 nanofibrous membranes at pH 2. Electrospun polyacrylonitrile nanofibrous membranes embedded with cerium oxide nanoparticles and zerovalent iron were prepared through electrospinning technique [120]. The cerium oxide embedded PAN nanofibers showed 96% Cr (VI) ion removal as compared to cerium oxide nanoparticles with an efficiency of 79%. Whereas the zerovalent iron embedded PAN nanofibrous membranes were 99.9% efficient in removal of Cr (VI) ions. The zerovalent iron nanofibers followed the Freundlich adsorption isotherm while in case of cerium oxide nanofibers Langmuir adsorption isotherm best fitted the adsorption data with an adsorption capacity 0f 28 mgg^{-1}. The adsorption of Cr (VI) ions using chitosan nanofibers cross-linked with glutaraldehyde was found to be twice in comparison to chitosan powder with the highest removal of Cr (VI) occurring at pH of 3.0. The adsorption best fitted pseudo-second-order kinetic model, Langmuir and Freundlich adsorption isotherms [121]. Surface modified PAN nanofibrous membranes with ethylenediaminetetraacetic acid utilising ethylenediamine as crosslinker were prepared for adsorption of Cr (VI) ions having maximum adsorption capacity of 66.24 mgg^{-1}

following pseudo-second-order kinetic model and Freundlich adsorption isotherm [122]. Adsorption of Cr (VI) ions has been reported using polyaniline/sepiolite nanofibrous membranes prepared via in-situ synthesis involving chemical oxidation polymerization method [123]. The adsorption of metal ions was dependent on pH and best fitted pseudo-second-order kinetic model and Langmuir isotherm with a maximum adsorption of 206.6 mgg^{-1} to 244.5 mgg^{-1} as the temperature increases from 25 °C to 45 °C. Electrospun polyacrylonitrile/thiol modified cellulose nanofibers were effective for removal of Cr (VI) ions from aqueous solutions with monolayer adsorption [124]. Magnesium hydroxide incorporated in polyamide nanofibers were efficient in adsorption of Cr (VI) ions from aqueous solutions [125]. Thermal plastic elastomer ester/iron alkoxide nanofibers were fabricated by Xu et al. [126] demonstrating Freundlich adsorption isotherm with multilayer adsorption of Cr (VI) ions. The adsorption mechanism involves the adsorption of Cr (VI) ions over iron alkoxide and formation of Cr (II) by reduction of Cr (VI) which is followed by Cr (III) precipitation on the membrane surface.

Table 2.3 Summary of various polymeric nanofibrous membranes used for adsorption of Cr (VI) ions

S. No.	Nanofibrous membrane	Adsorption capacity for Cr (VI) ions (mgg^{-1})
1.	PVP/alumina [127]	6.8
2.	Chitosan/MWCNT/Fe$_3$O$_4$ [128]	354
3.	NH$_2$ functionalised Cellulose acetate silica [129]	19.45
4.	Chitosan/graphene oxide [130]	310.4
5.	Polypyrrole/polyaniline [131]	227
6.	Iron nanoparticle polyaniline composite [132]	434.78
7.	Polyaniline deposition on PAN nanofibers [133]	202.53
8.	Chitosan/polymethylmethacrylate composite [134]	67
9.	Chitosan [121]	131.58
10.	Nylon 6,6 [135]	650.41

2.5 Clay based adsorbents

Clay minerals are hydrous aluminosilicates consisting of exchangeable cations and anions present on the surface. the clay minerals on the basis of their layered structure are divided into kaolinite, illite, smectite and chlorite groups. The properties of clay such as layered structure, higher specific surface area, higher cation exchange capacity make them suitable to be used as adsorbents [43, 136].

Montmorillonite clay belongs to the smectite group of the clay minerals composed of an octahedral alumina sheet sandwiched between two tetrahedral silica sheets. A common layer formation takes place between the tetrahedral layer tips and the hydroxyl layer of the octahedral alumina sheet with the common atom in the layer being oxygen rather than hydroxyl group. The sheets of montmorillonite are in the form of 2:1 structure with the presence of exchangeable cations balancing the negative charge created because of isomorphic substitution. Apart from the cation exchange, pH dependent metal uptake also occurs on montmorillonite with the binding of ions of adsorbate over the surface of the clay by ligand sharing with the cations of adsorbent. Precipitation of the metal ions occur as the pH or the concentration of adsorbate cation increases. The adsorption in montmorillonite can occur at the planar sites as well as the edge sites of the mineral. The properties of montmorillonite such as cation exchange, heat resistance, water sorption make it potential to be used as an adsorbent for heavy metal ions [137]. Several nanocomposites of montmorillonite have been prepared using dodecyl trimethyl ammonium chloride (DTAC), dodecyl amine (DA) and Al13 cations. The adsorption behaviour of the prepared montmorillonite nanocomposites against adsorption of Cr (VI) ions was studied with variation in pH, concentration of adsorbent, time and amount. The adsorption of hexavalent chromium ions over the montmorillonite nanocomposites was

mainly because of chemical adsorption and followed the pseudo-second-order kinetic model. The adsorption occurred as monolayer as well as on the heterogenous surface best fitting the Langmuir and Freundlich adsorption isotherm [14].

The clay minerals modified using metal oxides prepared by cationic ion exchange in the interlayers of the swelled clay are of immense importance due to the higher surface area, enhanced thermal stability and intrinsic catalytic activity. These intercalated species prevent the breakdown of interlayer spaces generating interlayer space. Further when heated, the intercalated species convert to the clusters of metal oxides resulting in a stable microporous network with a higher surface area [137].

Zinc oxide nanoparticles are amongst one of the significant metal oxides with various advantages such as low cost, biocompatibility, non- toxicity, chemical and thermal stability, long shelf life and robust in comparison to other metal oxides. These have been widely used as catalysts in wastewater treatment, antimicrobial additives and cosmetics [138]. Generally, zinc oxide is found in the following three phases, cubic rock salt, cubic zinc blende and hexagonal quartzite. The most common structure is wurtzite with each zinc atom being tetrahedrally coordinated to four oxygen atoms [138]. Zinc oxide nanoparticles have been used for the heavy metal ions removal from wastewater. Zinc oxide nanoparticles have been used as adsorbents for removal of cadmium (II), copper (II), lead (II) and nickel (II) ions [139]. The adsorption of metal ions increase with an increase in pH of the solution and the removal efficiency increased with an increase in the adsorbent amount. Zinc oxide nanoparticle reinforced silty clay composites have been developed as adsorbents for Pb (II) ions. The adsorption process is best interpreted by the Langmuir model and follows pseudo-

second-order kinetics. The adsorption of Pb (II) ions using zinc oxide reinforced clay composite is a feasible, spontaneous and endothermic process [140].

The clay minerals and their modified forms have attracted researchers, to be used as adsorbents for heavy metal ions present in aqueous solutions due to their easy availability and lower cost in comparison to activated carbon, membranes and zeolites [137]. However, the main drawback associated with the use of unaided clay is its tedious regeneration after its utilization. To overcome this limitation of clay, clay/ polymer nanocomposites are being developed for filtration applications. The addition of clay to polymers results in the enhancement of the membrane performance with better mechanical, barrier properties and improved thermal stability due to the dispersion of clay platelets and the interfacial interactions of the clay and polymeric membranes [42, 63, 141]. Electrospun cellulose acetate nanofibers were fabricated with sodium dodecyl sulfonate modified montmorillonite for the efficient adsorption of Cr (VI) ions by Cai et al. [41]. The solution pH, contact time and temperature had an appreciable effect on the adsorption of Cr (VI) ions.

Table 2.4 Summary of clay adsorbents for the adsorption of Cr (VI) ions.

S. No.	Clay	Adsorption capacity for Cr (VI) ions (mgg^{-1})
1.	Acid activated kaolinite [142]	8.0
2.	Kaolinite [142]	6.1
3.	Red clay [143]	1.3
4.	HDTMA modified red clay [143]	4.3
5.	Tetrabutylammonium kaolinite [142]	5.4
6.	Poly(oxozirconium) kaolinite [142]	5. 6
7.	Spent activated clay [144]	1.42
8.	Chitosan/bentonite composite [145]	89.13

24

2.6 Polyacrylonitrile based nanofibrous membranes

One of the widely used polymer for electrospinning is polyacrylonitrile (PAN) due to its ease to spinnability, commercial availability, stability and good mechanical properties [64]. The modified polyacrylonitrile nanofibrous membranes owing to their larger surface area, resistance to chemicals, lower flammability, better mechanical properties and thermal stability have been found to be efficient in PM2.5 filtration [8,17, 18, 83] as well as adsorption of heavy metal ions [40, 146-151]. The surface modification of PAN nanofibers results in its altered hydrophilicity and introduction of chelating groups which in turn are responsible to make them suitable for efficient adsorption [152, 153].

Liu et al. [154] grafted hyperbranched thiourea over electrospun polyacrylonitrile nanofibers. The grafted nanofibrous membranes were prepared initially by mixing hyperbranched poyethyleneimine with electrospun polyacrylonitrile nanofibers and finally reacting with methyl isothiocyanate and methanol resulting in a high density hyperbranched structure. These chemically grafted nanofibers were found to be effective adsorbents for Au (III) from aqueous

solutions resulting via coordination, electrostatic interaction and reduction. Cellulose/ polyacrylonitrile nanofibers have been prepared by Karki et al. [155] loading 15 weight % cellulose acetate solution in solvent mixture of N,N-Dimethylacetamide and acetone (1:2 by volume) and polyacrylonitrile (5 weight%) solution in dimethylformamide on two different syringes and connecting them through a plastic tube. The solutions were alternately pumped at similar conditions on the collector plate to obtain the composite nanofibers. Stacked layers of fibers having higher water permeation flux and better recyclability for the oil in water mixture solution separation.

Chitosan, a natural polymer is difficult to be electrospun due to its polycationic nature and higher degree of hydrogen bonding. Lou et al. [156] devised a two-step method to prepare chitosan polyacrylonitrile nanofibrous mats by coating chitosan over PAN nanofibers which were further found to improve the adsorption efficiency of the dye, Acid Blue-113. The morphology of the nanofibers revealed that the average diameter of chitosan coated PAN nanofibers (189±29 nm) was close to that of PAN nanofibers (186±37 nm). The chitosan coated PAN nanofibers were found to be of closed state and formed films of nanorange at the juncture of PAN nanofibers. These films provided the adsorption sites for the dye. The adsorption of dye over the nanofibers best fitted pseudo-second-order kinetic model and the Langmuir adsorption isotherm having maximum adsorption of 1708 mgg^{-1}.

In another study, surface modified polyacrylonitrile nanofibers were enhanced by addition of 2D titanium carbide Ti_3C_2X MXene nanosheets for the fabrication of air filter efficient in capturing PM2.5 [157]. The filtration efficiency is enhanced by stronger interaction with bacteria and PM 2.5 resulting from chemical delamination due to the presence of surface terminating groups such as OH, F and O in MXene nanosheets. Chen et al. [158] reported preparation of aminated PAN nanofibers by grafting of branched polyethyleneimine on the surface of electrospun PAN nanofibers of average diameter 595 nm. These aminated nanofibers were found to be efficient for removal of copper ions from wastewater effluents. The adsorption study results suggest pseudo-second-order kinetics model and follows Langmuir adsorption isotherm. Thermodynamically the process of adsorption is endothermic and spontaneous. Silver nanoparticle doped amidoxime modified PAN nanofibers have been prepared by a two-step process [159]. Initially polyacrylonitrile was added to silver nitrate dissolved in dimethylformamide. The solution was electrospun at a voltage of 18 kV, flow rate 2

mL/h and collector to tip distance of 15 cm. Further the AgNP doped PAN nanofibers were modified by amidoxime groups chemically by immersing the nanofibers in hydroxylamine hydrochloride and ammonia solution. Smooth, beadles and continuous nanofibers having crackles surface were obtained. This led to the fabrication of nanoplatform for signal amplification which was utilized for detecting CA 125 in patients of ovarian cancer. The major disadvantage associated with this method is, time consumption and negative signal which need to overcome. Electrospun polyacrylonitrile nanofibers when dyed via exhaust dyeing method using disperse dyes displayed excellent light fastness and very good washing fastness. The dyeing also resulted in improvement of tensile strength of PAN fibers [160].

PAN has been blended with polyacrylamidoxime (PANOx) (1: 1 weight%) in solvent containing mixture of dimethylformamide and dimethylsulfoxide (85:15 weight %) and electrospun into nanofibers of diameters ranging from 10 to 380 nm by Chen et al. [161]. These modified polyacrylonitrile polyacrylamidoxime nanofibers have found its application in self detoxifying protective clothing. One of the major developments in modification of polyacrylonitrile has been reported by Peng et al. [162] describing the production of microphase separated fibers using blends of polyacrylonitrile and poly(AN-co-MMA). The copolymer solutions were oxidized and carbonized and further pyrolysed producing porous structured fibers in nano range having diameter of 10 nm which were found to be interconnected on the surface as well as internally. Methyl methacrylate has been used instead of poy(methyl methacrylate) to blend with PAN due to the superior compatibility and solution stability of former with polyacrylonitrile while on blending latter with PAN a phase separation occurred during electrospinning process. These continuous nanofibrous membranes were found to be suitable to be used in electrochemical field.

Acrylonitrile based copolymers having porphyrin pendants have been blended and covalently immobilized via redox enzyme catalase which have been further electrospun into nanofibers by Wan et al. [163]. The nanofibrous membranes were found to have rough surface. The carbon nanofibers when blended with carbon nanotubes had protruding parts. The carboxyl groups were activated by N-(3-dimethylaminopropyl)-N'-ethylcarbodiimide hydrochloride and N-hydroxysuccinimide which resulted in immobilization of catalase on nanofibers. Polyacrylonitrile nanofibers of twotypes of fluorescent whitening agents: 1,4-bis(o-cyanostyryl) benzene (ER) and 1-(o-cyanostyryl)-4-(p-cyanostyryl) benzene (EB) were developed by Wang et al. The distinct structures and procedure of nanofiber production were due to the varying photoluminescence intensity of ER/PAN and EB/PAN nanofibers [164].

Polyacrylonitrile nanofibers have been modified via process modification. Doshi et al. [165] reported the production of nanofibers having parallel orientation to each other using the collector plate as a drum rotating at a higher speed. Polyacrylonitrile nanofibers have been prepared by needleless electrospinning by using wire electrode [166]. These resulted in formation of hollow fibers. A bobbin similar to wheel has been used as collector to generate nanofibers of parallel orientation by Zussman et al. [167]. The limitation of this method is that it cannot be used for production of well aligned nanofibers as a sharper edge of bobbin is required.

The fascinating chemical and electronic characteristics of metal oxides make them one of the suitable materials to be used as fillers or to be incorporated into fibers. The large interfacial surface area of metal oxide nanoparticles results into the desirable properties of these particles. Karimiyan et al. [168] reported the preparation of electrospun polyacrylonitrile/ graphene oxide nanofibers for microextraction of packed sorbent of

anaesthetic drugs namely lidocaine and prilocaine from plasma samples of humans. These nanofibers combined with polystyrene showed better efficiency for the extraction of these drugs compared to the conventional adsorbents. PAN/ biogenic silica nanocomposite nanofibers have been explored for degradation of malachite green dye photocatalytically by Mohamed and coworkers [169]. The nanocomposite nanofibers were prepared by submerging nanosilica obtained from rice straw or diatomite onto electrospun PAN nanofibers. The crosslinked composite nanofibers showed maximum dye degradation at 15 and 25 minutes for diatomite and rice straw membranes under visible light irradiation. 98% of the dye was found to degrade under 10 minutes at optimal conditions making it suitable to be used in fixed bed columns.

One of the recent studies describes the immobilization of calcium oxide chemically and mechanically on PAN fibers in the form of heterogenous catalyst for the conversion of Canola oil to biodiesel by transesterification reaction [170]. Calcium oxide powder was mixed into the polymeric solution and electrospun for the mechanical immobilization while for chemical immobilization, initially electrospun PAN fibers were activated by Pinner reaction and finally PAN fibers were amidated by dopamine hydrochloride-CaO. Polyacrylonitrile/ Graphene oxide-zinc oxide composite nanofibers were investigated to photodegrade organic dyes namely methylene blue and indigo carmine present in industrial wastewater with a degradation efficiency of 96% at 70 minutes and 98% merely after 27 minutes respectively under visible light irradiation [171]. Hashmi et al. [29] developed copper oxide loaded PAN nanofibrous membranes for antimicrobial respiratory mask use. The addition of copper oxide imparted mechanical, tensile strength, antibacterial properties and increased air permeability. Feng et al. [148] developed PAN/GO nanofibers by dispersion of polyacrylonitrile in graphene oxide solution in DMF solvent and further electrospinning the solution. The nanofibers were found to be effective Cr (VI) adsorption.

The adsorption process was spontaneous and endothermic thermodynamically and favored

Freundlich adsorption isotherm having an adsorption of 382.5 mg/g.

Table 2.5 Summary of various polyacrylonitrile nanofibrous membranes and their applications

S.No.	Nanofibrous membranes	Applications
1.	Eu^{3+}/Tb^{3+} doped PAN fibers [172]	Color display and optoelectronics
2.	Modified hydrophobic 3D PAN/ZnO composite fiber [173]	Separation of oil water mixture
3.	Polyacrylonitrile nanofibers decorated by activated carbon [174]	Extraction of fluoroquinolones from wastewater by solid phase dispersion
4.	Silica nanoparticle doped polystyrene/PAN nanofibers [175]	Hydrophobic protein adsorption
5.	PAN/lauric acid composite nanofiber [176]	Storage of thermal energy
6.	PAN/N-halamine nanofibers [177]	Protective antimicrobial face masks
7.	PAN/β-cylodextrin/GO nanofibers [178]	Cationic dye adsorption
8.	Zeolite/PAN nanofibers [179]	Wastewater polycyclic aromatic hydrocarbons extraction
9.	PAN/ amino functionalization on zirconium metal organic framework [180]	Analysis of pesticides in agricultural wastewater
10.	Cellulose/PAN nanofibers [181]	Improved mechanical and thermal properties
11.	PAN nanofibrous surface grafted with polyamidoamine [182]	Desalination and wastewater treatment
12.	Phosphorylated PAN nanofibers [147]	Heavy metal ion removal
13.	PAN/SAN/CNT composite [183]	Electrocatalysts
14.	Polyethylene-imine functionalized PAN nanofiber [184]	Adsorption of phenolic compounds
15.	Ag/PAN composite and AgNP/PAN nanofibers [185]	Antibacterial activity
16.	Graphite carbon nitride/silver phosphate/ PAN nanofibers [186]	Photocatalytic degradation of dyes and energy conversion
17.	Hydrous ZrO/PAN nanofibers [187]	Groundwater defluoridation
18.	In-situ self-polymerized gadolinium contained PAN [188]	Adsorption of thermal neutrons
19.	Porous CNF [189]	Adsorption and catalysts
20.	Pd modified PAN [190]	Determination of SO_2

2.7 Research gap and hypothesis

The detailed literature review on electrospun nanofibrous membranes for filtration of PM2.5 as well as for decontamination of heavy metal ions and clay based adsorbents suggested that the clay, modified clay, electrospun composite polymeric nanofibrous membranes have been utilized for the heavy metal ion adsorption as well as for capture of PM2.5 from atmosphere. To the best of our knowledge, polymeric nanofibrous membranes supported with montmorillonite and zinc oxide modified montmorillonite have not yet been utilised in filtration applications.

The adsorption capacity of clay and ZnO modified clay depends on the surface area available for adsorption of metal ions. If clay breaks down from stacked structure to two-dimensional nanostructure, larger surface will be available for the adsorption of metal ions. Through electrospinning, clay and ZnO modified clay can be exfoliated. Thus, the incorporation of ZnO modified clay in nanofibrous membranes can enhance the adsorption capacity. With the above hypothesis, Mt was modified with ZnO nanoparticles. In this study, we have utilized the properties of both PAN as well as montmorillonite to develop bifunctional PAN/Mt nanofibrous nanocomposites using electrospinning technique for effective filtration of PM2.5 particles present in atmosphere. The addition of Mt to PAN nanofibers results in the improvement of the stacked structure of Mt and the development of nanofibrous membranes having larger specific area and reactive functional groups, which are effective in adsorption of aerosols from the atmosphere as well as the heavy metal ions from water sources.

The bifunctional PAN/ZnO-Mt nanofibrous nanocomposites which can be effective against bacterial strains and also capture PM2.5 have been developed. The addition of montmorillonite to ZnO enhances its antibacterial properties. A series of thermally stable PAN/ZnO-Mt nanofibrous nanocomposites have been developed using electrospinning technique.

CHAPTER 3

EXPERIMENTAL METHODS

3.1 Overview

This chapter introduces the various chemicals and their source used to carry out the experiments. The chapter also includes the experimental procedure involved, specifications of characterization instruments used and the testing procedures. The experimental materials and methods are discussed as follows.

3.2 Materials

Zinc Oxide (ZnO) nanopowder having an average particle size of approximately 30 nm and clay nanopowder (composition: SiO_2-65%, Al_2O_3-15%, Fe_2O_3-1.3%, Ti_2O-0.19%, K_2O-1.3%, Na_2O-0.65%, CaO-3.31%, MgO-0.99%) having an average particle size of 80-150 nm and cation exchange capacity of 3-10 meq/100 g, were purchased from SRL, India. Zinc nitrate hexahydrate was also procured from SRL, India. Ammonium carbonate $((NH_4)_2CO_3)$ was purchased from Merck. Aloe vera gel was extracted from the aloe vera leaves plucked from the nursery of Delhi Technological University. Polyacrylonitrile (PAN) of average molecular weight 150,000 $gmol^{-1}$ was purchased from Sigma-Aldrich. N, N-Dimethylformamide (DMF) was purchased from Merck. Luria Broth, TM Media and agar agar (bacteriological grade) used to study the antimicrobial activity were purchased from Titan Biotech Ltd. and Fisher Scientific respectively. Potassium dichromate $(K_2Cr_2O_7)$ used for adsorption studies was purchased from Merck Specialties. Distilled water was used to carry out the experiment.

3.3 Preparation of zinc oxide modified montmorillonite using zinc oxide nanoparticles, ZnO-Mt (I)

To prepare ZnO-Mt (I), 3 g of Mt was added in 0.008 wt% ZnO nanoparticle dispersion in water and constantly stirred for a week at room temperature. The dispersion was ultrasonicated and centrifuged. The supernatant solution was discarded and clay was dried at 80 °C. The dried sample was grinded using mortar pestle. The schematic representation is as follows:
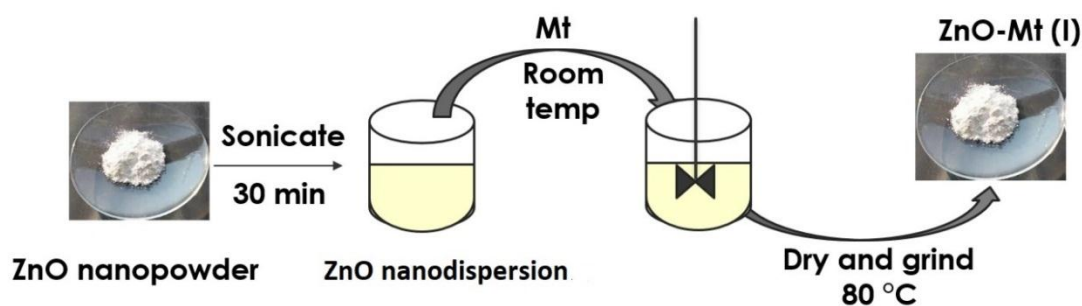
Fig 3.1 Schematic representation for preparation of ZnO-Mt(I)

3.4 Preparation of zinc oxide modified montmorillonite using zinc nitrate, ZnO-Mt (II)

ZnO-Mt (II) was synthesised via ion-exchange method, precipitation which was further followed by calcination [57]. To 30 ml solution of zinc nitrate ($Zn(NO_3)_2$, 1 mM), 3 g of Mt was added and the solution was continuously stirred for seven days at room temperature conditions. $(NH_4)_2CO_3$ solution (0.3 M) was added to the above solution and stirred for two days to precipitate the zinc ions in the form of zinc carbonate. The obtained solution was finally washed with distilled water till neutral pH was obtained. Further, the solution was dried at 50 °C and calcined for a time period of 2.5 h at 500 °C. Fig 3.2 shows the schematic preparation of ZnO-Mt (II).
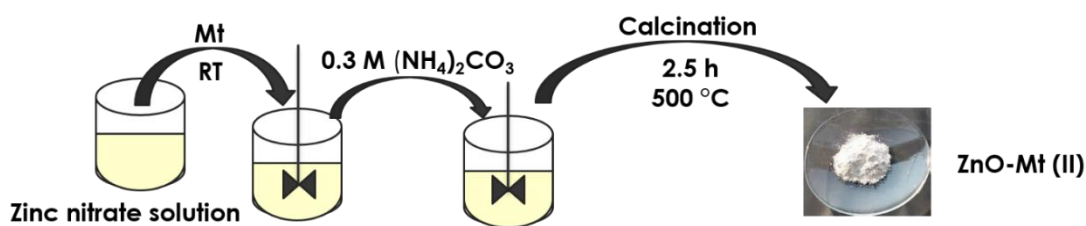
Fig 3.2 Schematic representation for preparation of ZnO-Mt (II)

3.5 Preparation of zinc oxide modified montmorillonite using aloe vera gel, ZnO-Mt (III)

The preparation of ZnO-Mt (III) was carried out using the method for synthesis of ZnO nanoparticles using aloe vera leaf [191] with some modifications. The aloe vera gel was extracted from boiled aloe vera leaves. The crushed gel was grounded to a thin paste by addition of distilled water which was further filtered using a fine mesh.

To prepare ZnO-Mt (III), 3g of Mt was added to aloe vera gel solution prepared in distilled water. The solution was continuously stirred for two days and further 20 mL of 1mM $Zn(NO_3)_2$ solution was added. The solution was vigorously stirred for five days and the supernatant was discarded. The obtained white solid was centrifuged after washing with distilled water. The resultant dried solid was calcined at 500 °C or 2.5 h (Fig 3.3).
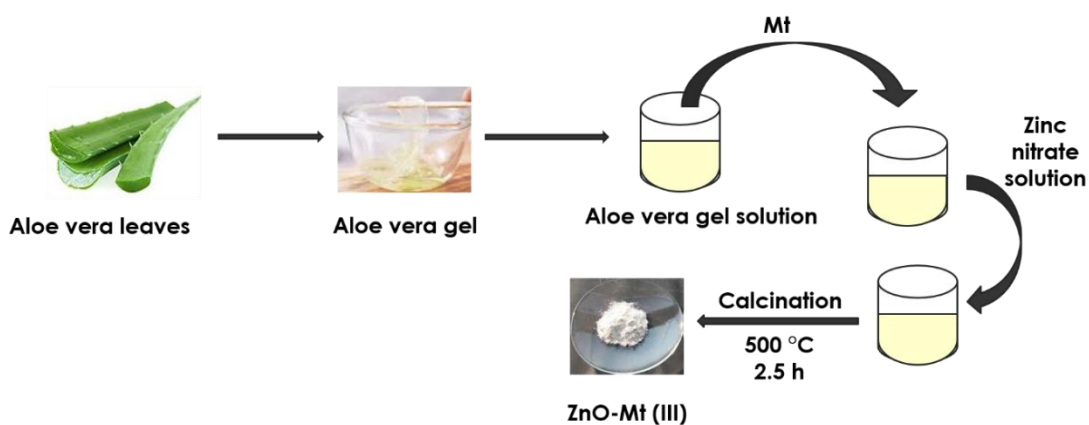
Fig 3.3 Schematic representation for preparation of ZnO-Mt (III)

3.6 Preparation of PAN and PAN/Mt dope solution

PAN (7% w/v) was dissolved in DMF by heating at 70 °C till a clear homogenous solution was obtained. Various PAN solutions comprising 0.25, 0.50, 0.75 and 1.00 wt% of Mt (w.r.t. PAN) were prepared by first sonicating Mt in DMF for 30 minutes and by further adding 7 wt% PAN to the solution. The solution was further heated at 70 °C till a homogenous solution was obtained. The solutions have been abbreviated as 0.25% PAN/Mt, 0.50% PAN/Mt, 0.75% PAN/Mt and 1.00% PAN/Mt.

3.7 Electrospinning of PAN and PAN/Mt nanofibrous nanocomposites

The dope solutions prepared were electrospun to produce nanofibers by placing a 12 mL syringe containing the solution on the pump. The solutions were further electrospun under a high voltage of 18 kV, at a flow rate of 6 mLh^{-1} at room temperature and were finally collected on the grounded drum roller covered with aluminium foil at a needle tip to collector distance of 12 cm. The various nanofibrous membranes prepared have been denoted as PAN, 0.25% PAN/Mt, 0.50% PAN/Mt, 0.75% PAN/Mt and 1.00% PAN/Mt. Fig 3.4 depicts the schematic representation for electrospinning of PAN/Mt nanofibrous nanocomposites.

X% =0%, 0.25%, 0.50%, 0.75% and 1.00%
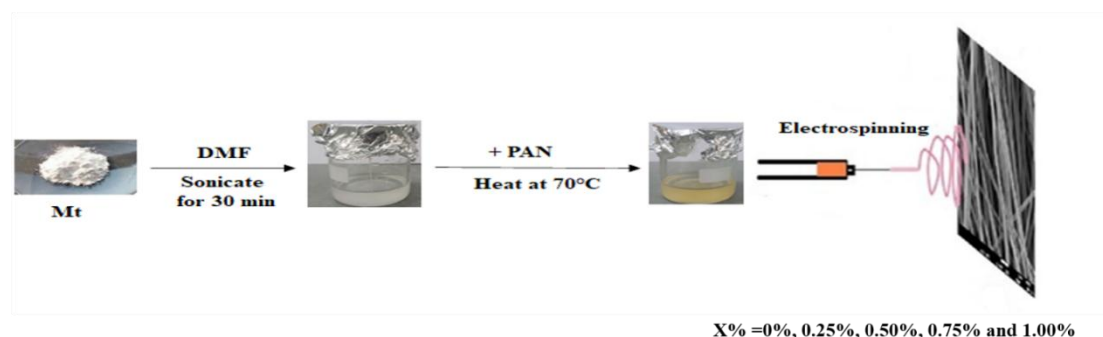
Fig 3.4 Schematic representation for electrospinning of PAN and PAN/Mt nanofibrous nanocomposites

3.8 Preparation of PAN/ZnO-Mt dope solution

ZnO-Mt (0.25% w/w w.r.t 7% w/v PAN) was ultrasonicated in 20 mL of DMF for 30 minutes and further PAN was added to the solution. The solution was heated at 70°C for 30 minutes till a homogenous solution was obtained. This solution was denoted as 0.25% PAN/ZnO-Mt (I) solution. Similarly, 0.50%, 0.75%, 1.00% PAN/ZnO-Mt (I), 0.75% PAN/ZnO-Mt (II) and 0.75% PAN/ZnO-Mt (III) solutions were prepared by varying the concentration of ZnO-Mt (I) from 0.50%, 0.75% to 1.00% and the concentration of ZnO-Mt (II) and ZnO-Mt (III) as 0.75% respectively. The solutions were brought to room temperature and used for electrospinning of nanofibrous nanocomposites.

3.9 Electrospinning of PAN/ZnO-Mt nanofibrous nanocomposites

Electrospun PAN/ZnO-Mt nanofibrous membranes were prepared by electrospinning machine (Royal Enterprises, India). A 12 mL syringe containing 0.25 % PAN/ ZnO-Mt (I) solution was placed on the pump. The process of electrospinning was carried through the needle tip to the grounded drum roller covered with aluminium foil. The solution was electrospun at room temperature conditions for 4 h at a flow rate of 6 mLh^{-1}, providing a high voltage of 18 kV to form stable jets and the nanofibers were collected on a grounded collector placed at a distance of 12 cm at room temperature conditions. The nanofibrous nanocomposites were electrospun under similar conditions using the prepared 0.50%, 0.75%, 1.00% PAN/ZnO-Mt (I), 0.75% PAN/ZnO-Mt (II) and 0.75% PAN/ZnO-Mt (III) solutions. The nanofibrous nanocomposites containing ZnO-Mt in varying concentrations have been denoted as 0.25% PAN/ZnO-Mt (I), 0.50% PAN/ZnO-Mt (I), 0.75% PAN/ZnO-Mt (I), 1.00% PAN/ZnO-Mt (I), 0.75% PAN/ZnO-

Mt (II) and 0.75% PAN/ZnO-Mt (III) nanofibrous nanocomposites. Fig 3.5 shows the schematic representation for electrospinning of PAN/Mt nanofibrous nanocomposites.

Here X%= 0.25%, 0.50%, 0.75% and 1.00%
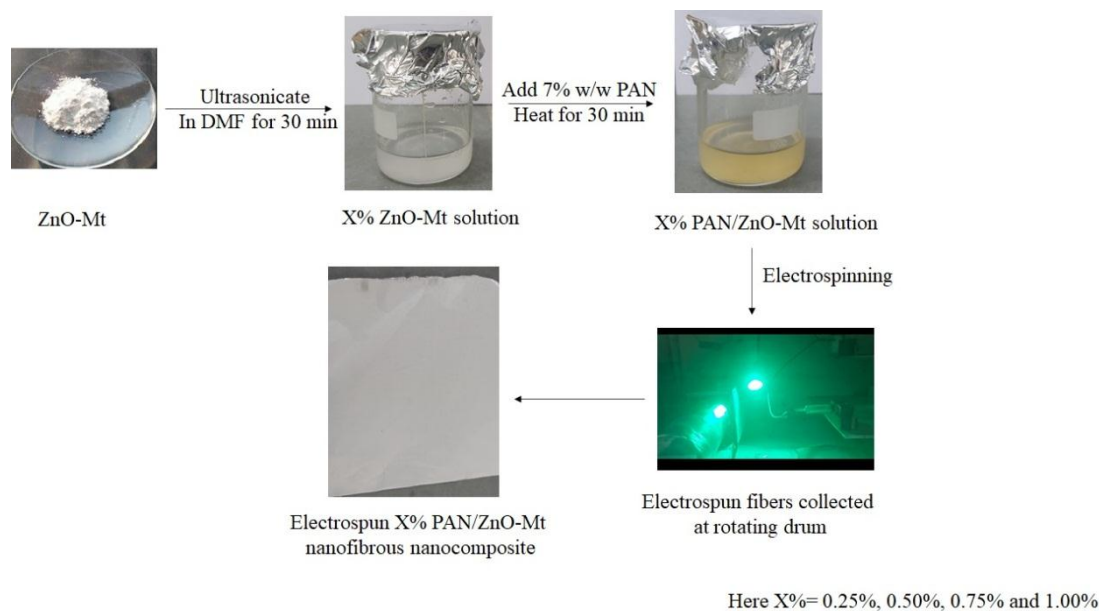
Fig 3.5 Schematic representation for electrospinning of PAN/ZnO-Mt nanofibrous nanocomposites

3.10 Particle size

The particle size of the modified clay was studied using Malvern Particle Size Analyzer. To study the particle size and zeta potential of Mt and ZnO-Mt, dispersed solutions of Mt and ZnO-Mt were prepared by sonicating 4 mg of Mt and ZnO-Mt in 10 mL methanol.

3.11 Viscosity and conductivity measurements

The viscosity of the dope solutions was measured via Anton Paar Modular compact rheometer 302 (MCR) of cone plate geometry (40-2°) of 0.21 mm gap at room temperature. The tests were carried out at a constant shear rate of 0.5 s^{-1}. The ionic conductivity of the solutions was measured using CON 700 conductivity meter at room temperature conditions.

3.12 Morphological and elemental characterization

The surface morphology of montmorillonite, zinc oxide modified montmorillonite and the nanofibrous nanocomposites was analyzed using the field emission scanning electron microscope (FESEM) with environmental SEM FEI Quanta 200 F with oxford EDS IE 250X Max 80, Netherlands. The surface of the samples was coated with platinum to study their morphology at an accelerating voltage of 15 kV. The deposition of zinc oxide over montmorillonite and zinc oxide modified montmorillonite on the surface of the nanofibrous membranes was studied by EDX analysis. The average diameter of the developed nanofibers was calculated by measurement of diameter of 20 nanofibers using ImageJ software. Transmission electron microscope -JEOL 2100 F was used to analyse the morphology of zinc oxide modified montmorillonite. A drop of sonicated aqueous solution of zinc oxide modified montmorillonite was casted on carbon coated copper HRTEM grid.

3.13 Structural characterization using X-ray diffraction

The exfoliation or intercalation of Mt with ZnO and Mt, ZnO-Mt with PAN was studied using Panlytical X'Pert Pro X-ray diffractometer by varying θ from 5° to 80°. The source of X-ray radiation was Cu Kα having wavelength of 0.154 nm.

3.14 Thermal analysis

The thermal stability of the samples was studied on Perkin Elmer Thermogravimetric Analyzer (TGA) instrument. For the thermal analysis of the samples, approximately 4 mg of the sample was weighed and the weight loss with respect to temperature was carried out under nitrogen atmosphere at a heating rate of 10 $°Cmin^{-1}$ from 30 °C to 800 °C.

3.15 BET surface area

The BET surface area of Mt and ZnO-Mt was analyzed using Quantachrome ASiQwin instruments under nitrogen gas.

3.16 Water vapor transmission rate

The water vapor transmission rate (WVTR) of the nanofibrous nanocomposites was measured using standard ASTM D 1653 method. In this method, the samples measuring 9.5 cm^2 were sealed on the beaker containing distilled water at room temperature conditions and weighed. After 24 hours the samples were weighed again. WVTR (gm^{-2}day^{-1}) of the nanofibrous nanocomposites was calculated by the equation given below:

$$WVTR = \frac{W_1 - W_2}{AX24}$$

Where W_1 and W_2 represent the weight of assembly before and after 24 h of water evaporation, respectively, and A represents the transmission area of the sealing samples.

3.17 Porosity

Liquid displacement method [192] was used to determine the porosity of the nanofibrous nanocomposites. Hexane was used as the displacement liquid because of its easy permeation through the pores of the fibers. A rectangular piece of dimensions 20X20 mm was immersed in 10 mL of hexane (V_1) in a graduated measuring cylinder for an interval of 10 minutes. The volume of hexane after immersing the samples was recorded (V_2). The residual hexane volume (V_3) in cylinder after removal of hexane impregnated sample was also recorded. The porosity was calculated by the equation:

$$Porosity\ (\%) = \frac{V_1 - V_3}{V_2 - V_3}X100$$

3.18 Air permeability

The air permeability of the nanofibrous nanocomposites was measured using air permeability tester WIRA and IS:11056-84 (RA 2006) test method. The air permeability is measured as the passage of volume of air (cm^3) through 1 cm^2 of the fiber per second at a differential pressure of 1 cm head of water.

3.19 Burst strength

The burst strength of the nanofibrous nanocomposites was measured using IS:1966 (Part-1) test method (Diaphragm Bursting, Materiau IngenierieI, France). The burst strength measures the application of maximum fluid pressure to a circular sample in expanding it to rupture.

3.20 PM2.5 filtration efficiency

The filtration efficiency of the nanofibrous nanocomposites was evaluated using Environmental Particle Air Monitor (EPAM-5000, HAZ-DUST, USA) having flow rate of 4 $lmin^{-1}$ and sample rate of 1 s for 6 h. The monitor of the equipment is highly sensitive and is based on the scattering of light for measurement of concentrations of particle in mgm^{-3}. The levels of PM10, PM2.5 and PM1.0 can be monitored using the interchangeable size selective impactors. The frequency of certain volume of collected air is termed as the sample rate of respirable suspended particulate matter (RSPM). In this test, the filters having pore size of 1 μm, 2.5 μm and 10 μm are selected to filter the particle size of 1 μm, 2.5 μm and 10 μm respectively, present in the volume ambient air are to be passed through the filter. The particle concentration of the sample was determined by calculating difference between the weight of the sample before and after the test. This is expressed as the concentration of particulate matter collected in mgm^{-3}.

Filtration efficiency of the nanofibrous membranes have been calculated using the following equation

$$Filtration\ efficiency\ (\%) = \frac{Y - X}{X} * 100$$

Where X and Y are the particle concentration of PAN nanofibers (control) and nanofibrous nanocomposites.

Fig 3.6 HAZ DUST EPAM 5000 instrument used for RSPM test

3.21 Pressure drop

The pressure drop or the differential pressure of the nanofibrous nanocomposites was measured using standard method IS 16289. The pressure drop of 1 cm^2 of nanofibrous samples was evaluated.

3.22 Antibacterial activity

The antibacterial activity of the nanofibrous membranes was studied by modified disc diffusion test (AATCC 30) against Gram positive *Staphylococcus aureus* and Gram negative *Eschericia coli* as described by Purwar et al. [96, 193]. Circular discs

(diameter=6mm) of the nanofibrous membranes were sterilized for 24 hours under UV light in laminar air flow which were further placed on cultured agar plates and incubated at 37 °C for 24 hours. The incubated samples were shaken in 10 mL sterilized water at 120 rpm for 30 minutes for the release of bacteria. The sample was further serially diluted upto 10^{-5} times. 20 μL of serially diluted sample was spread over the agar plates and further incubated at 37 °C for 16 hours. The experiment was performed in triplicates. The bacterial colonies were counted and % antibacterial activity was determined using the following equation.

$$Antibacterial\ activity\ (\%)\ = \frac{X - Y}{X} * 100$$

Where X and Y denote the number of colonies in control and treated sample.

3.23 Metal ion adsorption

Stock solution of $K_2Cr_2O_7$ (200 ppm) was used to prepare diluted solutions of 50 ppm to 150 ppm for adsorption study at λ_{max}= 350 nm. The minimum detectable concentrations for Cr (VI) ions in UV-Visible spectrophotometer were used to study the adsorption process of metal ions. The effect of pH, initial concentration, time and amount of adsorbent were analyzed. The experiments were performed in triplicates with a known amount of adsorbent (Mt and ZnO-Mt) i.e., 60 mg of the adsorbent was added to 25 mL of 100 ppm $K_2Cr_2O_7$ solution at pH 4.75. In case of nanofibrous nanocomposite, 3 mg of adsorbent was added to 25 mL of 100 ppm $K_2Cr_2O_7$ solution at pH 4.75. The solutions were uniformly stirred on magnetic shaker bath for 120 min to attain equilibrium. The solutions were further filtered, and the amount of metal ions adsorbed was analyzed using UV-Visible spectrophotometer. The percentage removal

of metal ions and adsorption capacity at equilibrium, q_e (mgg^{-1}) were calculated using the following equations

$$\% \, Removal = \frac{C_0 - C_e}{C_0} 100 \tag{3.1}$$

$$q_e = \frac{(C_0 - C_e)V}{M} \tag{3.2}$$

where C_0 and C_e are the initial and equilibrium concentration of metal ions in ppm, V is the volume of the solution and M is the mass of the adsorbent (g).

CHAPTER 4

PREPARATION AND CHARACTERIZATION OF ZINC OXIDE MODIFIED MONTMORILLONITE

4.1 Overview

Montmorillonite is a layered aluminosilicate clay with cation exchange capacity at its octahedral alumina layer which is fused between two tetrahedra silica layers. The excellent sorption ability, high surface area, catalytic property and ion exchange capacity of Mt makes it suitable to be used as an adsorbent. On the other hand, zinc oxide nanoparticles exhibit unique physical and chemical properties owing to its high density and limited size of corner or edges on their surface sites. The support of Mt over zinc oxide nanoparticles results in nanoparticles with enhanced surface area for adsorption and these materials also display the physicochemical properties of Mt and the metal oxide nanoparticle.

This chapter describes the preparation and characterization of zinc oxide modified montmorillonite, ZnO-Mt. ZnO-Mt has been prepared using three different starting material, (i) ZnO nanoparticles, (ii) zinc nitrate and (iii) aloe vera gel, which have been denoted as ZnO-Mt (I), ZnO-Mt (II) and ZnO-Mt (III) respectively. The reactions involved are as follows:

(i) using zinc oxide nanoparticles

$$ZnO + Mt \xrightarrow[\substack{Stir \\ 7\ days}]{Room\ temp.} ZnO\text{-}Mt$$

(ii) using zinc nitrate

$$Zn(NO_3)_2 + Mt \xrightarrow[\text{7 days}]{\text{Room temp.}} Zn(NO_3)_2\text{-}Mt \xrightarrow{+ (NH_4)_2CO_3} ZnCO_3\text{-}Mt \xrightarrow[\text{2.5 h}]{\text{500°C}} ZnO\text{-}Mt$$
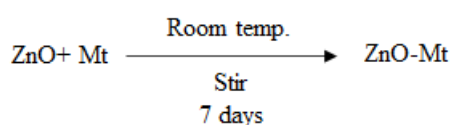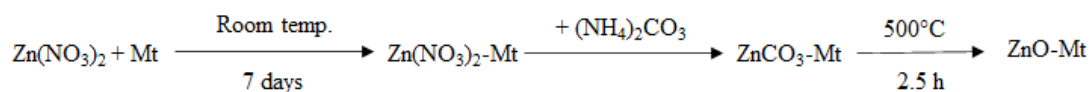
(iii) using aloe vera gel

A repetitive redox reaction occurs between zinc ions and the plant phytochemical involving conversion of carbohydrate to energy [194]].

$$Zn(NO_3)_2 \longrightarrow Zn^{2+} + NO_3^-$$

$$2NAD^+ + 2e^- \longrightarrow 2NAD$$

$$2NAD^+ + 2H^+ \longrightarrow 2NADH + 2e^-$$

$$Zn^{2+} + 2e^- \longrightarrow Zn^0 \xrightarrow{+Mt} ZnO\text{-}Mt$$
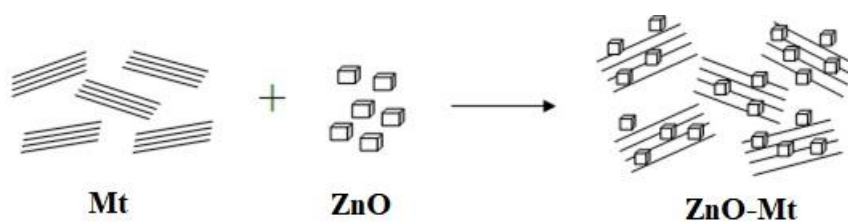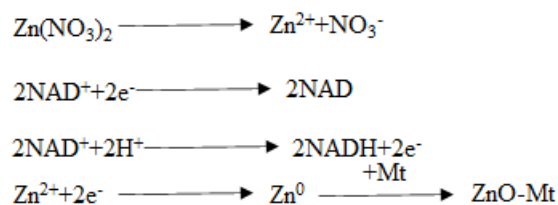
Fig 4.1 Representation of preparation of ZnO-Mt

To study the effect of modification of Mt to ZnO-Mt, morphological, structural and thermal properties of ZnO-Mt were analysed. The particle size and BET surface area of ZnO-Mt were analysed to study the changes in particle size and BET surface area of Mt on modification to ZnO-Mt. The morphology of modified montmorillonite was analysed using FESEM and HRTEM to study the changes on surface of Mt and inner structural changes in the morphology as Mt modifies to ZnO-Mt. The thermal stability of ZnO-Mt was also analysed. The results are summarized as follows.

4.2 Particle size of Mt and ZnO-Mt

The particle size of Mt and ZnO nanoparticles was analyzed using particle size analyzer. The average particle size of Mt was 71 nm. On modification, the size of ZnO-Mt (I), ZnO-Mt (II) and ZnO-Mt (III) was found to be 48 nm, 18 nm and 16 nm respectively. Hadjltaief et al. [59] and Akkari et al..[46] calculated size of ZnO on clay using Scherrer's equation and it was found to be around 13.65 nm and in the range of 7 to 10 nm respectively. Kumar et al. [57] prepared ZnO supported Mt for decontamination of sulfur mustard using ion-exchange, precipitation followed by calcination, the size of ZnO supported Mt was reported to be 3-6 nm by TEM and 6 nm from XRD.

4.3 Morphological properties

Mt was observed to be of flaky shape under scanning electron microscope (Fig 4.2 (a)). The cuboidal shaped ZnO nanoparticles are uniformly distributed over the surface of Mt (Fig 4.2 (b, c, d)). This change in surface of Mt demonstrates adsorption of ZnO nanoparticles over Mt surface. The morphology of ZnO-Mt was further analysed using high resolution transmission electron microscopy (HRTEM). HRTEM image of ZnO-Mt (I) (Fig 4.3) shows that the ZnO nanoparticles are uniformly present within the layers of Mt. Based on HRTEM results it has been observed that on modification of Mt by ZnO nanoparticles the spacing between the layers of Mt decreases and the ZnO nanoparticle gets inserted between the layers and are also uniformly distributed over the layers of Mt. This insertion of ZnO nanoparticles over the surface and between the layers of Mt results in change in size of ZnO-Mt in comparison to ZnO nanoparticle and Mt. Akkari et al. [46] observed homogenous distribution of ZnO nanoparticles prepared in situ along sepiolite fibers. Sani *et al.*. [58] demonstrated flower like shape of ZnO/ MMT nanocomposite.
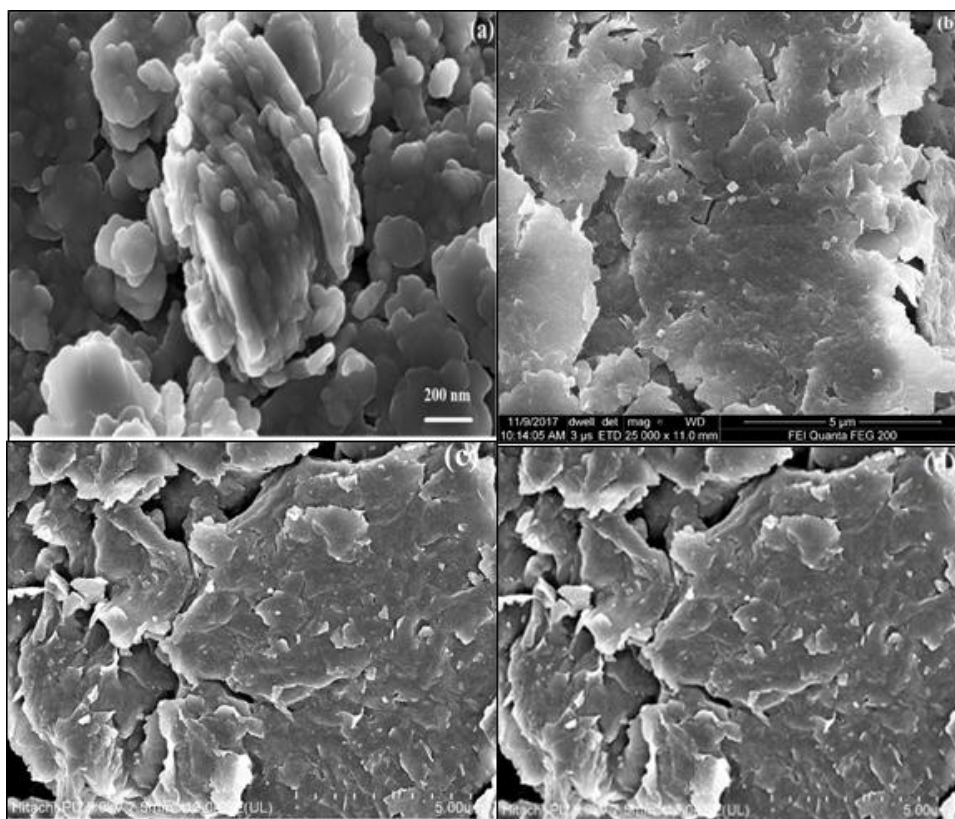
Fig 4.2 FESEM images of (a) Mt, (b) ZnO-Mt (I), (c) ZnO-Mt (II) and (d) ZnO-Mt (III)
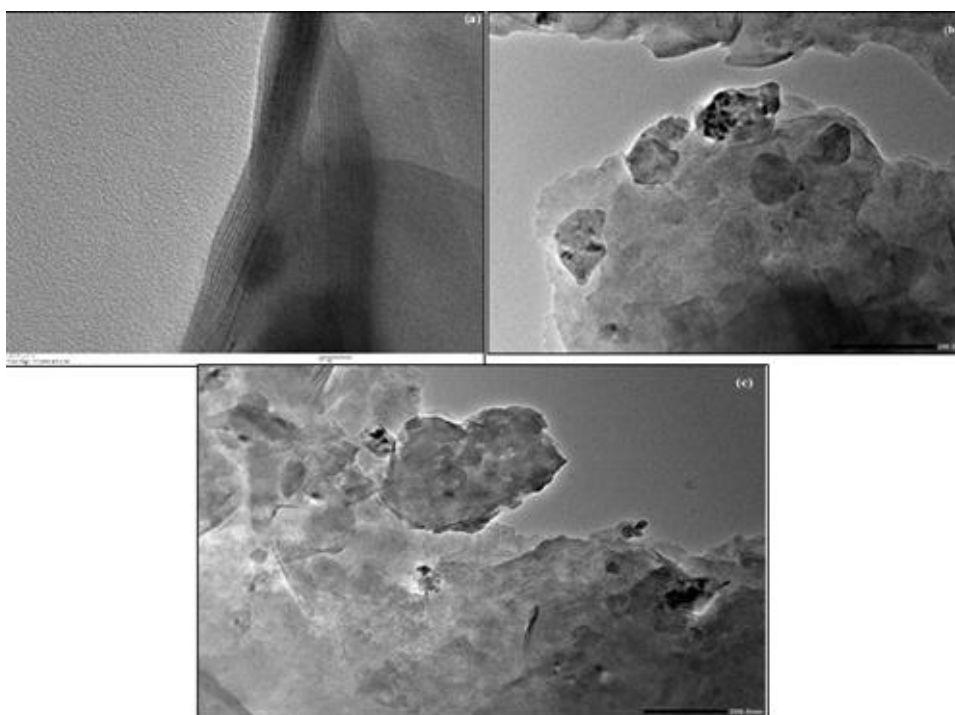
Fig 4.3 HRTEM images of (a) ZnO-Mt (I), (b) ZnO-Mt (II) and (c) ZnO-Mt (III)

The FESEM images of ZnO-Mt (II) and ZnO-Mt (III) clearly indicates the deposition of cuboidal shaped zinc oxide nanoparticles over the surface of flaky shaped montmorillonite (Fig 4.2 (c) and (d)). The formation of aggregates of ZnO on the montmorillonite surface was observed in the HRTEM images of ZnO-Mt (II) and ZnO-Mt (III). Non-uniform deposition of ZnO was observed over Mt in case of ZnO-Mt (II) and ZnO-Mt (III) (Fig 4.3 (b) and (c)).

4.4 Structural properties

A diffraction peak at 2θ equal to $7.12°$ for corresponding d-spacing of 1.24 nm appears in X-ray diffractogram of Mt (Fig 4.4 (a)). In case of ZnO-Mt (I), the X-ray diffractogram shows a minor shift in 2θ value. The 2θ value shifts to $7.32°$ (d spacing=1.21 nm) from $7.12°$. ZnO-Mt (II) shows a broad peak at $7.8°$ due to presence of Mt and diffraction peaks at $35.1°$ and $36.2°$ are due to presence of ZnO. ZnO-Mt (III) shows diffraction peaks at $6.9°$ and broadening of peak occurs at $35.5°$ (Fig 4.4 (b)). Broadening of peak appears in ZnO-Mt in comparison to Mt which indicates that ZnO nanoparticles get inserted within the layers of Mt with a negligible shift in 2θ value.
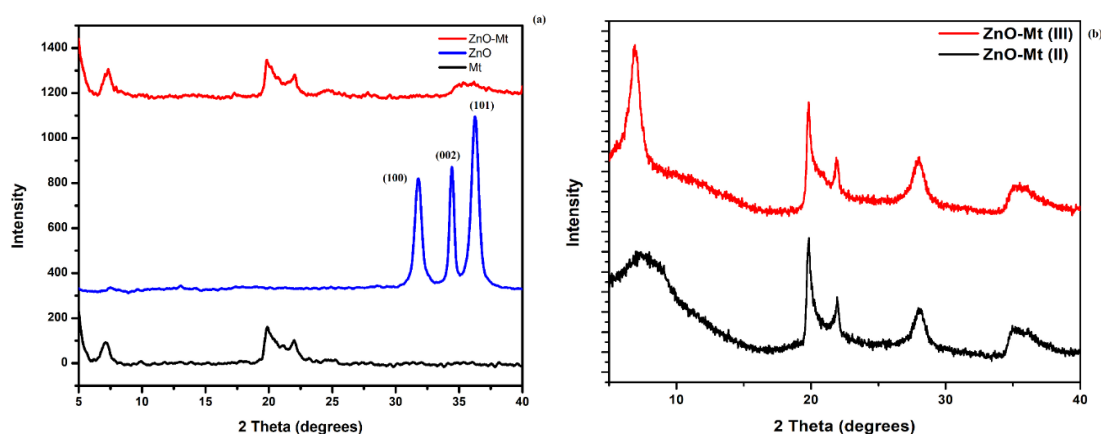
Fig 4.4 X-ray diffractogram of (a) Mt, ZnO and ZnO-Mt (I), and (b) ZnO-Mt (II) and ZnO-Mt (III)

4.5 BET surface area

The BET surface area of Mt was found to be 6.91 m^2g^{-1}. On modification of Mt with ZnO nanoparticles the surface area (11.16 m^2g^{-1}) increased by 1.6 times. The BET surface area of ZnO-Mt (II) and ZnO-Mt (III) was found to be 14.33 m^2g^{-1} and 15.23 m^2g^{-1}. The increase in surface area on modification suggest that the ZnO nanoparticle is present over and between the layers of Mt. This is in contradiction to the ZnO-Mt prepared by Kumar et al. the surface area of ZnO-Mt reduced in comparison to Mt suggesting blocking of pores of Mt by formation of ZnO-Mt over the surface of Mt [57]. The high surface area of ZnO-Mt would result in higher adsorption capacities of these materials.

4.6 Thermal properties

Mt, ZnO-Mt (I), ZnO-Mt (II) and ZnO-Mt (III) were analyzed for their thermal stability (Fig 4.5).
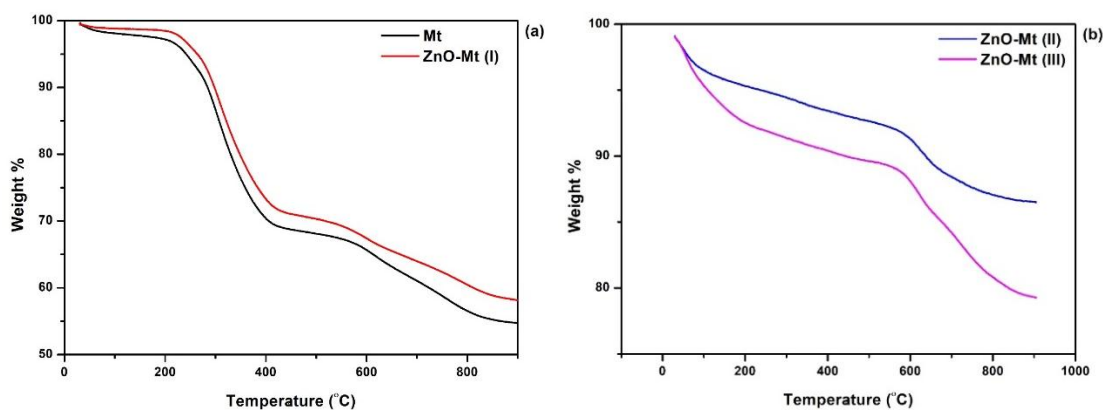
Fig 4.5 Thermogram of (a)Mt and ZnO-Mt (I) and (b) ZnO-Mt (II) and ZnO-Mt (III)

It was found that the first thermal degradation temperature of ZnO-Mt (I) was 235 °C whereas for Mt it was 203 °C. The residual mass obtained at 900 °C increased from 55% in Mt to 58% for ZnO-Mt (I). This implies an increase in the thermal stability of

Mt with addition of ZnO to Mt. The thermal degradation of ZnO-Mt (II) and ZnO-Mt (III) occurred at 561 °C and 539 °C respectively. The thermal stability of ZnO-Mt (II) and ZnO-Mt (III) was quite enhanced in comparison to Mt and ZnO-Mt (I). This enhancement in thermal stability could be due to smaller particle size of the fine powders. The smaller particle size of a crystallite results in stronger thermal stability of the crystallite [138].

4.7 Conclusions

ZnO-Mt was synthesised using zinc oxide nanoparticles, zinc nitrate and aloe vera gel. The particle size of Mt reduced from 71 nm in Mt to 16 nm in ZnO-Mt (III), on modification of Mt and an increase in BET surface area was observed for Mt on its modification with ZnO. The FESEM images showed the presence of cuboidal shaped ZnO over the surface of flaky shaped Mt and HRTEM images confirmed the presence of ZnO nanoparticles within the layers of Mt. The diffraction peaks broadened as observed from XRD which suggested the insertion of ZnO nanoparticles within the layers of Mt. Modification of Mt to ZnO-Mt enhanced the thermal stability of Mt.

CHAPTER 5

PREPARATION AND CHARACTERIZATION OF NANOFIBROUS NANOCOMPOSITES

This chapter has been divided into two parts. The first part of the chapter discusses the preparation and characterization of PAN and PAN/Mt nanofibrous nanocomposites. The second part of the chapter gives an account of the preparation and characterization of PAN/ZnO-Mt nanofibrous nanocomposites.

5.1 PREPARATION AND CHARACTERIZATION OF POLYACRYLONITRILE (PAN) AND POLYACRYLONITRILE/ MONTMORILLONITE (PAN/Mt) NANOFIBROUS NANOCOMPOSITES

5.1.1 Overview

In this chapter, preparation of PAN/Mt nanofibrous nanocomposites using electrospinning technique has been discussed. The nanofibrous nanocomposites were electrospun at room temperature conditions and the effect of addition of Mt in PAN was studied. Electrospun PAN/Mt nanofibrous nanocomposites were prepared by varying the concentration of Mt from 0.25% to 1.00% w/w (w.r.t PAN) and the electrospun nanofibrous nanocomposites were denoted as 0.25% PAN/Mt, 0.50% PAN/Mt, 0.75% PAN/Mt and 1.00% PAN/Mt nanofibrous nanocomposites. The changes in the viscosity and ionic conductivity of PAN/Mt dope solutions were studied to examine the effect of increasing concentration of Mt in PAN/Mt and was also compared with PAN dope solution. The electrospun nanofibrous nanocomposites were characterised using FESEM, XRD and TGA techniques. The FESEM micrographs suggested the changes in surface morphology of the nanofibrous nanocomposites as Mt was added to PAN

nanofibers. The increasing concentration of Mt in PAN/Mt nanofibrous nanocomposites also resulted in changes in the average diameter of the nanofibrous nanocomposites which was also a consequence of the variation in viscosity and conductivity of the dope solutions used for electrospinning. The intercalation in PAN/Mt nanofibrous nanocomposites was confirmed using X-ray diffraction analysis. The changes in thermal stability of PAN nanofibers and PAN/Mt nanofibrous nanocomposites was also examined. The effect of addition of Mt to PAN nanofibers on its morphology, structure and thermal stability have been discussed. The results are summarized as follows.

5.1.2 Viscosity and conductivity of PAN and PAN/Mt solution

The variation in viscosity of the dope solutions of PAN and PAN/Mt were studied to examine the effect of addition of Mt to PAN solution (Fig 5.1.1 (a)). It was observed that the addition of Mt increases the viscosity of PAN/Mt dope solution in comparison to PAN dope solution. The increase in viscosity of PAN/Mt solution might be due to the stronger interactions occurring between PAN and Mt layers. The increase in concentration of Mt from 0.25% to 0.75% results in a decrease in the viscosity of PAN/Mt solutions while a rapid increase in viscosity was observed for 1.00% PAN/Mt solution. A degradation in polymeric network occurs on addition of fillers resulting in a decrease in solution viscosity. But at a higher filler concentration, an increase in viscosity is observed resulting in difficulty in processing of the polymer solution [195, 196]. It has been reported that a reduction in solution viscosity is observed on weakening of force of interaction between the surface of clay. Creation of larger aggregates due to the interaction between platelets of clay results in an increase in viscosity at higher concentrations [197]. The reduction in viscosity can be attributed to the occurrence of breakdown in the platelet stacking of clay

and successive dispersion and exfoliation occurring under shear possibly resulting in slipping of chains over the platelets of clay [198].
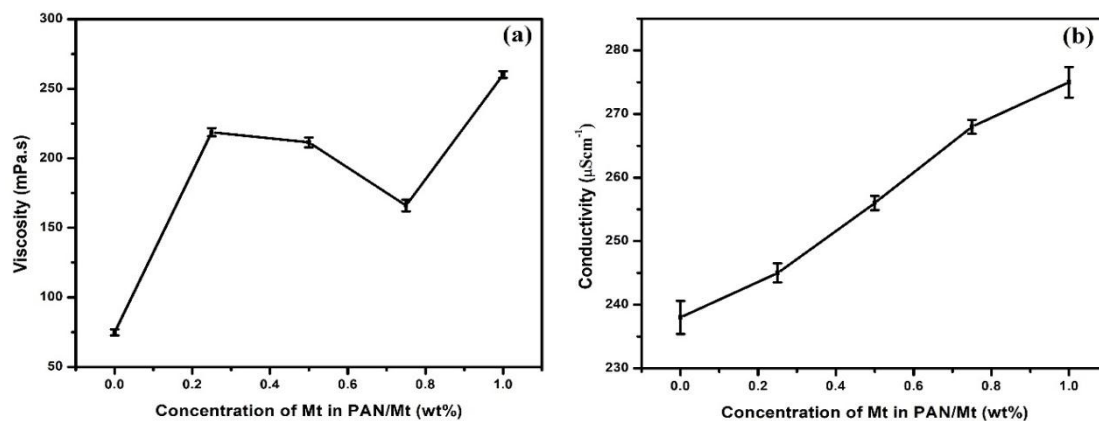
Fig 5.1.1 (a) Viscosity and (b) Conductivity of PAN and PAN/Mt solutions

The ionic conductivity of PAN solution increases on addition of Mt (Fig 5.1.1 (b)). As the concentration of Mt increases, a gradual increase in conductivity is observed in PAN/Mt solution. The ionic conductivity increases from 238 ± 2.6 μScm^{-1} in PAN to 275 ± 2.4 μScm^{-1} in 1.00% PAN/Mt solution. The ionic conductivity of a solution is dependent on the number of carrier ions and mobility of the ions. The crystallite structure of the polymer and the segmental mobility of the polymeric chains are responsible for the mobility of ions in a polymeric solution [199]. The increase in concentration of Mt increases the number of carrier ions and interaction between PAN and Mt enhances the mobility of the ions present in the solution thus resulting in increase in the conductivity of the PAN/Mt solution.

5.1.3 Surface morphology of PAN and PAN/Mt nanofibrous nanocomposites

The surface morphology of the PAN/Mt nanofibrous nanocomposites prepared by varying the concentration of Mt from 0.25% to 1.00% was analyzed using FESEM and is shown in Fig 5.1.2. It was observed that the addition of 0.25% Mt to PAN nanofibers increased the average diameter of the fibers from 269 nm in PAN nanofibers to 292 nm

for 0.25% PAN/Mt nanofibrous nanocomposites. The addition of Mt slightly increases the roughness of the fibers [200, 201]. As the concentration increased to 0.50% and 0.75% the diameter of PAN/Mt nanofibrous nanocomposites reduced to 228 nm and 206 nm respectively whereas a sharp increase in diameter was observed for 1.00% PAN/Mt nanofibrous nanocomposites. Agglomeration of Mt was visible at higher concentration of 1.00%. The change in diameter of the fibers is due to the addition of Mt to PAN and a change in viscosity of the solution. The increase in viscosity increases the fiber diameter with smooth fibrous surface [202]. The increased conductivity of PAN/Mt nanofibrous nanocomposites due to the layer charge present in Mt imparting higher polarity, is responsible for the formation of fine nanofibers [201, 203]. The charge density of ejected jets during electrospinning increases due to addition of a salt resulting in stronger forces of elongation on the jet due to the repulsion occurring among the excess charge when electric field is applied which in turn is responsible for production of substantially straight and small diameters of the fibers electrospun [203, 204]. The increase in ionic conductivity of PAN/Mt nanofibrous nanocomposites also account for a decrease in the average diameters of electrospun fibers [199, 203]. Almuhamed et al. [201] have prepared PAN/Na-Mt composite fibers with the concentration of Na-Mt varying from 5 to 19 wt%. The average diameter of the composite fibers electrospun at 13 kV ranged from 455 nm to 717 nm while the pristine PAN nanofiber had an average diameter of 747 nm.
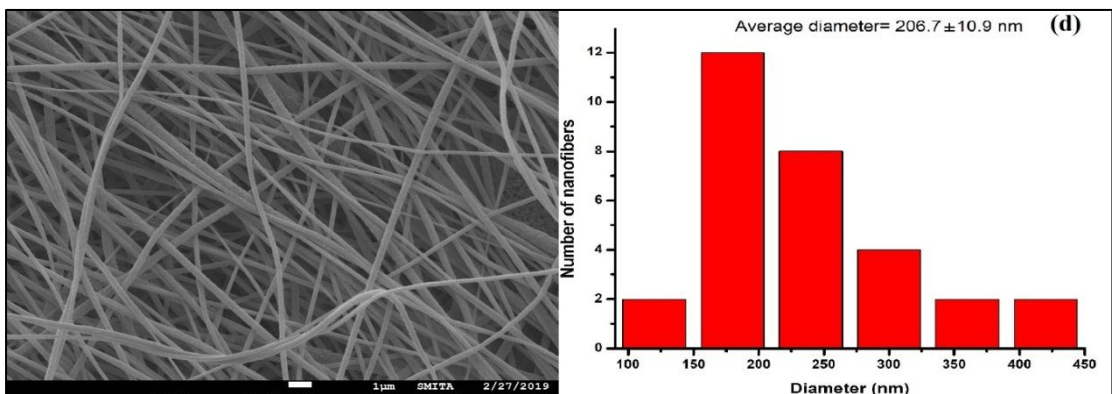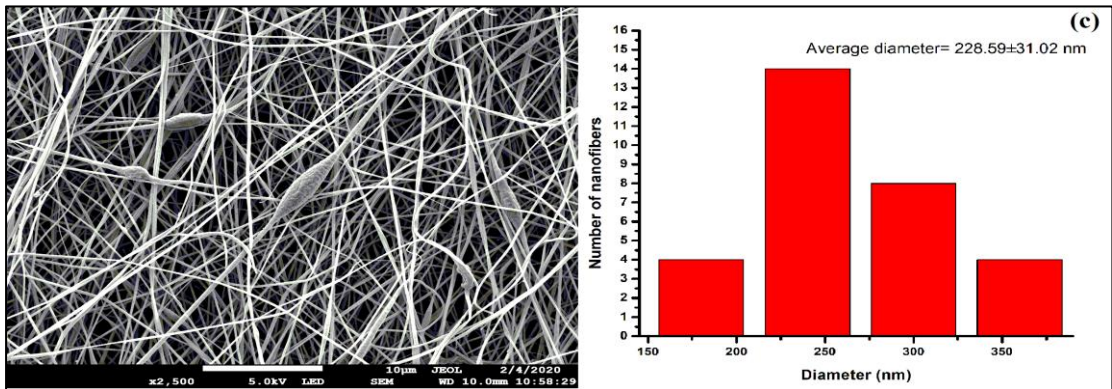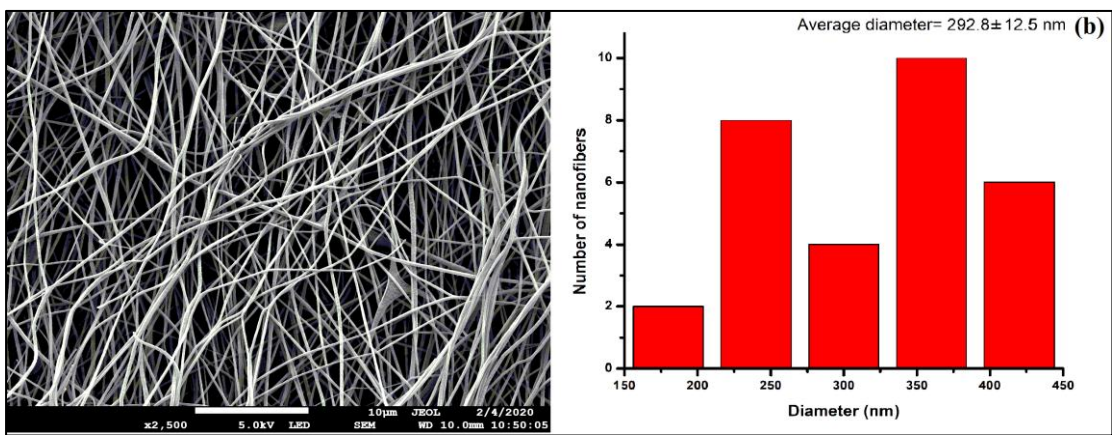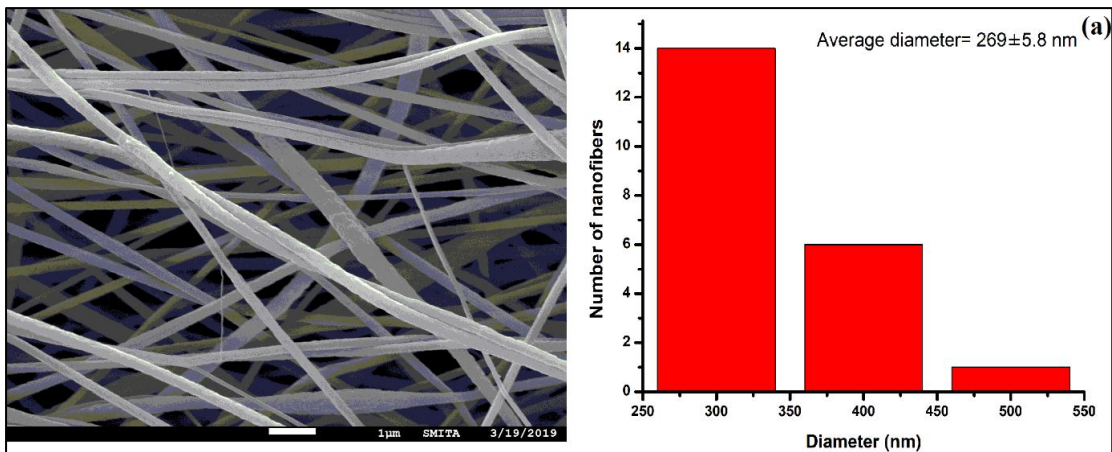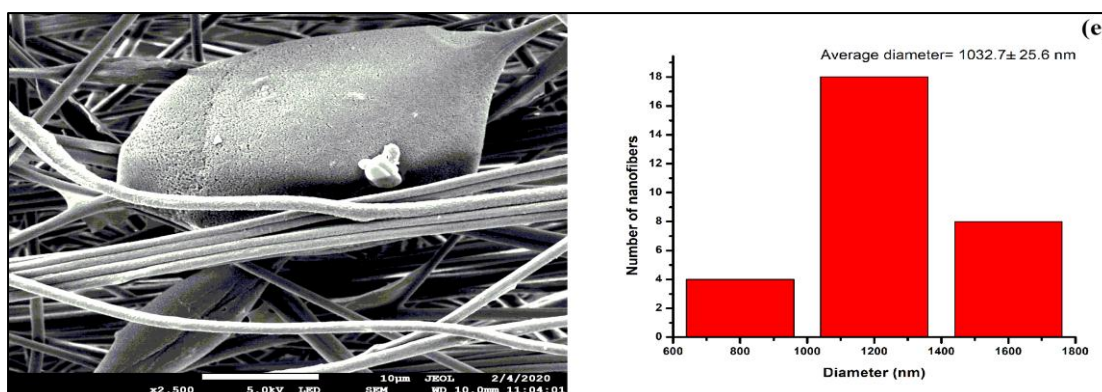
Fig 5.1.2   FESEM images of (a) PAN, (b) 0.25%, (c) 0.50%, (d) 0.75% and (e) 1.00% PAN/Mt nanofibrous nanocomposites

The dispersion of Mt into the PAN matrix was analysed using HRTEM images. The HRTEM image of 0.75% PAN/Mt nanofibrous nanocomposite clearly indicates the dispersion of Mt into PAN matrix. The surface roughness observed through HRTEM (Fig 5.1.3) is consistent with the SEM images of PAN/Mt nanofibers. The presence of Mt within PAN/Mt nanofibrous membranes was also confirmed from the EDX analysis.
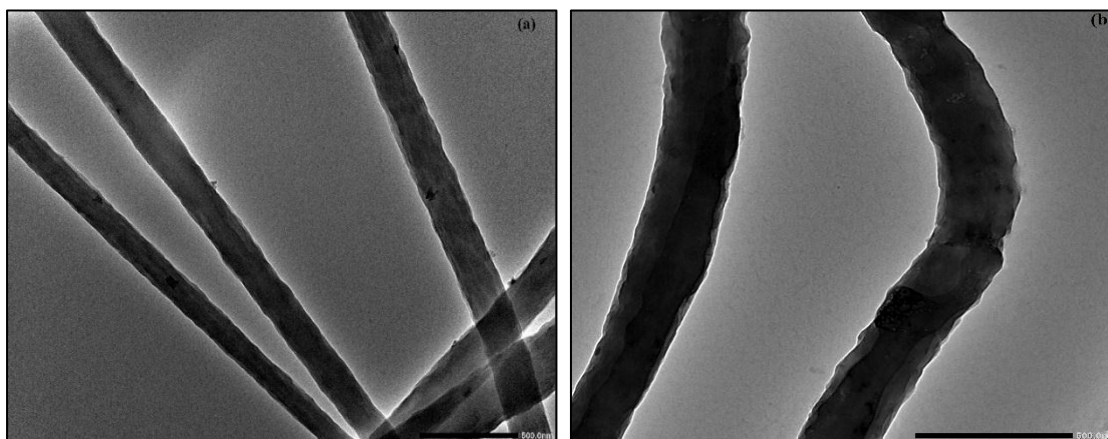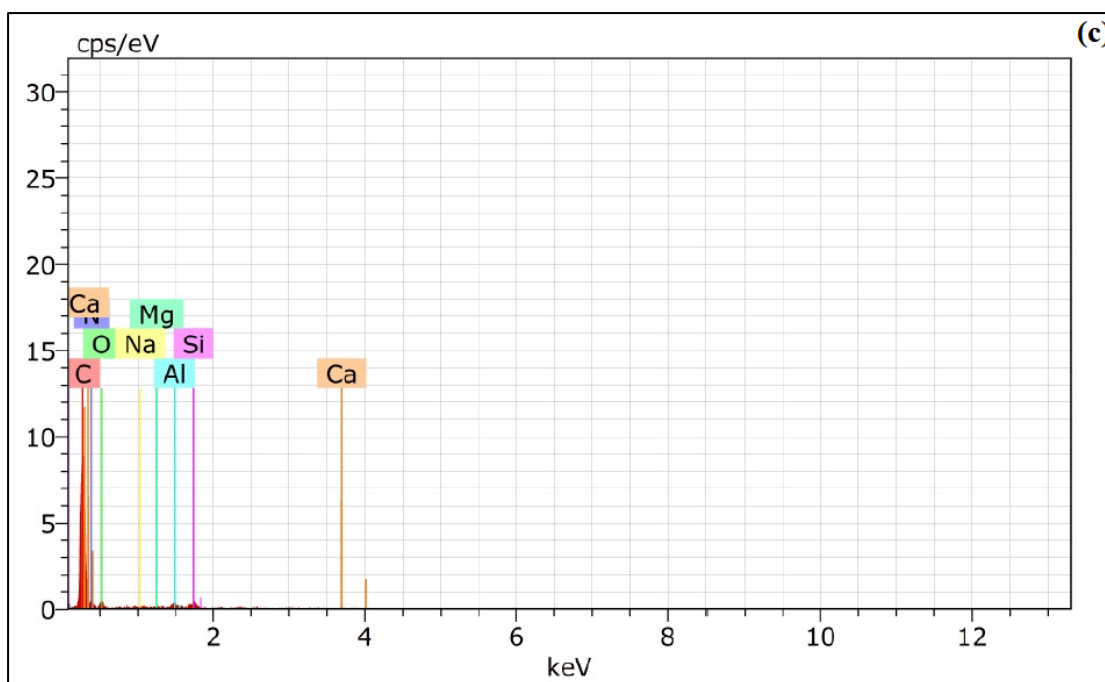
Fig 5.1.3 HRTEM image of (a) PAN and (b) 0.75% PAN/Mt nanofibrous nanocomposite (c) EDS of 0.75% PAN/Mt nanofibrous nanocomposite

The EDX spectra of 0.75% PAN/Mt nanofibrous membranes shows the presence of carbon (C), nitrogen (N), oxygen (O), calcium (Ca), sodium (Na), magnesium (Mg), silicon (Si) and aluminium (Al) elements, belonging to PAN and Mt (Fig 5.1.3 (c)).

5.1.4 Structural properties of PAN and PAN/Mt nanofibrous nanocomposites

The X-ray diffractogram of PAN nanofibers shows a strong diffraction peak at 2θ=16.9° whereas in case of PAN/Mt nanofibrous nanocomposites two peaks are observed at 2θ=7.7° due to presence of Mt and 2θ=16.9° which corresponds to PAN (Fig 5.1.4). As the concentration of Mt increases from 0.25% to 1.00%, the intensity of the peak at 7.7° increases while that of 16.9° decreases. This could be due to the intercalation of either PAN or DMF into the interlayer spacing of Mt [201]. The intercalation of water molecules into the galleries of Mt could also be responsible for this change [201].
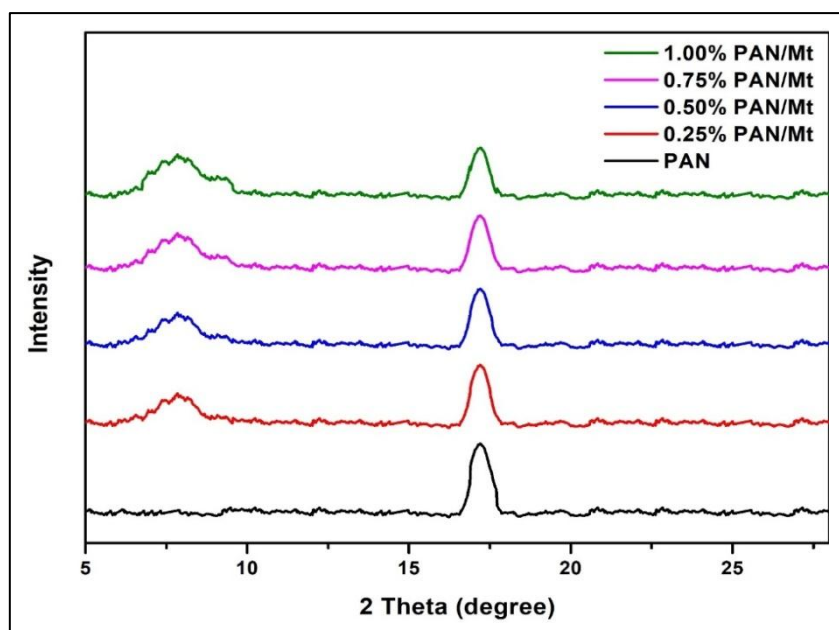
Fig 5.1.4 X-ray diffractogram of PAN and PAN/Mt nanofibrous nanocomposites

5.1.5 Thermal properties of PAN and PAN/Mt nanofibrous nanocomposites

The thermal stability of the nanofibrous nanocomposites was studied using thermogravimetric analysis. The thermograms were recorded and are shown in Fig 5.1.5.
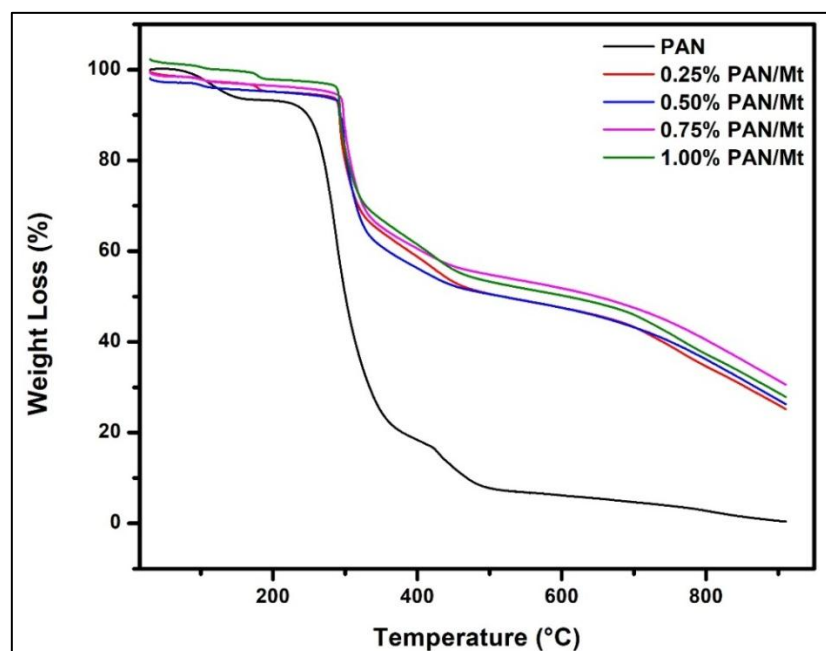
Fig 5.1.5 Thermogram of PAN and PAN/Mt nanofibrous nanocomposites

The electrospun nanofibrous membranes exhibited a similar behaviour till 165 °C exhibiting significant weight loss which is due to the desorption of water adsorbed. It was found that weight loss was negligible in PAN/Mt nanofibrous nanocomposites up to 290 °C while for PAN nanofibers it was up to 220 °C. This negligible weight loss was due to the process of cyclization [201, 205]. Further a swift weight loss was observed in nanofibrous nanocomposites which is due to the hydrogenation reaction [205]. The thermograms suggested that the addition of Mt to PAN resulted in lower weight loss in PAN/Mt nanofibrous nanocomposites compared to PAN nanofibers. The addition of Mt thus prevents the polymer degradation enhancing the thermal stability of nanofibrous nanocomposites. Similar results were reported by Almuhamed et al. [201], suggesting lowered weight loss and increased onset temperature as the amount of Mt increases in PAN.

5.1.6 Conclusions

The addition of Mt to PAN nanofibers introduced roughness on the surface of the nanofibrous nanocomposites. PAN/Mt nanofibrous nanocomposites were found to be thermally stable as the initial temperature of decomposition of the membranes increased and a lower weight loss in comparison to PAN nanofibers was observed.

5.2 PREPARATION AND CHARACTERIZATION OF POLYACRYLONITRILE/ ZINC OXIDE MODIFIED MONTMORILLONITE (PAN/ZnO-Mt) NANOFIBROUS NANOCOMPOSITES

5.2.1 Overview

This part of chapter discusses the preparation of thermally stable PAN/ZnO-Mt nanofibrous nanocomposites using electrospinning technique. PAN/ZnO-Mt (I), PAN/ZnO-Mt (II) and PAN/ZnO-Mt (III) nanofibrous nanocomposites were prepared by addition of ZnO-Mt (I), ZnO-Mt (II) and ZnO-Mt (III) to PAN solution in DMF respectively. The optimization was carried out using ZnO-Mt (I) and further the nanofibrous nanocomposites using ZnO-Mt (II) and ZnO-Mt (III) were prepared for the optimized concentration. The concentration of ZNO-Mt (I) was varied as 0.25%, 0.50%, 0.75% and 1.00% w/w (w.r.t 7% w/v PAN) and the electrospun PAN/ZnO-Mt (I) nanofibrous nanocomposites were labelled as 0.25% PAN/ZnO-Mt (I), 0.50% PAN/ZnO-Mt (I), 0.75% PAN/ZnO-Mt (I) and 1.00% PAN/ZnO-Mt (I) nanofibrous nanocomposites. Using ZnO-Mt (II) and ZnO-Mt (III), 0.75% PAN/ZnO-Mt (II) and 0.75% PAN/ZnO-Mt (III) nanofibrous nanocomposites were prepared. The viscosity and conductivity changes of dope solution with increasing concentration of ZnO-Mt (I) were studied. Viscosity and conductivity of PAN/ZnO-Mt (II) and PAN/ZnO-Mt (III) dope solutions were also analysed. The morphological, structural, physical, and thermal properties of nanofibrous nanocomposites have also been evaluated. The results are summarised as follows.

5.2.2 Viscosity and conductivity of PAN/ZnO-Mt solution

The variation of viscosity of the solution at a constant shear rate of 0.5 s^{-1} has been studied (Fig 5.2.1 (a)). It was found that addition of ZnO-Mt to PAN affects the

viscosity of the solution. The viscosity of the solution increases on the addition of ZnO-Mt (I) into PAN solution upto 0.50 % (w/w) concentration of ZnO-Mt (I) while decreases on further increase in the concentration of ZnO-Mt (I) (Fig 5.2.1 (a)). The viscosity of the PAN/ZnO-Mt (I) solution upto 0.75 % (w/w) was found to be higher than PAN solution. The increase in viscosity of the solution upto 0.50% PAN/ZnO-Mt (I) solution might be due to stronger interaction between PAN and ZnO-Mt in the solution. The stronger interaction could limit the polymeric chain mobility in the suspension resulting in higher entanglement of polymeric chains which facilitates extrusion of the solution during the process of electrospinning [206]. Whereas on increasing the concentration of ZnO-Mt (I) to 0.75% and 1.00% in PAN solution, the interaction between PAN and ZnO-Mt weakens due to accumulation of greater amount of ZnO-Mt resulting in a decrease in viscosity of the solution. The viscosity of PAN/ZnO-Mt (II) and 0.75% PAN/ZnO-Mt (III) was found to be 90.21±1.5 mPas and 87.32±1.6 mPas respectively which is approximately similar to the viscosity of PAN/ZnO-Mt (I) (88.82±1.8 mPas). Researchers have reported enhancement as well as reduction in viscosity of polymer solution on incorporation of clay [207, 208]. The dispersion and exfoliation of platelets during mixing reduces the shear viscosity of the nanocomposites in comparison to pristine polymer [196].
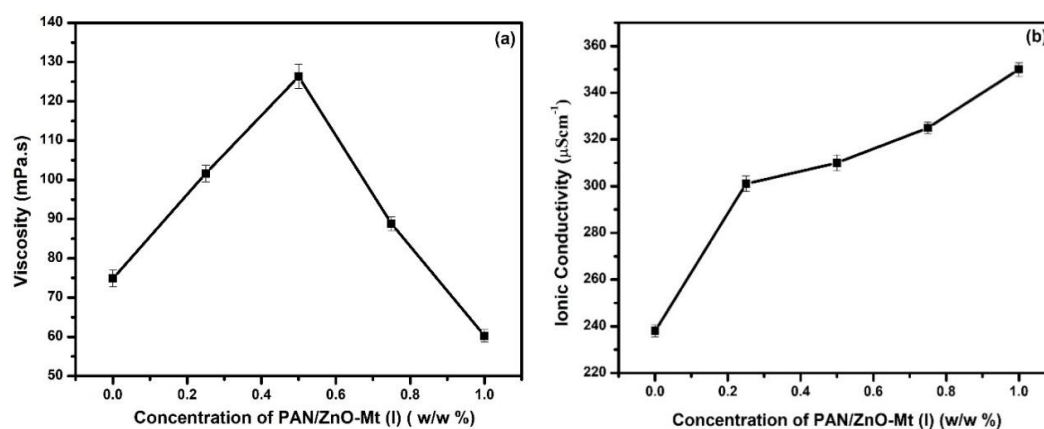
Fig 5.2.1 (a) Viscosity and (b) Ionic conductivity of PAN/ZnO-Mt (I) dope solutions

The ionic conductivity of pure PAN solution was found to be 238 μScm^{-1} solution and further increased on addition of ZnO-Mt (I) into PAN solution upto 350 μScm^{-1}. The ionic conductivity of the solution is governed by two factors, the mobility of the ions and the amount of the carrier ions in olution. The amount of carrier ions in a solution is affected by the concentration of ions present in the solution. Mt possesses negative charge and OH group linked to Al or Si. This charge is responsible for the interaction between Mt and PAN. The ionic conductivity of PAN solution increases on addition of ZnO-Mt as the number of charged ions increases in the solution (Fig 5.2.1 (b)). The ionic conductivity of 0.75% PAN/ZnO-Mt (II) was 346 μScm^{-1} whereas for 0.75% PAN/ZnO-Mt (III), it was found to be 349 μScm^{-1}. Sikkanthar et al. [209] reported that the ionic conductivity of polyacrylonitrile-ammonium bromide polymer electrolyte increased from $1.3X10^{-4}$ Scm^{-1} in 95:5 composition to $2.5X10^{-3}$ Scm^{-1} in 70:30 composition due to the increase in mobility of the charge carriers.

5.2.3 Surface morphology of PAN/ZnO-Mt nanofibrous nanocomposites

The nanofibrous membranes have been developed by varying the concentrations of ZnO-Mt (I) in PAN solution from 0.25% to 1.00%. 0.75% PAN/ZnO-Mt (II) and 0.75% PAN/ZnO-Mt (III) nanofibrous nanocomposites have also been electrospun. The field emission scanning electron micrographs of the PAN/ZnO-Mt nanofibrous nanocomposites are shown in Fig 5.2.2.

The surface morphology of the nanofibrous nanocomposites suggested that on addition of ZnO-Mt (I) into the PAN matrix, the roughness on the surface of the nanofibers increased. PAN nanofibrous membranes (Fig 5.2.2 (a)) were smooth in comparison to PAN/ZnO-Mt (I) nanofibrous nanocomposites. As the concentration of ZnO-Mt (I) increases in PAN/ZnO-Mt (I) nanofibrous nanocomposites respectively, the fibers

changed their orientation from beaded to beadless uniformly densely packed nanofibers. But as the concentration increased to 1.00%, beaded and less dense nanofibers were formed. An increase in the concentration results in instability of the solution at the tip of spinneret during electrospinning resulting in formation of beaded fibers with a thicker diameter [15]. The diameter of the fibers increased at higher concentration due to viscosity changes in the solution which is due to the entanglement of the molecules of the polymeric chain [206].

In case of ZnO-Mt (II) and ZnO-Mt (III), 0.75% PAN/ZnO-Mt (II) and 0.75% PAN/ZnO-Mt (III) were prepared as 0.75% concentration was optimized from the results of PAN/Mt and PAN/ZnO-Mt nanofibrous nanocomposites. The FESEM images for PAN/ZnO-Mt (II) and PAN/ZnO-Mt (III) nanofibrous nanocomposites are shown in Fig 5.2.2 (f) and (g). The average diameter of 0.75% PAN/ZnO-Mt (II) and 0.75% PAN/ZnO-Mt (III) nanofibrous nanocomposites was found to be 219.94 nm and 225.61 nm respectively which was comparable to 0.75% PAN/ZnO-Mt (I) nanofibrous nanocomposite. The surface roughness of 0.75% PAN/ZnO-Mt (II) and 0.75% PAN/ZnO-Mt (III) was significantly enhanced as compared to PAN nanofibers.
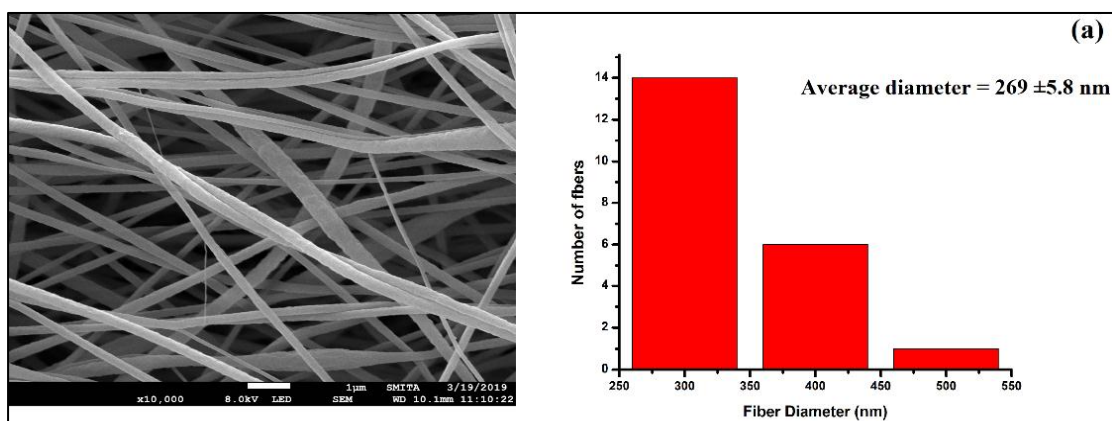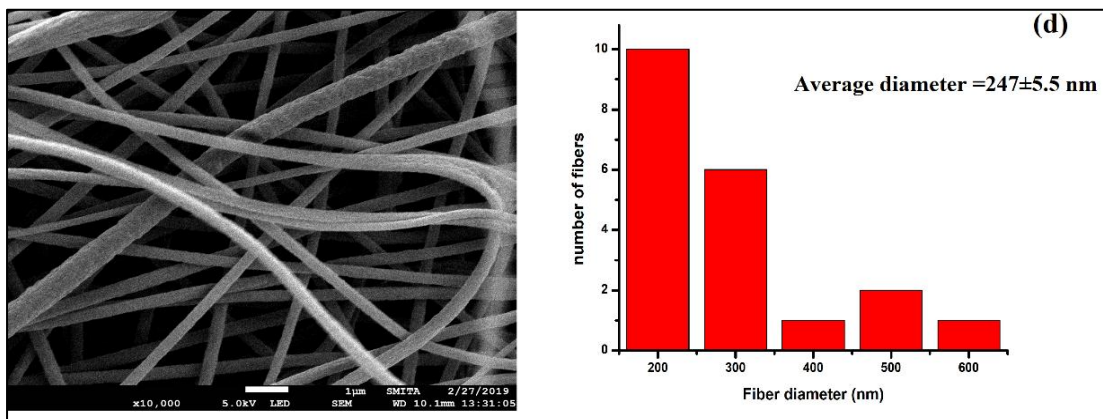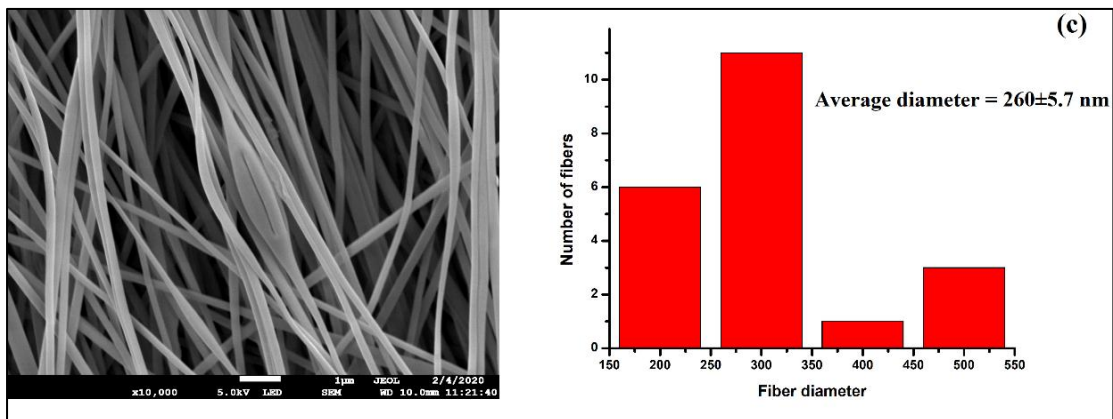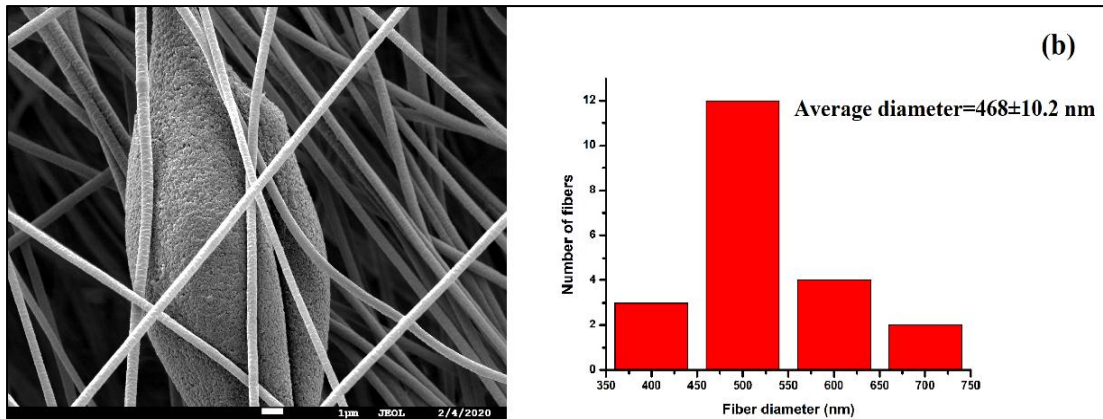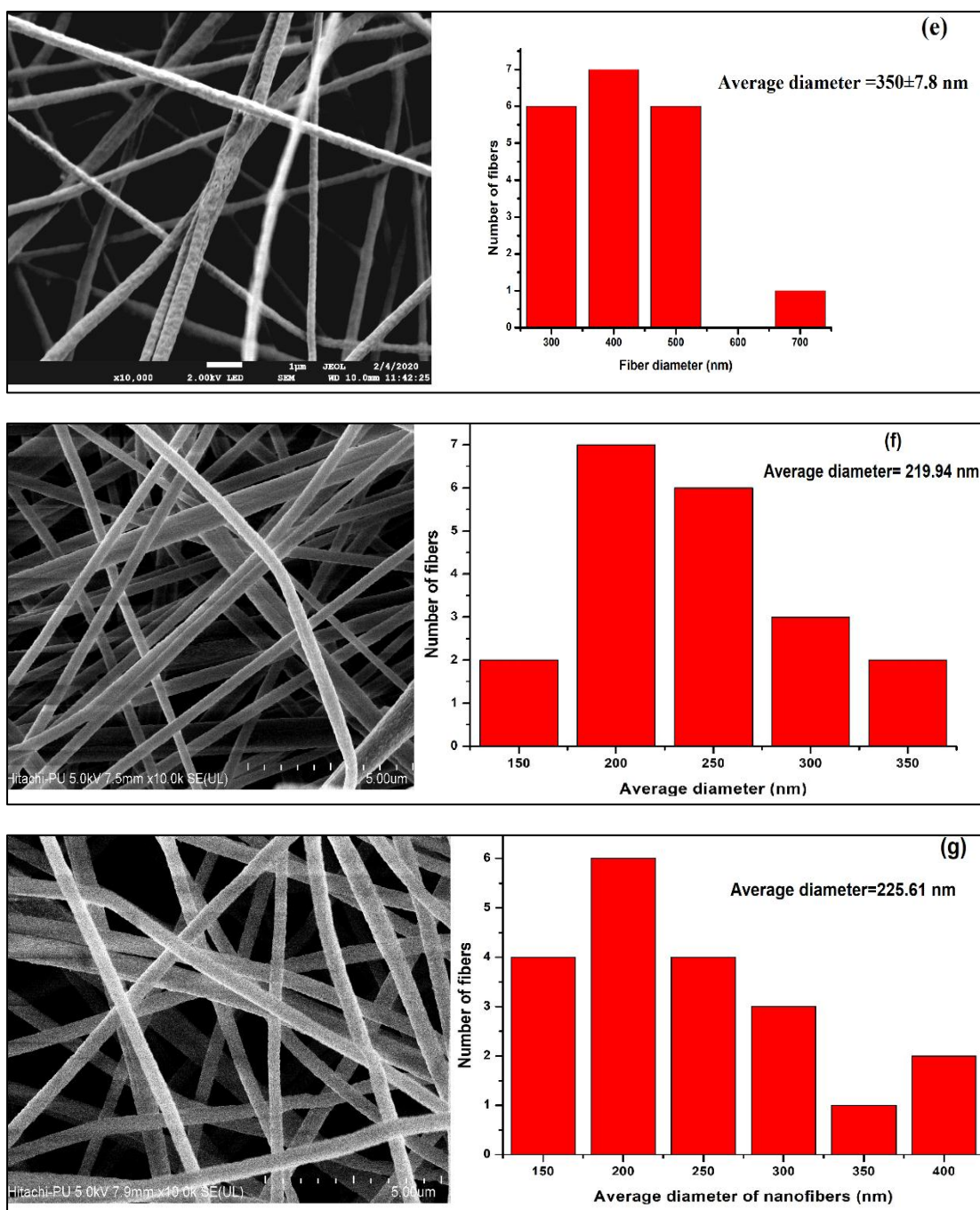
Fig 5.2.2 FESEM images and average diameter of (a) PAN, (b) 0.25%, (c) 0.50%, (d) 0.75%, (e) 1.00% PAN/ZnO-Mt (I) nanofibrous nanocomposites, (f) 0.75% PAN/ZnO-Mt (II) and (g) 0.75% PAN/ZnO-Mt (III) nanofibrous nanocomposites

The viscosity and electrical conductivity of the dope solution has a major effect on the diameter of the nanofibers. The size of the fiber and its uniformity is dependent on the viscosity of the polymer solution [93]. Non-uniform beaded fibers are formed at lower

viscosities whereas at a higher viscosity the electrospinning jet experiences a difficulty in ejection. The increase in conductivity is also responsible for a decrease in the diameter of the fibers as the electrospinning spinneret jet carries higher amount of electric charges which results in application of much higher forces of elongation on the surface of the fiber and finer diameter fibers are formed. Thus, a solution of an optimum viscosity and conductivity is required for electrospinning [15]. A regular trend in average diameter of nanofibers was not observed due to the combined effect of viscosity and conductivity of the solution resulting in formation of nanofibers. 0.75% PAN/ZnO-Mt (I) nanofibrous nanocomposites had the smallest average diameter of 247 nm amongst the series of nanofibers developed. The addition of clay increases the fiber diameter as an increase in clay content increases the viscosity as well as electrical conductivity of the solution [210]. Liu et al. [18] reported that the average diameter of polyacrylonitrile/polyacrylic acid nanofibers is dependent both on the viscosity and conductivity of the dope solution. Similar results have been obtained by the addition of sodium montmorillonite into PAN matrix which resulted in an increase in the surface roughness of the produced composite nanofibers and decrease in average diameter of the nanofibers with respect to their pristine counterpart [201].

The HRTEM images of PAN/ZnO-Mt (I), 0.75% PAN/ZnO-Mt (II) and PAN/ZnO-Mt (III) nanofibrous nanocomposites indicate the dispersion of ZnO-Mt in PAN nanofibrous membranes (Fig 5.2.3 (a), (b) and (c)). The surface roughness was visible in the HRTEM images. From the images it is evident that ZnO-Mt (I), Zn)-Mt (II) and ZnO-Mt (III) are present over and within the PAN matrix. The presence of ZnO-Mt within PAN/ZnO-Mt nanofibrous membranes was also confirmed from the EDX analysis. The EDX spectra of 0.75% PAN/ZnO-Mt (I), 0.75% PAN/ZnO-Mt (II) and 0.75% PAN/ZnO-Mt (III)

nanofibrous membranes shows the presence of carbon (C), nitrogen (N), oxygen (O), calcium (Ca), sodium (Na), magnesium (Mg), silicon (Si), aluminium (Al) and zinc (Zn) (Fig 5.2.3 (d), (e) and (f)) elements, belonging to PAN and ZnO-Mt.
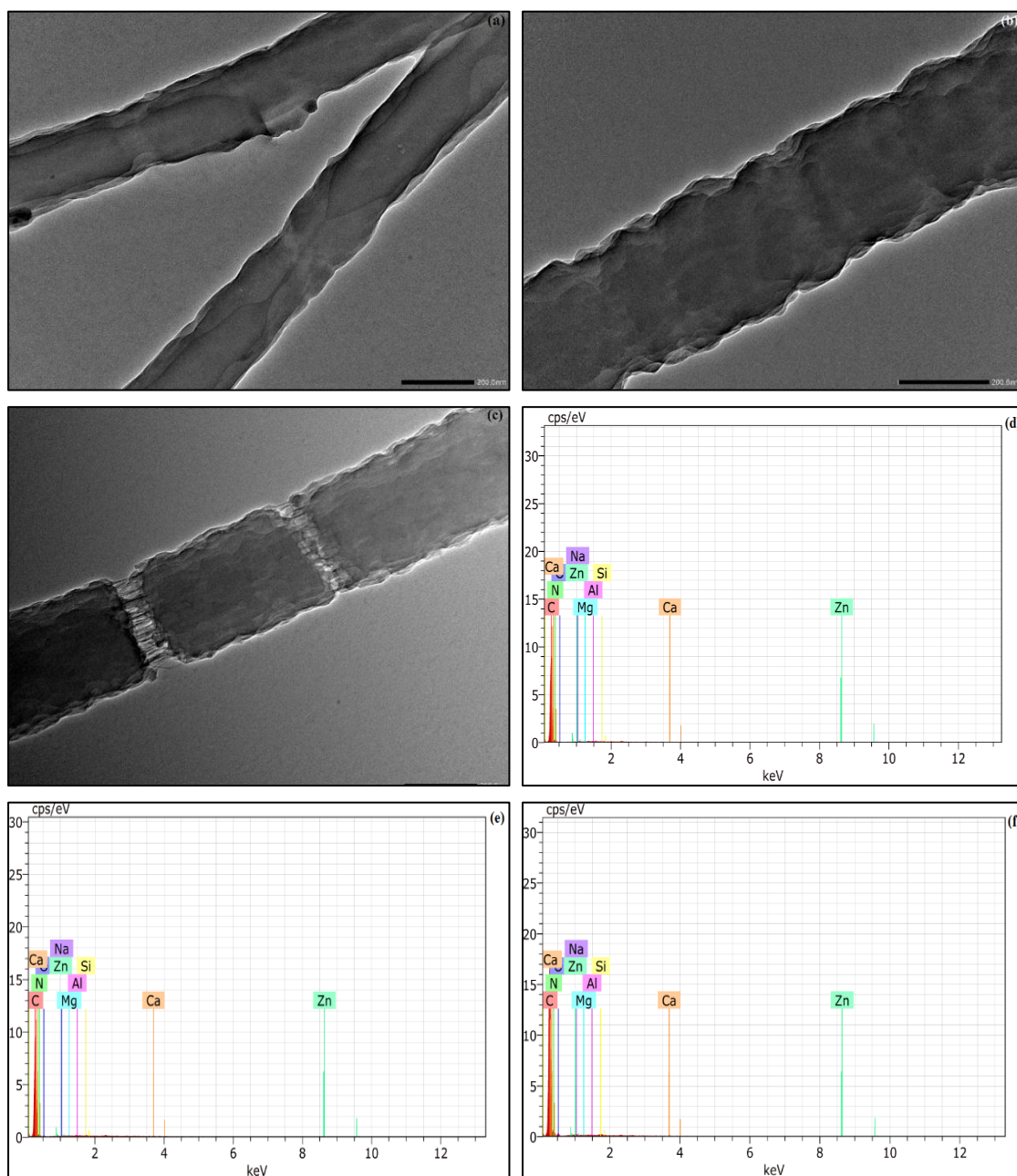
Fig 5.2.3 HRTEM image of (a) 0.75% PAN/ZnO-Mt (I), (b) 0.75% PAN/ZnO-Mt (II), (c) 0.75% PAN/ZnO-Mt (III), EDS of (d) 0.75% PAN/ZnO-Mt (I), (e) 0.75% PAN/ZnO-Mt (II) and (f) 0.75% PAN/ZnO-Mt (III) nanofibrous nanocomposites

5.2.4 Structural properties of PAN/ZnO-Mt nanofibrous nanocomposites

The presence of ZnO-Mt in the nanofibrous membranes was analyzed using XRD (Fig 5.2.4). XRD pattern shows a peak at 16.9° for PAN nanofibers whereas for PAN/ZnO-Mt (I) nanocomposite nanofiber two peaks were observed at 16.9° and 31.8°. Strong anatase peaks of ZnO are observed at 31°, 34° and 36° [40], the modification of Mt with ZnO resulted in broadening of peak. It was observed that with addition of ZnO-Mt to PAN nanofibers the peak appeared at 16.5° for PAN was broadening, suggesting localization of ZnO-Mt into the nanofibrous membranes. The fiber diffraction pattern for PAN having hexagonal crystal system shows two equatorial peaks at $2\theta=29.5°$ and $2\theta=17°$ with degree of crystallinity of PAN fibers in the range 8.8% to 11.27%. The crystallization slows down during electrospinning because of rapid solidification of stretched chains of polymer at higher elongation rates hindering crystal formation [211-213]. The degree of crystallinity of PAN was found to be 13.33% whereas on addition of ZnO-Mt to the PAN nanofibrous membranes, the degree of crystallinity increased in the order 0.25% PAN/ZnO-Mt (I) (38.10%)> 0.50% PAN/ZnO-Mt (I) (28.03%)> 0.75% PAN/ZnO-Mt (I) (26.82%)> 0.75% PAN/ZnO-Mt (II) (24.23%)> 0.75% PAN/ZnO-Mt (III) (24.11%)> 1.00% PAN/ZnO-Mt (17.65%). The zinc oxide modified clay may act as nucleating site and enhanced the crystallinity of nanocomposite fibers. However, higher amount of clay in nanofibrous matrix affects the crystallization behavior of polyacrylonitrile polymer chain and reduces the crystallinity. Two diffraction peaks were observed for PAN/ZnO-Mt (II) and 0.75% PAN/ZnO-Mt (III) nanofibrous nanocomposites at 16.9° and 27.1°. The appearance of diffraction peaks at 27° to 33.1° suggested the presence of ZnO in ZnO-Mt.
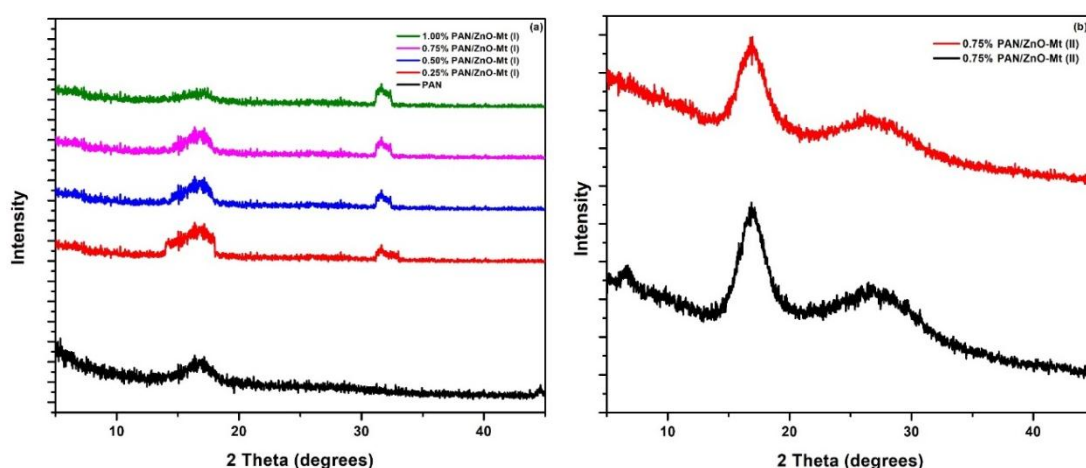
Fig 5.2.4 X-ray diffractogram of PAN/ZnO-Mt nanofibrous nanocomposites

5.2.5 Thermal properties of PAN/ZnO-Mt nanofibrous nanocomposites

The performance of the nanofibrous nanocomposites under thermal conditions was studied by thermogravimetric analysis. The thermal degradation of the nanofibrous nanocomposites was found to be a two-step degradation process whereas for PAN nanofibers it was a three-step degradation process (Fig 5.2.5). On addition of ZnO-Mt (I) into PAN nanofibrous membranes the onset temperature of first step of degradation was found to increase from 92 °C in PAN nanofibers to 288 °C in nanofibrous nanocomposites. The second step of thermal decomposition starts at 188 °C for PAN nanofibers and increases to 381 °C in nanofibrous nanocomposites. The nanocomposite fibers show only 40% weight loss at 900 °C higher in comparison to PAN nanofibers due to stability of ZnO-Mt (I) at higher temperatures. Addition of ZnO-Mt enhances the thermal stability of PAN nanofibers due to the synergistic effect of ZnO-Mt. The tremendous improvement in thermal properties of nanofibers suggests uniform dispersion of ZnO-Mt in nanofibrous matrix. The addition of ZnO-Mt into PAN nanofibers resulted in much more thermally stable nanofibrous nanocomposites in comparison to PAN nanofibers as the presence of ZnO-Mt prevents degradation of PAN. ZnO nanoparticles

70

have also been reported to enhance the thermal stability of PAN nanofibers [40]. Similar results have been reported by Almuhamed et al. [201] for electrospun PAN/Na-MMT hybrid nanofibers comprising 5, 10 and 19 wt% Na-MMT, an increase in thermal stability of the nanofibers was observed with incorporation of Na-MMT in PAN.

The thermal decomposition temperature was found to increase in case of 0.75% PAN/ZnO-Mt (II) and 0.75% PAN/ZnO-Mt (III) nanofibrous nanocomposites. This increase could be attributed to the smaller particle size of ZnO-Mt (II) and ZnO-Mt (III).
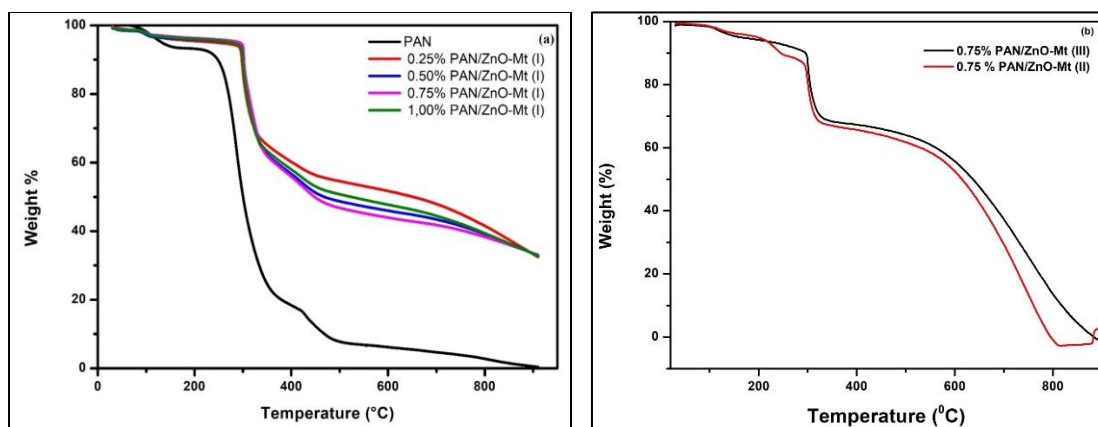
Fig 5.2.5 Thermogram of PAN/ZnO-Mt nanofibrous nanocomposites

5.2.6 Conclusions

PAN/ZnO-Mt (I) nanofibrous nanocomposites were developed by varying concentration of ZnO-Mt (I) from 0.25% to 1.00%. ZnO-Mt (II) and ZnO-Mt (III) were used to prepare 0.75% PAN/ZnO-Mt (II) and 0.75% PAN/ZnO-Mt (III) nanofibrous nanocomposites. The average diameter of the nanofibrous nanocomposites was found to be in the range of 260±5.7 nm to 350±7.8 nm. The surface roughness of the nanofibrous nanocomposites was increased as compared to PAN nanofibers on addition of ZnO-Mt.

The broadened peak observed in X-ray diffractogram suggested localization of ZnO-Mt within nanofibrous membranes. The addition of ZnO-Mt enhanced the thermal stability of the nanofibrous nanocomposites in comparison to PAN nanofibers.

CHAPTER 6

FILTRATION OF PM2.5 AND ANTIBACTERIAL ACTIVITY OF NANOFIBROUS NANOCOMPOSITES

6.1 Overview

Air pollution and presence of heavy metal ions in water resources are amongst the significant environmental issues adversely affecting the health of the public, production efficiency and the ecosystem. One of the harmful pollutants giving rise to atmospheric pollution is particulate matter (PM) pollution which is majorly due to the emission of various solid and liquid particles into the atmosphere, adversely affecting the human health, due to its easy penetration into the respiratory and cardiovascular systems. The electrospun fibrous membranes have emerged as a promising material for efficient filtration of PM particles. The nanofibrous membranes produced using electrospinning have diameters ranging from 40 to 2000 nm, higher surface-to-volume ratio, good network connectivity, tunable geometries and controllable structure. These properties of the nanofibrous membranes make them promising filtration materials.

The nanofibrous nanocomposites were analysed for their ability to capture PM2.5 from atmosphere. This chapter discusses about the PM2.5 filtration efficiency of PAN/Mt and PAN/ZnO-Mt nanofibrous nanocomposites. The addition of ZnO to Mt enhances its antibacterial properties. This chapter also focuses on the antibacterial properties of PAN/ZnO-Mt nanofibrous nanocomposites against Gram-positive and Gram-negative bacterial strains. The physical properties such as porosity, burst strength, air permeability and water vapor transmission rate of PAN/Mt and PAN/ZnO-Mt nanofibrous nanocomposites were examined. The porosity, burst strength, air permeability and

WVTR of nanofibrous nanocomposites depend on the average fiber diameter. These properties have a significant effect on the PM2.5 capture efficiency of the nanofibrous nanocomposites. The results are discussed as follows.

6.2 Porosity of nanofibrous nanocomposites

The nanofibrous membranes are known to be porous which accounts for its ability to absorb and retain the electrolyte which in turn imparts high ionic conductivity. The average porosities of the nanofibrous nanocomposites are tabulated in Table 6.1. Increase in the concentration of Mt from 0.25% to 0.75% increases the porosity of PAN/Mt nanofibrous nanocomposites while a slight decrease is observed as the concentration of Mt reaches to 1.00%. The porosity of PAN nanofibrous membranes increased from 50% to 75% in 0.75% PAN/Mt nanofibrous nanocomposite. It has been found that the porosity of the nanofibrous nanocomposites increases with a decrease in fiber diameter. The difference in porosity is due to the loosely bound fibrous network and average diameter of the fibrous membrane. The well-developed interconnected fibrous network is also responsible for the superior porosities of the nanofibrous membranes [199].

0.75% PAN/ZnO-Mt (II) nanofibrous nanocomposites were found to have the highest porosity of 88% respectively. The porosity of the nanofibrous nanocomposites were found to increase with an increase in the concentration of ZnO-Mt upto 0.75% w/w. whereas 1.00% PAN/ZnO-Mt nanofibrous nanocomposite had porosity equal to PAN nanofibers. It was observed that the porosity of the nanofibrous nanocomposites increased with decrease in fiber diameter suggesting that uniformly developed interconnected network of fibers was accountable for better porosities of the

nanofibrous nanocomposites. The porosity of 0.75% PAN/ZnO-Mt (II) and 0.75%

PAN/ZnO-Mt (III) was found to be in close proximity with 0.75% PAN/ZnO-Mt (I)

Table 6.1 Parameters of nanofibrous nanocomposites

	Porosity (%)	Burst Strength (Nmm^{-2})	Water Vapor Transmission Rate (kgm^{-2}day^{-1})	Air Permeability (Lm^{-2}s^{-1})
PAN	50	8.9	0.79	5.4
0.25% PAN/Mt	33	11.3	0.21	6.1
0.50% PAN/Mt	67	16.7	0.93	11.1
0.75% PAN/Mt	75	18.1	5.41	19.8
1.00% PAN/Mt	63	9.8	0.83	10.0
0.50% PAN/ZnO-Mt (I)	80	21.6	1.04	14.2
0.75% PAN/ZnO-Mt (I)	86	27.8	7.81	25.3
1.00% PAN/ZnO-Mt (I)	50	25.4	2.86	6.6
0.75% PAN/ZnO-Mt (II)	88	26.5	8.77	27.1
0.75% PAN/ZnO-Mt (III)	86	24.3	7.98	26.5

6.3 Burst strength of nanofibrous nanocomposites

The ability of a material to maintain its continuity on application of pressure is defined

as the burst strength of the material. The burst strength increased from 8.9 N mm^{-2} in

PAN nanofibers to 18.1 N mm^{-2} on addition of Mt to PAN nanofibers. The increase in

concentration of Mt from 0.25% to 0.75% resulted in an increase in burst strength of

PAN/Mt nanofibrous nanocomposites from 11.3 N mm^{-2} to 18.1 N mm^{-2} whereas a

slight decrease was observed as the concentration of Mt increases to 1.00%. The

exfoliated clay acts as a reinforcing filler for the nanofibrous membranes. The increase

in concentration of clay increases the burst strength of the sample [96].

The burst strength of the PAN/ZnO-Mt nanofibrous nanocomposites was found to increase from 15.7 to 27.8 Nmm^{-2}. As the concentration of ZnO-Mt increases to 0.75% in PAN nanofibers, the burst strength increases as the modified clay present within the nanofibers act as a reinforcing filler whereas a slight decrease was observed for 1.00% PAN/ZnO-Mt (I) nanofibrous nanocomposites which might be due to a less dense structure of the membrane as observed from FESEM.

6.4 Water vapor transmission rate and air permeability of nanofibrous nanocomposites

The transportation characteristics of nanofibrous membranes is essential to determine the suitability of the membrane as a filter which were studied by evaluation of water vapor transmission rate of the nanofibrous nanocomposites. WVTR of PAN nanofibrous membranes was found to be 0.79 $kgm^{-2}day^{-1}$. On addition of Mt to PAN the WVTR increased to 5.41 $kgm^{-2}day^{-1}$ in for 0.75% PAN/Mt nanofibrous nanocomposite while a decrease was observed in 1.00% PAN/Mt nanofibrous nanocomposite. WVTR was found to be linearly related to porosity of the nanofibrous nanocomposites. An increase in porosity resulted in increase in WVTR of the nanofibrous membranes. WVTR was found to increase with an increase in the concentration of ZnO-Mt in PAN/ZnO-Mt nanofibrous nanocomposites. The increase in WVTR in case of PAN/ZnO-Mt in comparison to PAN is due to enhancement of porosity. The change in the morphology of the nanofibrous membranes results in variation in WVTR of the nanofibrous nanocomposites. PAN nanofibers were more densely packed compared to PAN/ZnO-Mt and had lower pore size which resulted in lower water vapor transmission rate of the nanofibrous nanocomposites. As indicated from FESEM images, the addition of ZnO-Mt to PAN nanofibers resulted in an

increased pore size and lower nanofiber diameters which increased its water vapor transmission rate compared to PAN.

The measurement of passage of air through a specified area of a fiber is termed as air permeability [214]. The air permeability is also one of the important measures to study the permittivity of the membrane for filters. The air permeability of a fiber is majorly dependent on the porosity, pore size and diameter of the fiber influencing its openness [215]. The air permeability of the nanofibrous membranes was directly related to the porosity of the nanofibrous membranes. The air permeability was found to increase from 5.4 $Lm^{-2}s^{-1}$ in PAN to 19.8 $Lm^{-2}s^{-1}$ for 0.75% PAN/Mt nanofibrous nanocomposites. The air permeability increased by five times in 0.75% PAN/ZnO-Mt in comparison to PAN nanofibrous membranes. It has been reported that the fluffy structure of PAN nanofibrous membranes exhibit WVTR of 13.7 $kgm^{-2}day^{-1}$ and an air permeability value of 23.6 $Lm^{-2}s^{-1}$. On increasing the concentration of polydimethylsiloxane in PAN, the WVTR and air permeability decreases due to the transformation in structure from being fluffy to adhesive resulting in decreased porosity of the membranes[216]. Roche et al. [217] developed laminated PAN nanofibers for air filtration having air permeability of 4 $Lm^{-2}s^{-1}$ which was comparatively lower due to adhesion method reducing the porosity of the membrane. Wang et al. [218] fabricated waterproof and breathable electrospun PAN nanofibers modified with waterborne fluorinated polyurethane having an air permeability of 5.9 $Lm^{-2}s^{-1}$ suitable for protective clothing.

6.5 Filtration performance of nanofibrous nanocomposites

The filtration performance of the nanofibrous nanocomposites was evaluated by environment particle air monitor test. The capture of PM2.5 was performed in environmental conditions (the machine containing the filter samples was kept at busy roadside to capture the PM2.5 for 6 hours). To evaluate the filtration efficiency of the nanofibrous nanocomposites, PAN nanofibers were used as a control. The addition of Mt to PAN has an appreciable effect on the filtration performance of PAN/Mt nanofibrous nanocomposites. The addition of Mt enhanced the filtration efficiency of nanofibrous nanocomposites in comparison to PAN nanofibrous membranes. As the concentration of Mt increased from 0.25% to 0.75% the filtration efficiency and particle concentration increased significantly to 98.7% and 62.93 mgm^{-3} respectively. It was observed that the particle concentration increases from 31.67 mgm^{-3} in PAN nanofibers to 62.93 mgm^{-3} in 0.75% PAN/Mt nanofibrous nanocomposite. The improvement observed in filtration efficiency might be due to the decrease in fiber diameter which as a result enhances the porosity of nanofibrous nanocomposites. Further, addition of Mt to the PAN nanofibers increases the surface area and roughness as clearly visible from SEM and HRTEM images. Such enhancement is responsible for better filtration efficiency of nanofibrous nanocomposites. Similar results of increase in filtration efficiency due to smaller and narrower diameter distribution have been shown by Zhu et al. for poly(vinyl alcohol)/poly(acrylic acid) composite membranes doped with silica and silver nanoparticles. The highest concentration of PM2.5 was filtered by 0.75% PAN/Mt nanofibrous nanocomposite. It has also been observed that as the concentration increased from 0.75% to 1.00%, filtration efficiency remarkably decreased to 36.83%. This decrease in behaviour could be due to distorted fibrous

structure of 1.00% PAN/Mt nanofibrous nanocomposite as shown in the FESEM images. Thus, the addition of Mt to PAN nanofibrous membranes upto 0.75% enhances the filtration of particles having size lesser than 2.5 μm. Wang et al. [20] reported that the composite membranes comprising attapulgite nanorods are able to enhance the sieving effect due to the network-like hierarchical structure having larger surface area and a smaller pore size effective in capturing ultrafine particulates compared to PAN nanofibers.

As the concentration of ZnO-Mt (I) in nanofibrous nanocomposites increased from 0.25% to 0.75% the filtration efficiency of the membrane increased and further decreased as the concentration increases to 1.00%. The RSPM test analysis showed that 0.75% PAN/ZnO-Mt (III) nanofibrous nanocomposites adsorbed the highest amount of PM2.5 while PAN nanofibers were comparatively less efficient in filtering PM2.5. This suggests that the addition of ZnO-Mt enhances PM2.5 capture over the nanofibrous membranes. The filtration efficiency of the nanofibrous membranes increased from 56.5% to 99.6% as concentration increased from 0.25% to 0.75% whereas a rapid decrease to 26.5% was observed in case of 1.00% PAN/ZnO-Mt (I) (Table 6.2). The particle concentration of PM2.5 increases from 31.67 mgm^{-3} in PAN nanofibers to 79.58 mgm^{-3} in 0.75% PAN/ZnO-Mt (I) nanofibrous nanocomposite. Further a decrease in particle concentration to 50.43 mgm^{-3} was observed for 1.00% PAN/ZnO-Mt (I) nanofibrous nanocomposite. This trend in filtration efficiency of the nanofibrous membranes is due to the increasing amount of ZnO-Mt (I) which decreases the diameter of the nanofibers which is further responsible for an efficient capture of PM2.5. As the surface roughness of the fiber increases, it provides larger number of sites for adsorption of PM2.5, thereby increasing the filtration efficiency which is evident from

the RSPM test of the nanofibrous membranes. The addition of nanofibers accounts for the interception due to diffusion mechanism for filtration of particles with size upto 100 nm and an increase in filtration occurs as the fiber size decreases. The interception mechanism considers the flow of particle along the gas streamline adhering to the surface of the fiber when the distance between the surface of the fiber and the particle is lower than the radius of the considered spherical particle. The diffusion as well as interception mechanism was effective for the diffusion of particles upto 150 nm for the nanofibrous membranes with higher porosity whereas interception favoured for particles having size above 150 nm [218]. From the above studies it was found that 0.75% PAN/ZnO-Mt (III) nanofibrous nanocomposites had the highest filtration efficiency.

Table 6.2 Filtration efficiency of nanofibrous nanocomposites

S.No.	Nanofibrous nanocomposites	Filtration efficiency (%)	Particle concentration (mgm^{-3})
1	PAN		31.67
2	0.25% PAN/Mt	46.5	46.40
3	0.50% PAN/Mt	86.5	59.06
4	0.75% PAN/Mt	98.7	62.93
5	1.00% PAN/Mt	16.3	36.83
6	0.25% PAN/ZnO-Mt (I)	56.5	49.56
7	0.50% PAN/ZnO-Mt (I)	94.6	61.63
8	0.75% PAN/ZnO-Mt (I)	99.6	63.21
9	1.00% PAN/ZnO-Mt (I)	26.5	40.06
10	0.75% PAN/ZnO-Mt (II)	99.8	63.28
11	0.75% PAN/ZnO-Mt (III)	99.9	63.31

The surface morphology of 0.75% PAN/Mt, 0.75% PAN/ZnO-Mt (I), 0.75% PAN/ZnO-Mt (II) and 0.75% PAN/ZnO-Mt (III) nanofibrous nanocomposite before and after the RSPM test was analyzed as it showed the highest particle concentration of PM2.5 (Fig 6.1). The FESEM images show that PM2.5 gets attached to the surface of the nanofibrous nanocomposites as a beaded structure and aggregates were formed when these particles got attached one above the other.
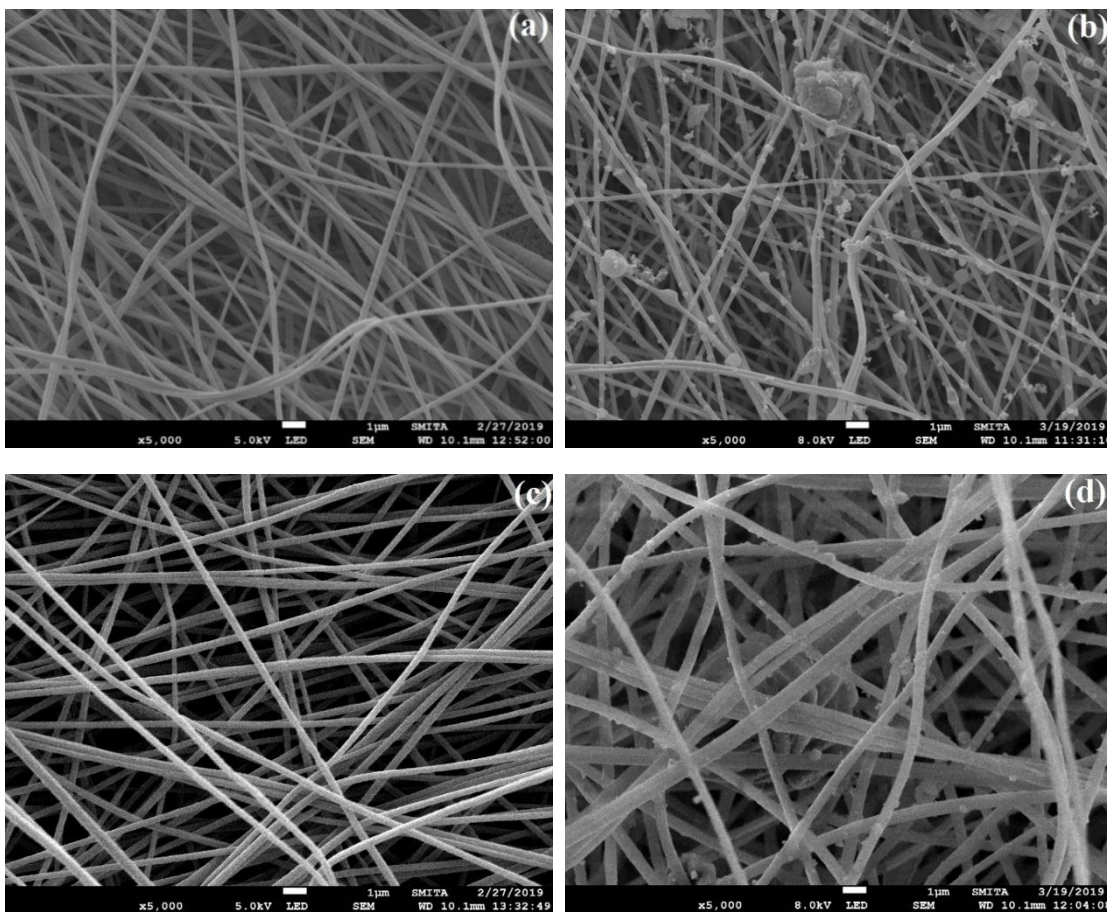
Fig 6.1 FESEM images of (a) 0.75% PAN/Mt before, (b) after, (c) 0.75% PAN/ZnO-Mt (I) before, (d) after RSPM test of nanofibrous nanocomposites

It was found that the particles got attached one above other on the nanofibrous membranes forming agglomeration or bigger sized particles which can also be due to the affinity of these particles to get attached on the surface of these nanofibers. The

attachment of PM particles over nanofibrous nanocomposites suggest that the nanofibrous surface has affinity for these PM2.5 leading to contact area enlargement [26]. The dust particles of PM2.5 accumulated on the nanofibrous membranes via van der Waals interaction [219]. The particles of PM2.5 move and merge as larger particles along the nanofibrous membranes, leaving surface for absorption of more particles the particles attach over one another forming agglomeration of larger sizes [220]. Similar results of agglomeration of PM2.5 wrapped and deposited over nanofibrous network has been observed for PAN/DEAP nanofibers [8]. Jing *et al.* [8] enhanced capture of PM2.5 generated by cigarette burning using electrospun PAN/ionic liquid nanofibers in comparison to PAN nanofibers mainly due to improvement in surface roughness, dipole moment and hydrophilicity of PAN on modification. PAN/PAA nanofibrous membranes with weight ratio 6:4 have been reported with filtration efficiency of 99.994% for sodium chloride aerosol particles (300-500 nm) [18]. The RSPM test for 0.75% sericin/PVA/clay nanofibers having burst strength 10 N/mm^2 filtered 0.725 $mg/m^3/s$ of particulate matter compared to other concentrations [96].

The pressure drop of the nanofibrous nanocomposites decreased as the concentration of Mt increased in PAN/Mt nanofibrous nanocomposites (Fig 6.2 (a)). The pressure drop of 0.75% PAN/Mt was found to be 46.8 Pa which was lowest amongst these developed nanofibrous nanocomposites. The lowered pressure drop might be due to the mitigation in stacked layers of nanofibrous membranes by addition of Mt as its dispersion between the polymeric layers enhanced the interlayer spacing further broadening the passage of air flow [20]. The pressure drop decreased from 96.5 Pa to 46.8 Pa as the concentration of Mt increased from 0% to 0.75% in PAN/Mt nanofibrous nanocomposites. This decrease in pressure drop might be due to a decrease in fiber diameter as nanofibrous

membrane developed due to smaller fibers has a higher porosity allowing easy passage of air molecules [26].

As the concentration of ZnO-Mt (I) in nanofibrous nanocomposites increased from 0.25% to 0.75% the pressure drop of the membrane decreased from 71.62 Pa to 41.18 Pa and further increased to 100.56 Pa as the concentration increases to 1.00%. As the surface roughness of the fiber increases, it provides larger number of sites for adsorption of PM2.5, thereby increasing the filtration efficiency and decreasing its pressure drop (Fig 6.2 (b)).
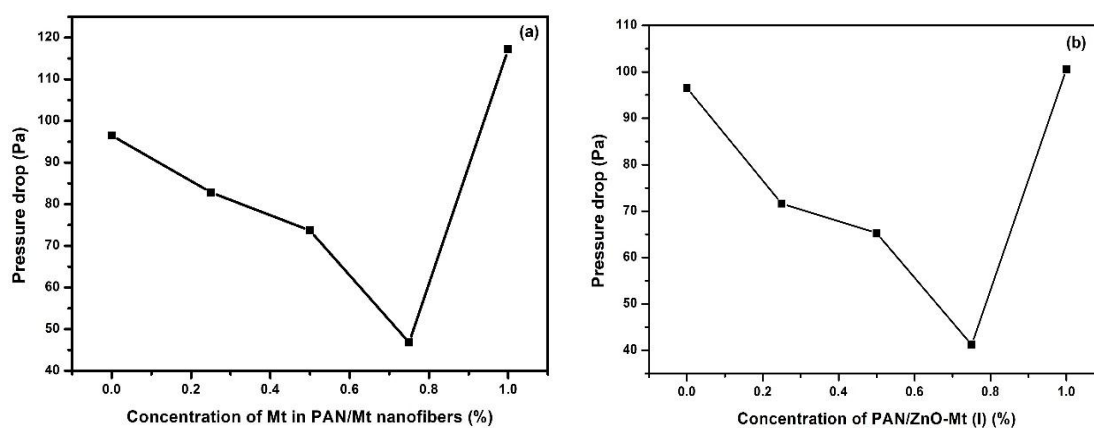
Fig 6.2 Pressure drop versus concentration of (a) PAN/Mt and (b) PAN/ZnO-Mt (I) nanofibrous nanocomposites

The pressure drop of PAN/ZnO-Mt (II) and PAN/ZnO-Mt (III) nanofibrous nanocomposites was found to be 38.41 Pa and 26.72 Pa respectively. The increase in surface roughness of the nanofibrous nanocomposites with increase in concentration results in an increase in filtration efficiency of the nanofibrous nanocomposites with a lower pressure drop and higher quality factor [206]. The smaller size of the nanofibrous membranes helps in collision of aerosol particles with the surface of the nanofibrous membrane which results in deposition of the particles over the surface of the nanofibrous membrane and in turn increasing the filtration efficiency [221]. The filtration efficiency

increases from 41.6% for PAN nanofibers to 99.9% for 0.75% PAN/ZnO-Mt nanofibrous nanocomposites. The increase in concentration to 1.00% decreases the filtration efficiency to 21.5%. A saturation point is achieved and higher concentration does not enhance the filtration performance [222]. According to the "slip effect" theory, the smaller diameter fibers results in lower pressure drop across the filter media as the airflow bypasses the fiber causing lower airflow resistance [223]. Higher filtration efficiency is achieved for the thinner fibers. As the fiber diameter decreases to mean free path of molecules of the air, the air moves over the fibrous membrane and reduces the pressure drop of the fiber [224]. On the basis of pressure drop and filtration efficiency, 0.75% PAN/ZnO-Mt nanofibrous nanocomposites were found to be suitable to be used as a filter membrane.

6.6 Antibacterial activity of nanofibrous nanocomposites

The antibacterial activity of the PAN/ZnO-Mt nanofibrous nanocomposites was studied against Gram-positive *S. aureus* and Gram-negative *E. coli* bacterial strains (Fig 6.3). The zone of inhibition was absent around the nanofibrous mats and no growth of bacteria was observed beneath PAN/ZnO-Mt nanofibrous nanocomposites suggesting antibacterial activity in the nanofibrous mats having non-leaching or barrier mechanism (i.e., negligible migration of ZnO-Mt from the nanofibrous nanocomposites). 0.75% PAN/ZnO-Mt (III) nanofibrous nanocomposites showed excellent antibacterial activity of 99.58% and 99.71% against *E. coli* and *S. aureus* respectively (Table 6.3).
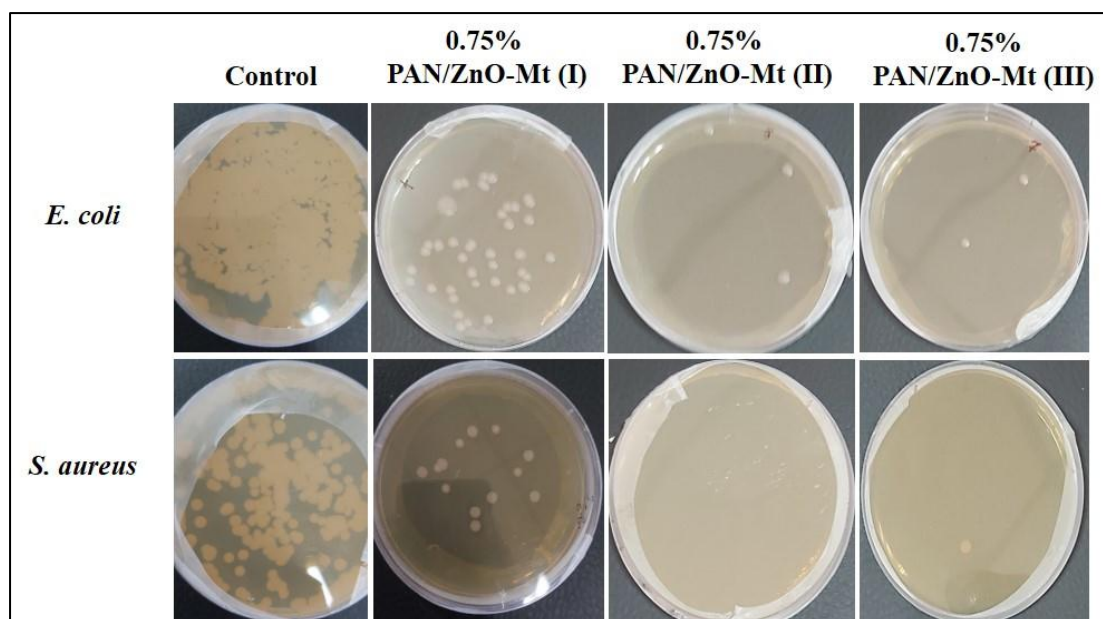
Fig 6.3 Antibacterial activity of PAN/ZnO-Mt nanofibrous nanocomposites

ZnO has been used at micro and nanoscale as an antibacterial agent. When the size of the particle reduces to nanoscale, it comes in interaction with the surface and/or core of the bacteria, entering the cell and exhibits significant bactericidal activity [225]. The antibacterial activity of ZnO nanoparticles depends on several factors such as size of the particle, concentration of solution, morphology, surface modification and defects [226, 227]. Various mechanisms have been reported for the antibacterial activity of ZnO nanoparticles namely, destruction of bacterial cell integrity when ZnO nanoparticles comes in direct contact with the bacterial cell wall, release of antimicrobial Zn^{2+} ions and formation of reactive oxygen species [228, 229].

Table 6.3 Antibacterial activity of nanofibrous nanocomposites

S.No.	PAN/ZnO-Mt nanofibrous nanocomposites	*Escherichia coli*		*Staphylococcus aureus*	
		CFU/mL x 10^5	Antibacterial activity (%)	CFU/mL x 10^5	Antibacterial activity (%)
1	Control	504.00±5.3	-	438.00±7.9	-
2	0.25% PAN/ZnO-Mt (I)	180.38±2.9	64.21±3.6	67.23±3.8	84.65±2.8

3	0.50% PAN/ZnO-Mt (I)	138.30±3.1	72.56±2.1	45.55±4.6	89.60±1.5
4	0.75% PAN/ZnO-Mt (I)	41.00±3.6	91.86±0.7	14.00±2.6	96.80±0.6
5	1.00% PAN/ZnO-Mt (I)	46.82±2.7	90.71±0.8	35.61±2.5	91.87±0.9
6	0.75% PAN/ZnO-Mt (II)	4.25±1.2	99.15±1.2	12.43±2.1	97.16±1.4
7	0.75% PAN/ZnO-Mt (III)	2.13±1.4	99.58±1.5	1.25±1.1	99.71±1.1

The clay modified with ZnO can easily penetrate inside the bacterial cell wall due to its small size, destructing the cell integrity. When ZnO-Mt is incorporated in the polyacrylonitrile nanofibrous mat, stacked structure of the clay further breakdowns providing more surface to ZnO to interact with bacterial cell wall. In this case ZnO has not leached out/released in the agar medium from polymeric matrix, the bacterial cell which comes in contact of the fibrous matrix gets killed. The non-leaching phenomenon of ZnO nanoparticle from the nanofibrous surface may be due to formation of weak complex acrylonitrile with Zn cation or $CH_2CH(CN)^-$-----Zn. It was observed that ZnO nanoparticles incorporated alginate/polyvinyl alcohol nanofibrous nanocomposite diffuse out from the matrix and show zone of inhibition. It was also mentioned that the release of higher concentration of zinc oxide (2%) highly toxic to the cells. However, the bacterial cells when comes in contact with the surface of the fibrous matrix, their growth gets inhibited [230].

6.7 Conclusions

Electrospun PAN/Mt and PAN/ZnO-Mt nanofibrous nanocomposites have been utilized in effective filtration of ultrafine PM2.5 particles. These nanofibrous nanocomposites had a filtration efficiency of 99.9% compared to PAN nanofibers for PM2.5 particles on exposure to environmental conditions for 6 hours. The pressure drop of the PAN/Mt nanofibrous membranes decreased from 96.5 Pa to 46.8 Pa on addition

of Mt to PAN nanofibers. The addition of Mt to PAN nanofibers introduced roughness on the surface of the nanofibrous nanocomposites which provided larger surface are for capturing PM2.5. A lower pressure drop makes this nanofibrous membrane suitable to be utilized as filter. 0.75% PAN/Mt had the highest water vapor transmission rate of 5.41 $kgm^{-2}day^{-1}$ and an air permeability of 19.8 $Lm^{-2}s^{-1}$. The efficient capturing of PM2.5 using 0.75% PAN/Mt nanofibrous nanocomposite makes it a promising material to be developed as a breathable filtration media.

The addition of ZnO-Mt into PAN nanofibrous membranes increased its ability to capture PM2.5 from the atmosphere. PAN/ZnO-Mt nanofibrous nanocomposites were found to be effective against Gram-positive and Gram-negative bacterial strains. The antimicrobial efficiency increased with an increase in concentration of ZnO-Mt. 0.75% PAN/ZnO-Mt nanofibrous nanocomposite was found to have 99.58% and 99.71% antibacterial activity against *E. coli* and *S. aureus* bacterial strains. Thus, 0.75% PAN/ZnO-Mt nanofibrous nanocomposites can be a promising filter membrane for PM2.5 and microorganisms. Thereupon the nanofibrous nanocomposites serves as a bifunctional membrane which can simultaneously capture PM2.5 and inhibit the growth of microorganisms and can also provide future approach for its development to be an effective antimicrobial air filter.

CHAPTER 7

DECONTAMINATION OF CHROMIUM (VI) IONS USING NANOFIBROUS NANOCOMPOSITES

7.1 Overview

One of the major challenges currently is the availability of clean drinking water. The non-biodegradable toxic metal ions like chromium (Cr) released from industries mainly in its hexavalent state are injurious to human health and aquatic environment when their tolerance limit exceeds in water bodies. Cr (VI) is amongst one of the highly toxic metal ions due to its carcinogenicity, mutagenicity, tetragenicity in living organisms and is hundred times more toxic than its trivalent state.

This chapter discusses the adsorption behaviour of PAN/ZnO-Mt (I) and PAN/Mt nanofibrous nanocomposites for Cr (VI) ion in comparison to ZnO-Mt (I) and Mt. The properties of 0.75% PAN/ZnO-Mt (I), 0,75% PAN/ZnO-Mt (II) and 0.75% PAN/ZnO-Mt (III) nanofibrous nanocomposites were found to be quite comparable, so for adsorption of Cr (VI) ions 0.75% PAN/ZnO-Mt (I) nanofibrous nanocomposites have been used. The effect of pH, concentration, amount of adsorbent and contact time on adsorption of Cr (VI) ions using Mt, ZnO-Mt, PAN/Mt and PAN/ZnO-Mt nanofibrous nanocomposites were studied. The adsorption kinetics was studied to determine the rate controlling step of the adsorption of Cr (VI) over adsorbents. To determine the mechanism of adsorption of Cr (VI) ions, adsorption isotherm was also evaluated.

7.2 Effect of pH

The effect of pH on the adsorption of Cr (VI) ions using Mt, ZnO-Mt (I), PAN/Mt nanofibrous nanocomposites and PAN/ZnO-Mt (I) nanofibrous nanocomposites is shown in Fig 7.1.
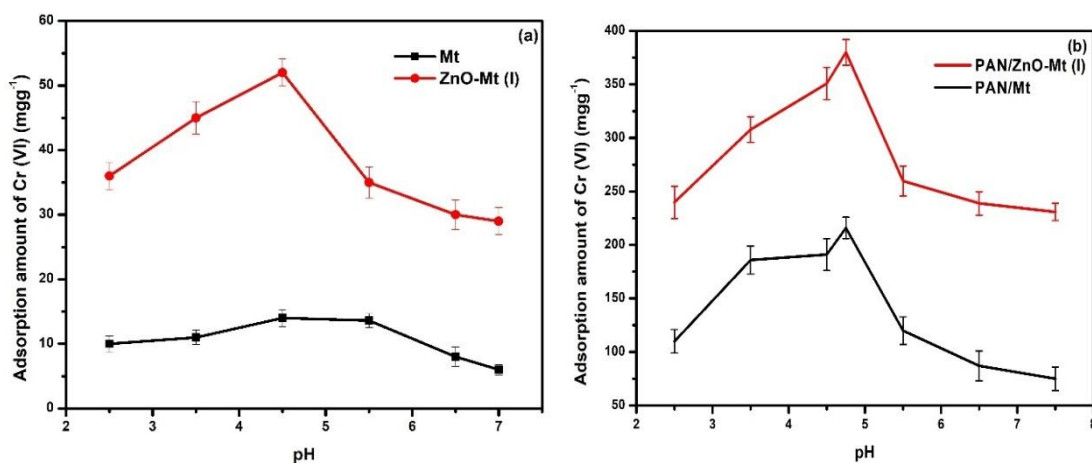
Fig 7.1 Effect of pH on the adsorption of Cr (VI) using (a) Mt and ZnO-Mt (I) and (b) PAN/Mt and PAN/ZnO-Mt (I) nanofibrous nanocomposites

The maximum adsorption of Cr (VI) ions was found to occur at a pH of 4.5 for Mt and ZnO-Mt (I) whereas for nanofibrous nanocomposites it was observed at pH 4.75. The amount of Cr (VI) ions adsorbed using Mt, ZnO-Mt (I), PAN/Mt nanofibrous nanocomposites and PAN/ZnO-Mt (I) nanofibrous nanocomposites was 14.10 mgg^{-1}, 52.61 mgg^{-1}, 216.21 mgg^{-1} and 350.16 mgg^{-1} respectively. The adsorption of Cr (VI) ions increased initially with an increase in pH and after attaining an optimum value adsorption decreased with increasing pH. The acidity of the solution is one of the important factors governing the adsorption of Cr (VI) ions. The point of zero charge of Mt, ZnO-Mt (I), PAN/Mt nanofibrous nanocomposite and PAN/ZnO-Mt (I) nanofibrous nanocomposite was found to be 5.9, 6.7, 6.4 and 7.2 respectively. The point of zero charge of PAN/ZnO fibers have been reported to be 6.4 [231]. According to the point of zero charge, the surface of the adsorbents will be positively charged below pH 5.9 for Mt, pH 6.7 for ZnO-Mt (I), pH 6.4 for PAN/Mt and pH 7.2 for PAN/ZnO-Mt (I) nanofibrous nanocomposites and negatively charged above this pH. The adsorption of Cr (VI) ions will be higher at pH below point of zero charge as the anionic form of Cr (VI) ion will bind with the positively charged surface of the adsorbent in acidic media.

The difference in the adsorption of Cr (VI) ions at different pH is attributed to the ability of the adsorbent to bind with the various Cr (VI) ion species (H_2CrO_4, $Cr_2O_7^{2-}$, CrO_4^{2-} and $HCrO_4^{4-}$) present in the solution at different pH values [221].

7.3 Adsorption kinetics

The metal ion adsorption of PAN/ZnO-Mt (I) nanofibrous nanocomposites, PAN/Mt nanofibrous nanocomposites, ZnO-Mt (I) and Mt were studied for hexavalent, Cr (VI) ions which is known to be the most toxic form and is reported as carcinogenic and mutagenic to living organisms. Mt can adsorb metal ions via two different ways (i) through cation exchange at the interlayers resulting from interactions between ions and negative permanent charge, and (ii) through the formation complexes with Si-O and Al-O groups at the clay particle edge. Both the mechanisms are pH dependent [40]. In case of ZnO nanoparticles, the surface area of the particle is responsible for adsorption of metal ions and forms metal ion/ZnO hybrid which is dependent on the pH of the solution. The predicted mechanism of Cr (VI) adsorption on ZnO or clay in the acidic pH (pH=4.75) is associated with electrostatic attraction between the surface hydroxyl groups of metal oxides ($ZnOH^{2+}$) or protonated silanol and aluminol groups on edge of clay and CrO_4^{2-} or $Cr_2O_7^{2-}$. Therefore, the present adsorption study was carried out at pH 4.75 for Cr (VI) ion. In case of nanofibrous nanocomposites, both Mt and ZnO-Mt get exfoliated during electrospinning, providing greater surface area for removal of Cr (VI) ions.

A rapid and stable kinetics of adsorption is necessary for an adsorbent to determine its efficiency in removal of heavy metal ions from aqueous solutions. The adsorption of Cr (VI) ion with respect to time of contact with adsorbent shows that as the time of contact

90

increases adsorption of metal ions initially increases rapidly upto 60 minutes, further a slower increase in adsorption of the metal ion is observed (Fig 7.2).
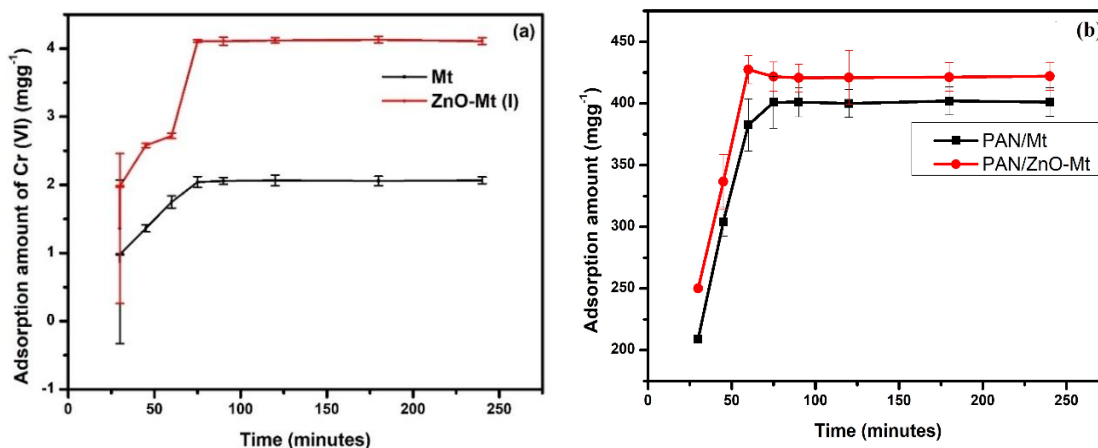
Fig 7.2 Effect of contact time on removal of Cr (VI) (Experimental conditions: Concentration of Cr (VI): 100 ppm, amount of Mt and ZnO-Mt (I) 60 mg in Cr (VI), amount of PAN/Mt and PAN/ZnO-Mt (I): 3 mg)

Addition of ZnO to Mt enhanced the adsorption of Cr (VI) ions by two times. However, for PAN/Mt and PAN/ZnO-Mt (I) nanofibrous nanocomposites the amount of Cr (VI) adsorbed was found to be 401 mgg^{-1} and 421 mgg^{-1} respectively in comparison to 2.06 mgg^{-1} for Mt and 4.11 mgg^{-1} for ZnO-Mt, suggesting an enhanced adsorption for Cr (VI) ions in case of nanofibrous nanocomposites. This difference in behavior may be attributed to higher specific surface area and porosity of nanofibrous nanocomposites as compared to ZnO-Mt and Mt, providing greater number of active sites for adsorption and possibly partial access to inter and intra fibrous network resulting in better adsorption of metal ions while as time increases the diffusion rate is reduced. The addition of Mt and ZnO-Mt to nanofibrous nanocomposites has substantially improved the adsorption of Cr (VI) ions over the adsorbents. The BET surface area of the adsorbents was found to increase in the order: Mt (6.910 m^{2}g^{-1}) < ZnO-Mt (I) (11.165 m^{2}g^{-1}) < PAN/Mt (23.665 m^{2}g^{-1}) < PAN/ZnO-Mt (I) (46.567 m^{2}g^{-1}) which was also one

91

of the major factors governing the adsorption. Amongst the various adsorbents studied, PAN/ZnO-Mt (I) nanofibrous nanocomposites with highest specific surface area imparted the highest adsorption (421 mgg^{-1}) for Cr (VI) ions.

One of the important factors to determine the applicability of adsorption process is to predict the rate of adsorption. To examine the reaction kinetics, pseudo-first-order and pseudo-second-order models were studied. Various factors such as the morphology and type of adsorbent, physicochemical properties of adsorbent and adsorbate, affect the reaction kinetics and the process performance.

Pseudo-first-order and pseudo-second-order kinetic models are represented using equation 7.1 and 7.2 respectively,

$$\frac{dq_t}{dt} = k_1(q_e - q_t) \tag{7.1}$$

$$\frac{dq_t}{dt} = k_2(q_e - q_t)^2 \tag{7.2}$$

The linear form of the pseudo-first-order and pseudo-second-order reaction kinetic models can be represented, using equation 7.3 and 7.4 respectively.

$$\ln(q_e - q_t) = \ln q_e - k_1 t \tag{7.3}$$

$$\frac{t}{q_t} = \frac{1}{k_2 q_e^2} + \frac{t}{q_e} \tag{7.4}$$

where t, q_e, q_t, k_1 and k_2 are time, amount of Cr (VI) ion adsorbed at equilibrium (mgg^{-1}) and time t (min), rate constant of first-order (min^{-1}) and second-order (lmin^{-1}) respectively.

From the linear plot of ln (q_e-q_t) versus t (Fig 7.3 (a) and (b)), the value of rate constant, k_1 was found to be 0.0401 min^{-1}, 0.0138 min^{-1}, 0. 0757 min^{-1} and 0.1071 min^{-1} for Cr

(VI) for Mt, ZnO-Mt (I), PAN/Mt and PAN/ZnO-Mt (I) nanofibrous nanocomposites respectively.
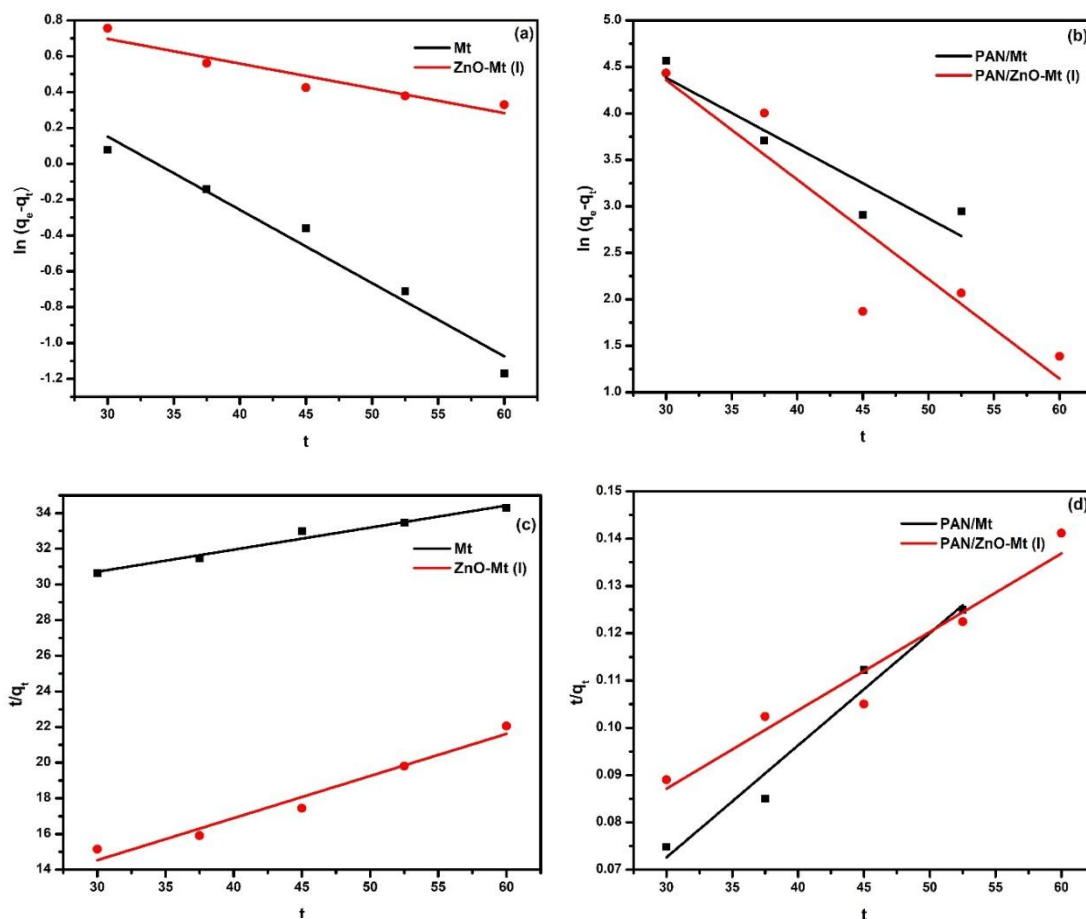
Fig 7.3 Pseudo-first-order kinetic plot (a) Mt and ZnO-Mt (I), (b) PAN/Mt and PAN/ZnO-Mt (I) nanofibrous nanocomposite, Pseudo-second-order kinetic plot of (c) Mt and ZnO-Mt and (d) PAN/Mt and PAN/ZnO-Mt nanofibrous nanocomposite

The value of second-order rate constant k_2 was calculated from the linear plot of t/q_t versus t (Fig 7.3 (c) and (d)) and was found out to be 5.67×10^{-4} lmin^{-1}, 75.12×10^{-4} lmin^{-1}, 38.40×10^{-4} lmin^{-1} and 0.76×10^{-4} lmin^{-1} for Cr (VI) for Mt, ZnO-Mt (I), PAN/Mt and PAN/ZnO-Mt (I) nanofibrous nanocomposites respectively.

The value of q_e was also calculated from the plots and was found to be in good agreement with the experimental value. The various parameters calculated from the

pseudo-first-order and pseudo-second-order kinetic models have been summarized in
Table 7.1.

Table 7.1 Model parameters of Pseudo-first-order and pseudo-second-order kinetic models for Cr (VI)

		Mt	ZnO-Mt (I)	PAN/Mt nanofibrous nanocomposites	PAN/ZnO-Mt (I) nanofibrous nanocomposites
Pseudo-first-order	q_e(experimental)	2.06	4.11	401	421
Pseudo-first-order	$k_1 \times 10^{-2}$ (min^{-1})	4.01	1.38	7.57	10.71
	q_e (mgg^{-1})	3.97	3.04	777.51	1945.16
	R^2	0.9709	0.9073	0.8766	0.8597
	AARD (%)	31.77	9.4	6.28	16.17
Pseudo-second-order	$k_2 \times 10^{-4}$ (lmin^{-1})	5.67	75.12	38.40	0.76
	q_e (mgg^{-1})	8.08	4.23	416.67	488.23
	R^2	0.9718	0.9650	0.9686	0.9507
	AARD (%)	0.51	2.49	3.43	3.35

The value of R^2 ($R^2 > 95\%$) i.e., the correlation coefficient was used to fit the models to the experimental data. Average absolute relative deviation ($AARD = \frac{1}{n} \Sigma \left(\frac{y_i - y_{fit,i}}{y_i}\right)$, where y_i and $y_{fit, i}$ are left hand side of equations 7.5 and 7.6), an error metric was also used for evaluation of the kinetic model to best fit the experimental data. The higher values of R^2 revealed best fit between experimental data and model. Mt best fitted both pseudo-first-order as well as pseudo-second-order kinetic model but in case of pseudo-first-order kinetic model, value of q_e was not in good agreement with experimental data which was also depicted from higher value of AARD. The experimental data of kinetic study suggest that the adsorption of Cr (VI) ions over adsorbent best fits the pseudo-second-order kinetic model (low AARD and high R^2) which suggests that the rate controlling step is chemically governed or involves chemisorption involving shared or

exchanged electrons between adsorbent and adsorbate. Similar results were obtained in amidoximated polyacrylamide/organobentonite composite for adsorption of copper ions [231]. The adsorption of lead ion on clay/poly(methoxyethyl)acrylamide composite [221] and Cr (VI) ions on aromatic polyamide and s-triazine core silane coupling agent modified ZnO nanocomposite [40] also follow the pseudo second order kinetic model. PAN/ZnO nanofibrous nanocomposites follow the second order kinetic model for Cd (II) and Pb (II) ions [232].

The effect of amount of adsorbent on removal of Cr (VI) ions was studied and it was observed that the increase in the amount of adsorbent increases the adsorption of Cr (VI) ions (Fig 7.4).
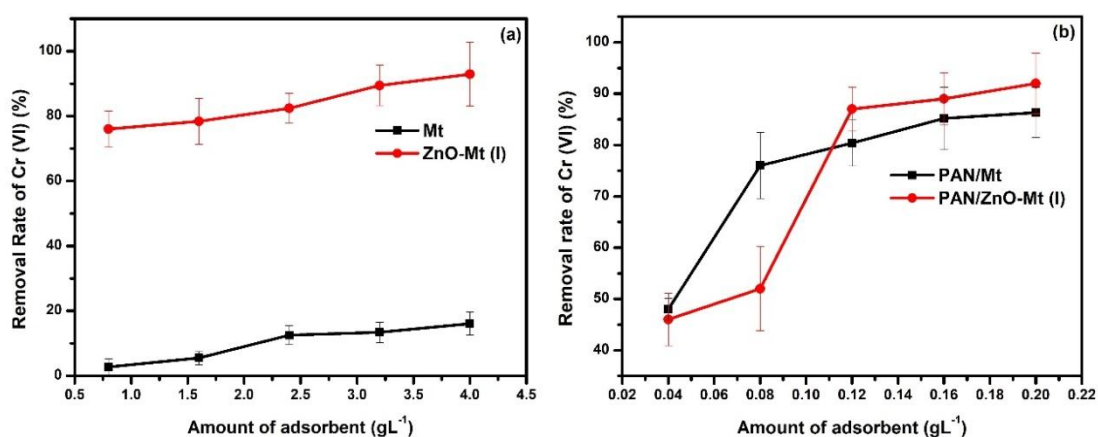
Fig 7.4 Effect of amount of adsorbent on removal of (a and b) Cr (VI) (Experimental conditions: Concentration of Cr (VI): 100 ppm, contact time: 120 min)

The amount of adsorbent affects the removal efficiency of Cr (VI) ion as it determines the number of available active sites. On increasing the amount of adsorbent in same volume of solution greater number of active sites are available for binding to metal ions. The percentage removal of metal ions increases as the surface area of the adsorbent increases on increasing the amount of adsorbent [40]. Initially Cr (VI) ions are adsorbed

over and between the layers of adsorbent resulting in rapid increase of removal of Cr (VI) ions. After attaining an optimum value, the adsorption of Cr (VI) ions increases at a slower rate due to formation of clusters over the surface of adsorbent as more and more of metal ions get adsorbed over the surface of adsorbent which doesn't allow Cr (VI) ions to be adsorbed between the layers of adsorbent.

It is observed that the incorporation of Mt and ZnO-Mt (I) into PAN nanofibers reduces the amount of adsorbent required for removal of metal ions. On incorporation of Mt and ZnO-Mt (I) into nanofibers, the amount of adsorbent required for removal of Cr (VI) ions reduces by 20 times. The optimum dosage of adsorbent required for removal of metal ions is lower in case of ZnO-Mt (I) in comparison to Mt. This is because of ZnO-Mt (I) being smaller in size provides greater number of active sites for binding of metal ions. Cr (VI) adsorbed through electrostatic interaction with clay as well as ZnO. When Mt and ZnO-Mt (I) are incorporated in PAN nanofibers, the surface area of the adsorbent for the metal ion increases and the pore size of the nanofibrous nanocomposites decreases resulting in lower amount of adsorbent required for adsorption of metal ions compared to Mt and ZnO-Mt (I). Haddad and Alharbi [107] found that 123 % increment in the adsorption of Cd (II) ion on PAN/ZnO nanofibrous mat as compared to PAN nanofibrous mat and adsorption equilibrium reached within 60 min. When kaolinite and kaolinite modified with acid were used as an adsorbent for the adsorption of Cr (VI) ions, it has been reported that the adsorption increases with an increase in amount of adsorbent added [59].

The effect of initial concentration of Cr (VI) ions over the adsorbent shows that as the concentration of Cr (VI) ions increases the adsorption amount of metal ion increases

rapidly without attaining any equilibrium (Fig 7.5). It was observed that the adsorption of metal ions was higher in case of PAN/ZnO-Mt (I) nanofibrous nanocomposite and ZnO-Mt (I) as compared with PAN/Mt nanofibrous nanocomposite and Mt respectively. This increase in removal of metal ions using nanofibrous nanocomposites as an adsorbent is observed due to enhancement of surface to volume ratio and surface area of Mt and ZnO-Mt (I) during fabrication of nanofibrous nanocomposites. ZnO was immobilized over Tunisian clay and found a decrease in degradation ratio of dyes with initial concentration of the dye [142]. It has been reported that kaolinite and acid modified kaolinite decreases the extent of adsorption and an increase in amount adsorbed per unit mass as the concentration of metal ions increase [40].
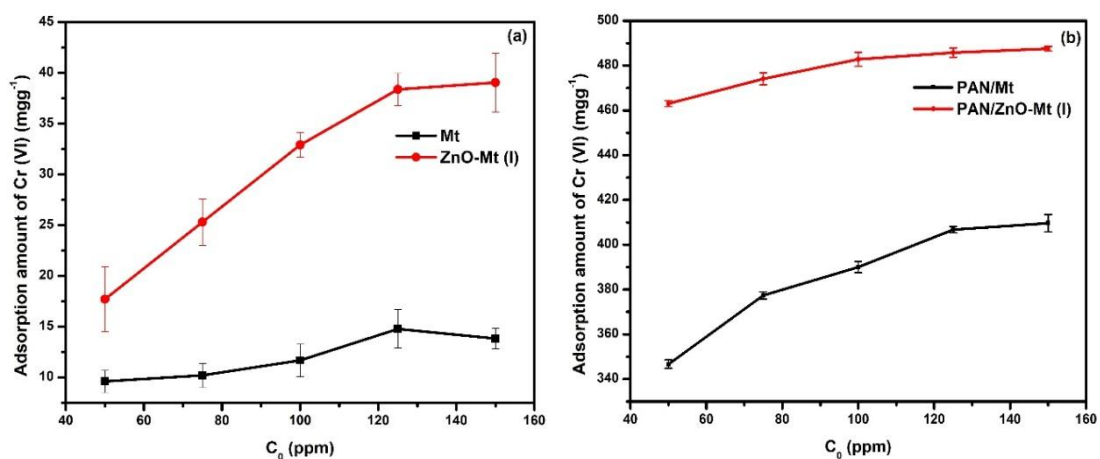
Fig 7.5 Effect of concentration of adsorbent on percent removal of Cr (VI) metal ion (Experimental conditions: Amount of Mt and ZnO-Mt (I) is 60 mg, amount of PAN/Mt and PAN/ZnO-Mt (I) is 3 mg, contact time is 120 min)

7.4 Adsorption isotherms

The equilibrium adsorption isotherms are the promising tools to understand the mechanism of adsorption. The Langmuir and Freundlich isotherms are represented using equation 7.5 and 7.6 respectively.

$$q_e = \frac{bq_mC_e}{1+bC_e} \tag{7.5}$$

$$q_e = k_f C_e^{\frac{1}{n}} \tag{7.6}$$

The linear form of the Langmuir and Freundlich isotherms were analyzed using equations 7.7 and 7.8 respectively.

$$\frac{C_e}{q_e} = \frac{1}{bq_m} + \frac{C_e}{q_m} \tag{7.7}$$

$$\ln q_e = \ln k_f + \frac{1}{n}\ln C_e \tag{7.8}$$

In which C_e and q_e are the adsorbate concentration at equilibrium in mgl^{-1} and equilibrium amount of heavy metal adsorbed in mgg^{-1} respectively, b and q_m are adsorption energy and saturated monolayer sorption capacity respectively related to Langmuir constant, k_f and n are intensity of adsorption and Freundlich constant related to adsorption capacity respectively. Langmuir adsorption depicts the adsorption of gas-solid phase and is used to study the adsorptive efficiency of adsorbents. It describes the surface coverage by the study of dynamic equilibrium between adsorption and desorption. The Langmuir constant related to adsorption capacity is related to surface area and the porosity of adsorbent which suggest that greater surface area and pore size increase adsorption efficiency. Separation factor, R_L was calculated to determine the favorable conditions of adsorption using equation 7.9. The adsorption is said to be favorable when $0< R_L<1$ and unfavorable when $R_L>1$.

$$R_L = \frac{1}{1+bC_0} \tag{7.9}$$

The adsorption process occurring over heterogenous surfaces are described by Freundlich isotherm. For Langmuir isotherm of Cr (VI), a plot of C_e/q_e versus C_e was plotted representing a straight line (Fig 7.6 (a) and (b)z). A plot of $\ln q_e$ and $\ln C_e$ was plotted to study the Freundlich isotherm of Cr (VI). A straight line was obtained in case of Freundlich isotherm (Fig 7.6 (c) and (d)). The values of b, q_m, R_L, n and k_f for Cr (VI) ions have been tabulated (Table 7.2).
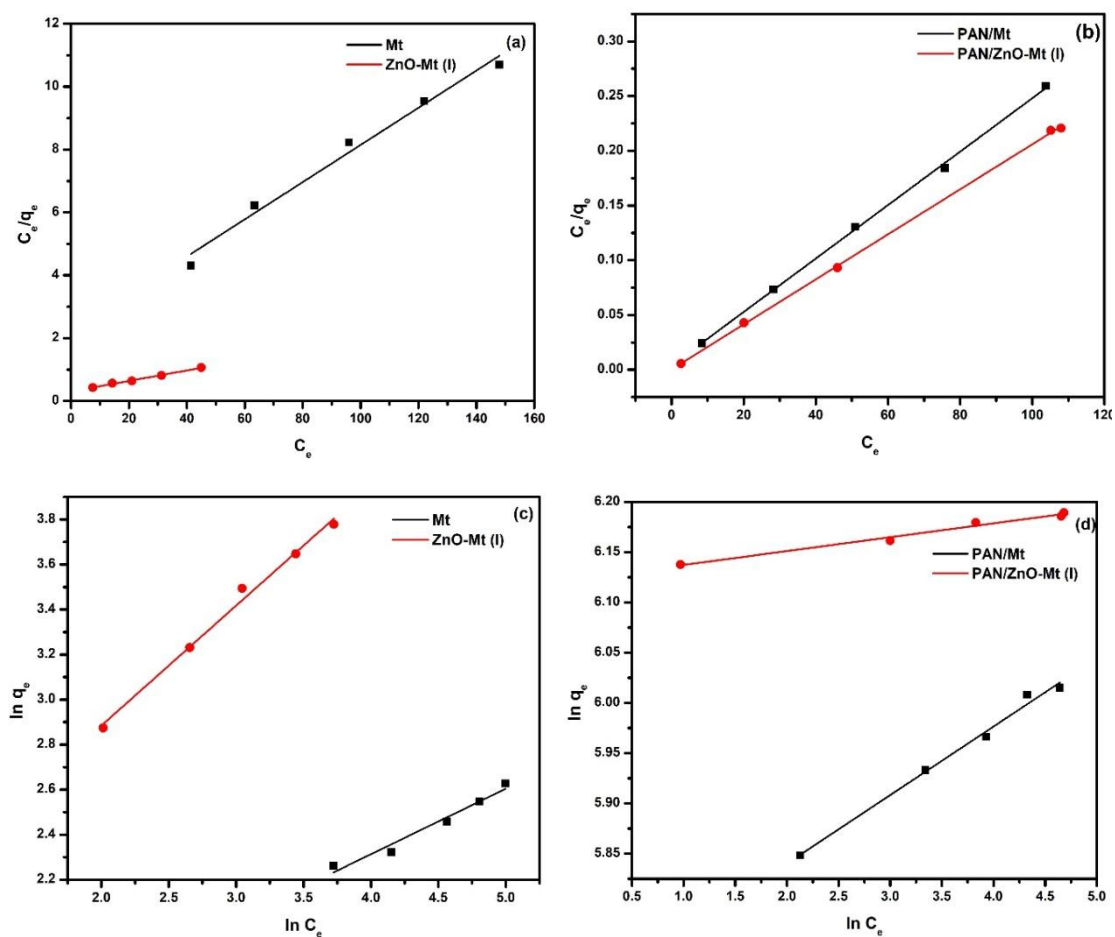
Fig 7.6 (a and b) Langmuir isotherm and (c and d) Freundlich isotherm for adsorption of Cr (VI) ions

Table 7.2 Various parameters of Langmuir and Freundlich isotherm for adsorption of Cr (VI) ions

Isotherm		Mt	ZnO-Mt (I)	PAN/Mt nanofibrous nanocomposites	PAN/ZnO-Mt (I) nanofibrous nanocomposites
Langmuir	q_m (mgg^{-1})	16.89	59.88	416.67	476.19
	B	0.03	0.06	0.60	7.00
	R^2	0.9855	0.9962	0.9991	0.9997
	AARD (%)	4.13	0.53	1.06	0.63
	R_L	0.25	0.14	0.02	0.001
Freundlich	k_f	3.16	6.16	300..01	456.46
	N	3.44	2.87	3.46	4.54
	R^2	0.9671	0.9613	0.9919	0.9847
	AARD (%)	1.15	0.51	0.26	0.21

By linear curve fitting, it was found that the adsorption of Cr (VI) follows Langmuir and Freundlich isotherm. The error metrics (AARD) was used for fitting of experimental data. It was observed that R^2 was higher in case of Langmuir model. The Langmuir model is based on the assumption that none of the interactions are present between adjacent adsorbed species and all the available sites of adsorption are equivalent in energy. The fitting for Langmuir adsorption isotherm suggested homogenous distributed adsorption sites on the surface of the adsorbent [233]. The Freundlich isotherm assumes that adsorption occurs on heterogeneous surface with the stronger binding sites occupied first and that the binding strength decreases with an increasing degree of site occupation [1231]. For the Freundlich model, the value of k_f at equilibrium is 3.16 to 456 for different adsorbent and adsorbate system. The Freundlich constant n is a measure of the deviation from linearity of the adsorption. If the value for n is below unity, it implies that the adsorption process is governed by a chemical

mechanism, but the value for n above unity suggests that the adsorption is a favorable physical process [234]. The value of n at equilibrium are lying between 2.87 to 4.54 suggesting physical mechanism of adsorption. From the linear plots, the R^2 and AARD value was lower in case of Freundlich model as compared to Langmuir model. Lower values of AARD suggest that the adsorbents best fit the Freundlich adsorption isotherm suggesting heterogenous adsorption of Cr (VI) ions on the surface of Mt, ZnO-Mt (I), PAN/Mt and PAN/ZnO-Mt (I) nanofibrous nanocomposites. In Fig 7.7 the possible interaction of Cr (VI) with nanocomposite nanofibers has been described. PAN/ ZnO-Mt (I) nanofibrous nanocomposites were found to be most efficient in adsorption of Cr (VI) ions which is attributed to larger number of surface active sites for metal ion adsorption because of its porous structure and surface polar nature of positively (Zn) and negatively charged (O) ions [142].
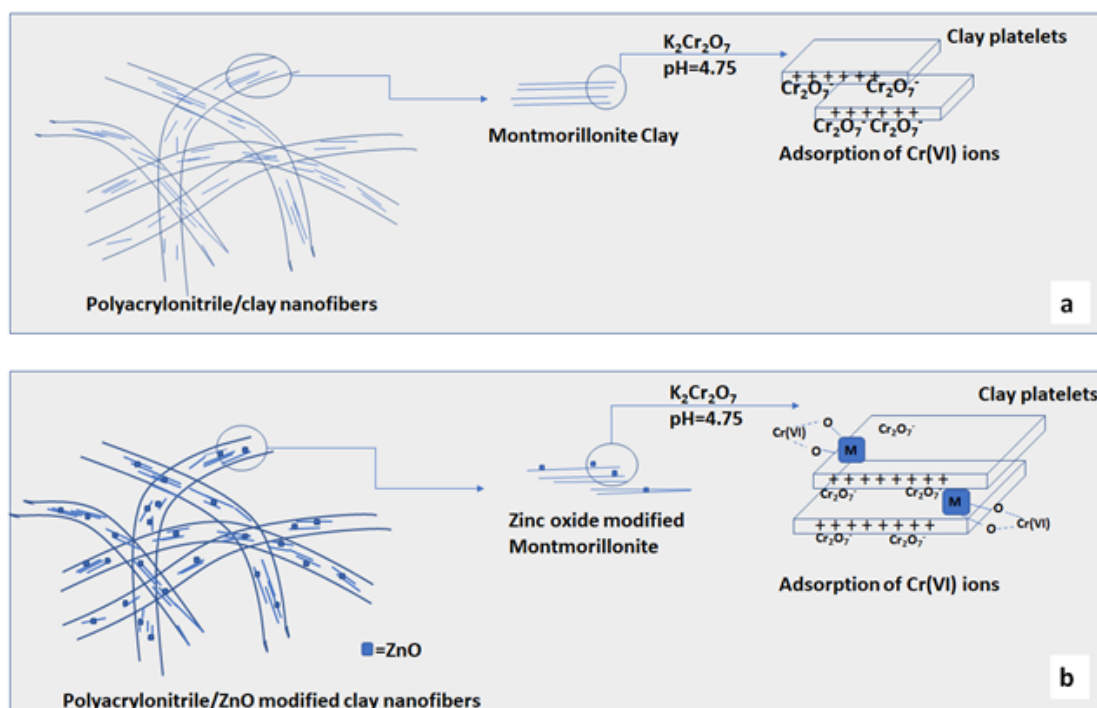
Fig 7.7 Mechanism of adsorption of Cr (VI) ions on (a) PAN/ Mt (b) PAN/ZnO-Mt (I) nanofibrous nanocomposites

The heterogenous adsorption in presence of ZnO-Mt (I) can also be explained by XRD (Fig 4.3). The XRD analysis of ZnO-Mt suggests that the spacing between the layers of Mt decreases on addition of ZnO nanoparticles and ZnO gets inserted between the layers and are also uniformly distributed over the layers of Mt (Fig 4.3). This insertion of ZnO nanoparticles over the surface and between the layers of Mt results in change in size of ZnO-Mt in comparison to ZnO and Mt. Reduction in size of clay after modification with ZnO enhanced the surface area which further helps in improving adsorption efficiency of ZnO-Mt. When Mt is added to PAN nanofibers, Mt gets completely exfoliated as well as on addition of ZnO-Mt to PAN nanofibers, ZnO-Mt gets exfoliated. The porous structure of the nanofibers also supports the heterogenous adsorption of metal ions on nanofibrous nanocomposites. Cr (VI) ion adsorption on kaolinite clay [221] and aromatic polyamide/s-triazine heterocyclic ring modified ZnO nanocomposite [235] follow both Langmuir and Freundlich isotherm. The value of n lies between 2 to 9. Amidoximated polyacrylonitrile/ organobentonite composite [40] show best correlation with Langmuir isotherm for removal of Cu (II) ions. In case of PAN/ZnO nanofibrous nanocomposite show Langmuir isotherm is best fit for adsorption of Cd (II) and Pb (II) ions [40]. The addition of ZnO-Mt to PAN nanofibers enhances its adsorption efficiency for Cr (VI). Various adsorbents and their adsorption capacities for Cr (VI) have been tabulated in Table 7.3.

Table 7.3 Cr (VI) ion adsorption capacity of various adsorbents

Adsorbent material	Amount of adsorbent (gL^{-1})	Initial Cr (VI) concentration (mgL^{-1})	q_m (mg g^{-1})
Chitosan/nylon 6 nanofibers [115]	1.00	30-200	23.90
Tannin/nylon 6 nanofibers [115]	1.00	30-200	62.70
HCl activated Akadama Clay [114]	5.00	112.5	7.47
Acid activated montmorillonite clay [236]	10.00	250	4.51
Cerium oxide nanoparticles [237]	0.32	80	121.95
Mt (This study)	2.40	100	16.89
ZnO-Mt (I) (This study)	2.40	100	59.88
PAN/Mt (This study)	0.12	100	416.67
PAN/ZnO-Mt (I) (This study)	0.12	100	476.19

7.5 Conclusions

The effect of concentration, amount of adsorbent and time on removal of metal ions show that when Mt and ZnO-Mt (I) are incorporated in PAN nanofibers better adsorption of metal ions is observed owing to increase in specific surface area available for adsorption and the uniform distribution of pore size compared to Mt and ZnO-Mt (I). The intercalation of ZnO-Mt over PAN nanofibers resulted in a decrease in amount of adsorbent and contact time for removal of metal ions compared to ZnO-Mt. PAN/Mt nanofibrous nanocomposites are found to be more effective adsorbent for heavy metal ions compared to Mt. The adsorption studies suggest that PAN/Mt nanofibrous nanocomposites and PAN/ZnO-Mt (I) nanofibrous nanocomposites can be used as an adsorbent for removal of Cr (VI) ions from aqueous solutions. The adsorption of Cr (VI) ions over Mt, ZnO-Mt (I), PAN/Mt nanofibrous nanocomposites and PAN/ZnO-Mt (I) nanofibrous nanocomposites follows pseudo-second-order kinetics suggesting

chemisorption between adsorbate and adsorbent. The adsorption isotherm analysis suggested that homogenous and heterogenous adsorption of Cr (VI) ions occur over the adsorbent and thus best fit the Langmuir and Freundlich adsorption isotherm. The addition of Mt and ZnO-Mt (I) to electrospun PAN nanofibers enhances the adsorption of Cr (VI) ions over the adsorbent site.

CHAPTER 8

CONCLUSIONS AND FUTURE PROSPECTS

8.1 Conclusions

Zinc oxide modified montmorillonite has been successfully synthesised using three different precursors, zinc oxide nanoparticles, zinc nitrate and aloe vera gel. The average particle size of montmorillonite reduced from 71 nm to 16 nm on modification to zinc oxide modified montmorillonite. The structural analysis of zinc oxide modified montmorillonite suggested distribution of cuboidal shaped zinc oxide nanoparticles over the surface of flaky shaped montmorillonite. The broadening of peaks in X-ray diffractogram suggested the insertion of zinc oxide nanoparticles within the layers of montmorillonite in zinc oxide modified montmorillonite. These zinc oxide modified montmorillonite were incorporated in polyacrylonitrile nanofibrous membranes using electrospinning. Polyacrylonitrile/ montmorillonite and polyacrylonitrile/ zinc oxide modified montmorillonite nanofibrous nanocomposites have been successfully developed using electrospinning technique. The addition of montmorillonite and zinc oxide modified montmorillonite to polyacrylonitrile introduces surface roughness in polyacrylonitrile/montmorillonite nanofibrous nanocomposites and polyacrylonitrile/ zinc oxide modified montmorillonite nanofibrous nanocomposites in comparison to polyacrylonitrile nanofibrous membranes. The average diameter of the nanofibrous nanocomposites was found to be in the range of 206.7±10.9 nm to 1032.7±25.8 nm. The nanofibrous nanocomposites were found to be much more thermally stable than polyacrylonitrile nanofibrous membranes as the addition of montmorillonite and zinc oxide modified montmorillonite prevents degradation of polyacrylonitrile. The

nanofibrous nanocomposites were analysed for their efficiency in filtration of particulate matter and effectiveness against *S. aureus* and *E. coli* bacterial strains. Nanofibrous nanocomposites had a filtration efficiency of 99.9% compared to polyacrylonitrile nanofibers for PM2.5 particles on exposure to environmental conditions for 6 hours. 0.75% PAN/ZnO-Mt had the highest water vapor transmission rate of 8.77 $kgm^{-2}day^{-1}$ and an air permeability of 27.1 $Lm^{-2}s^{-1}$. 0.75% Polyacrylonitrile/zinc oxide modified montmorillonite nanofibrous nanocomposite was found to have an antibacterial activity of 99.58% and 99.71% against *E. coli* and *S. aureus* bacterial strains respectively. The developed polyacrylonitrile/zinc oxide modified montmorillonite nanofibrous nanocomposites could serve as a bifunctional membrane which can simultaneously capture PM2.5 and inhibit the growth of microorganisms and can also provide future approach for its development to be an effective antimicrobial air filter. Adsorption of Cr (VI) ions over montmorillonite, zinc oxide modified montmorillonite, polyacrylonitrile/montmorillonite nanofibrous nanocomposites and polyacrylonitrile/ zinc oxide modified montmorillonite nanofibrous nanocomposites follows pseudo-second-order kinetics suggesting chemisorption between adsorbate and adsorbent. Adsorption isotherm analysis suggested that homogenous and heterogenous adsorption of Cr (VI) ions occurs over the adsorbent and thus best fit the Langmuir and Freundlich adsorption isotherms. The addition of montmorillonite and zinc oxide modified montmorillonite to electrospun polyacrylonitrile nanofibers enhances the adsorption of Cr (VI) ions over the adsorbent site. Thus, the developed multifunctional nanofibrous nanocomposites could be potential materials in the field of filtration mainly bacteria, PM2.5 from atmosphere and Cr (VI) ions from water sources.

8.2 Future prospects

The potential in this field lies in the development of polyacrylonitrile nanofibers by incorporation of clay, metal oxides and metal oxide modified clay which can further be used in sensors, protective clothing, biomedical, decontamination of metal ions from wastewater and carbon based high performance fibers. It is expected that in the coming era various other applications and potential of polyacrylonitrile based nanofibers will be explored by the scientific community. The future study of nanofibrous membranes should also involve development of cost-effective methods in drainage industrial wastewater treatment.

REFERENCES

1. Apte JS, Marshall JD, Cohen AJ, Brauer M (2015) Addressing Global Mortality from Ambient PM2.5. Environmental Science and Technology 49:8057–8066. https://doi.org/10.1021/acs.est.5b01236

2. Xie M, Hannigan MP, Barsanti KC (2014) Impact of gas/particle partitioning of semivolatile organic compounds on source apportionment with positive matrix factorization. Environmental Science and Technology 48:9053–9060. https://doi.org/10.1021/es5022262

3. Naeher LP, Smith KR, Leaderer BP, et al. (2001) Carbon monoxide as a tracer for assessing exposures to particulate matter in wood and gas cookstove households of highland Guatemala. Environmental Science and Technology 35:575–581. https://doi.org/10.1021/es991225g

4. Mannucci PM, Harari S, Martinelli I, Franchini M (2015) Effects on health of air pollution: a narrative review. Internal and Emergency Medicine 10:657–662. https://doi.org/10.1007/s11739-015-1276-7

5. Brook RD, Rajagopalan S, Pope CA, et al. (2010) Particulate matter air pollution and cardiovascular disease: An update to the scientific statement from the american heart association. Circulation 121:2331–2378. https://doi.org/10.1161/CIR.0b013e3181dbece1

6. Li P, Wang C, Zhang Y, Wei F (2014) Air filtration in the free molecular flow regime: A review of high-efficiency particulate air filters based on Carbon Nanotubes. Small 10:4543–4561. https://doi.org/10.1002/smll.201401553

7. Turner MC, Krewski D, Pope CA, et al. (2011) Long-term ambient fine particulate matter air pollution and lung cancer in a large cohort of never-smokers. American Journal of Respiratory and Critical Care Medicine 184:1374–1381. https://doi.org/10.1164/rccm.201106-1011OC

8.   Jing L, Shim K, Toe CY, et al. (2016) Electrospun Polyacrylonitrile-Ionic Liquid Nanofibers for Superior PM2.5 Capture Capacity. ACS Applied Materials and Interfaces 8:7030–7036. https://doi.org/10.1021/acsami.5b12313

9.   Mohraz MH, Golbabaei F, Yu IJ, et al. (2019) Preparation and optimization of multifunctional electrospun polyurethane/chitosan nanofibers for air pollution control applications. International Journal of Environmental Science and Technology 16:681–694. https://doi.org/10.1007/s13762-018-1649-3

10.   Douwes J, Thorne P, Pearce N, Heederik D (2003) Bioaerosol health effects and exposure assessment: Progress and prospects. Annals of Occupational Hygiene 47:187–200. https://doi.org/10.1093/annhyg/meg032

11.   Desai K, Kit K, Li J, et al. (2009) Nanofibrous chitosan non-wovens for filtration applications. Polymer 50:3661–3669. https://doi.org/10.1016/j.polymer.2009.05.058

12.   Chen L (2009) Next Generation of Electrospun Textiles for Chemical and Biological Protection and Air Filtration

13.   Liu H, Cao C, Huang J, et al. (2020) Progress on particulate matter filtration technology: basic concepts, advanced materials, and performances. 437–453. https://doi.org/10.1039/c9nr08851b

14.   Wang G, Hua Y, Su X, et al. (2016) Cr(VI) adsorption by montmorillonite nanocomposites. Applied Clay Science 124–125:111–118. https://doi.org/10.1016/j.clay.2016.02.008

15.   Bhardwaj N, Kundu SC (2010) Electrospinning: A fascinating fiber fabrication technique. Biotechnology Advances 28:325–347. https://doi.org/10.1016/j.biotechadv.2010.01.004

16.   Zhu M, Han J, Wang F, et al. (2017) Electrospun Nanofibers Membranes for Effective Air Filtration. Macromolecular Materials and Engineering 302:1–27. https://doi.org/10.1002/mame.201600353

17. Zhang S, Liu H, Yin X, et al. (2016) Anti-deformed Polyacrylonitrile/ Polysulfone Composite Membrane with Binary Structures for Effective Air Filtration. ACS Applied Materials and Interfaces 8:8086–8095. https://doi.org/ 10.1021/acsami.6b00359

18. Liu Y, Park M, Ding B, et al. (2015) Facile electrospun Polyacrylonitrile/poly(acrylic acid) nanofibrous membranes for high efficiency particulate air filtration. Fibers and Polymers 16:629–633. https://doi.org/10. 1007/s12221-015-0629-1

19. Cao M, Gu F, Rao C, et al. (2019) Improving the electrospinning process of fabricating nanofibrous membranes to filter PM2.5. Science of the Total Environment 666:1011–1021. https://doi.org/10.1016/j.scitotenv.2019.02.207

20. Wang B, Sun Z, Sun Q, et al. (2019) The preparation of bifunctional electrospun air filtration membranes by introducing attapulgite for the efficient capturing of ultrafine PMs and hazardous heavy metal ions. Environmental Pollution 249:851–859. https://doi.org/10.1016/j.envpol.2019.03.122

21. Wang N, Zhu Z, Sheng J, et al. (2014) Superamphiphobic nanofibrous membranes for effective filtration of fine particles. Journal of Colloid and Interface Science 428:41–48. https://doi.org/10.1016/j.jcis.2014.04.026

22. Wang N, Yang Y, Al-Deyab SS, et al. (2015) Ultra-light 3D nanofibre-nets binary structured nylon 6-polyacrylonitrile membranes for efficient filtration of fine particulate matter. Journal of Materials Chemistry A 3:23946–23954. https://doi.org/10.1039/c5ta06543g

23. Matulevicius J, Kliucininkas L, Martuzevicius D, et al. (2014) Design and characterization of electrospun polyamide nanofiber media for air filtration applications. Journal of Nanomaterials 2014:. https://doi.org/10.1155/2014/859656

24. Yan S, Yu Y, Ma R, Fang J (2019) The formation of ultrafine polyamide 6 nanofiber membranes with needleless electrospinning for air filtration. Polymers for Advanced Technologies 30:1635–1643. https://doi.org/10.1002/pat.4594

25. Lee S, Cho AR, Park D, et al. (2019) Reusable Polybenzimidazole Nanofiber Membrane Filter for Highly Breathable PM 2.5 Dust Proof Mask. ACS Applied Materials and Interfaces 11:2750–2757. https://doi.org/10.1021/acsami.8b19741

26. Zhang Q, Li Q, Young TM, et al. (2019) A Novel Method for Fabricating an Electrospun Poly(Vinyl Alcohol)/Cellulose Nanocrystals Composite Nanofibrous Filter with Low Air Resistance for High-Efficiency Filtration of Particulate Matter. ACS Sustainable Chemistry and Engineering 7:8706–8714. https://doi.org/10.1021/acssuschemeng.9b00605

27. Hao Z, Wu J, Wang C, Liu J (2019) Electrospun Polyimide/Metal-Organic Framework Nanofibrous Membrane with Superior Thermal Stability for Efficient PM 2.5 Capture. ACS Applied Materials and Interfaces 11:11904–11909. https://doi.org/10.1021/acsami.8b22415

28. Ma S, Zhang M, Nie J, et al. (2019) Design of double-component metal–organic framework air filters with PM2.5 capture, gas adsorption and antibacterial capacities. Carbohydrate Polymers 203:415–422. https://doi.org/10.1016/j.carbpol.2018.09.039

29. Hashmi M, Ullah S, Kim IS (2019) Copper oxide (CuO) loaded polyacrylonitrile (PAN) nanofiber membranes for antimicrobial breath mask applications. Current Research in Biotechnology 1:1–10. https://doi.org/10.1016/j.crbiot.2019.07.001

30. Upadhyay RK, Soin N, Roy SS (2013) Role of graphene/metal oxide composites as photocatalysts, adsorbents and disinfectants in water treatment: a review. RSC Advances 4:3823–3851. https://doi.org/10.1039/C3RA45013A

31. Ngwenya N, Ncube EJ, Parsons J (2013) Recent Advances in Drinking Water Disinfection: Successes and Challenges. Rev Environ Contam Toxicol 222:111–170. https://doi.org/10.1007/978-1-4614-4717-7_4

32. Ahmad M, Zhang B, Wang J, et al. (2019) New method for hydrogel synthesis from diphenylcarbazide chitosan for selective copper removal. International Journal of Biological Macromolecules 136:189–198. https://doi.org/10.1016/j.ijbiomac.2019.06.084

33. Yi J, Li Y, Yang L, Zhang LM (2019) Kinetics and thermodynamics of adsorption of Cu^{2+} and methylene blue to casein hydrogels. Journal of Polymer Research 26: 1-14. https://doi.org/10.1007/s10965-019-1870-x

34. Li L, Wang Z, Ma P, et al. (2015) Preparation of polyvinyl alcohol/chitosan hydrogel compounded with graphene oxide to enhance the adsorption properties for Cu(II) in aqueous solution. Journal of Polymer Research 22:1–10. https://doi.org/10.1007/s10965-015-0794-3

35. Li T, Liu X, Li L, et al. (2019) Polydopamine-functionalized graphene oxide compounded with polyvinyl alcohol/chitosan hydrogels on the recyclable adsorption of Cu(II), Pb(II) and cd(II) from aqueous solution. Journal of Polymer Research 26: 1-12. https://doi.org/10.1007/s10965-019-1971-6

36. Manzoor K, Ahmad M, Ahmad S, Ikram S (2019) Removal of Pb(II) and Cd(II) from wastewater using arginine cross-linked chitosan-carboxymethyl cellulose beads as green adsorbent. RSC Advances 9:7890–7902. https://doi.org/10.1039/C9RA00356H

37. Manzoor K, Ahmad M, Ahmad S, Ikram S (2019) Synthesis, Characterization, Kinetics, and Thermodynamics of EDTA-Modified Chitosan-Carboxymethyl Cellulose as Cu(II) Ion Adsorbent. ACS Omega 4:17425–17437. https://doi.org/10.1021/acsomega.9b02214

38. Cheng R, Ou S, Xiang B, et al. (2009) Adsorption behavior of hexavalent chromium on synthesized ethylenediamine modified starch. Journal of Polymer Research 16:703–708. https://doi.org/10.1007/s10965-009-9276-9

39. Li P, Dai X, Yan Q, et al. (2020) A novel modification method for polystyrene microspheres with dithizone and the adsorption properties for Pb^{2+}. Journal of Polymer Research 27:1-10. https://doi.org/10.1007/s10965-020-02180-8

40. Haddad MY, Alharbi HF (2019) Enhancement of heavy metal ion adsorption using electrospun polyacrylonitrile nanofibers loaded with ZnO nanoparticles. Journal of Applied Polymer Science 136:1-11. https://doi.org/10.1002/app.47209

41.   Cai J, Lei M, Zhang Q, et al. (2017) Composites: Part A Electrospun composite nanofiber mats of Cellulose @ Organically modified montmorillonite for heavy metal ion removal: Design, characterization, evaluation of absorption performance. Composites Part A 92:10–16. https://doi.org/10.1016/j.compositesa.2016.10.034

42.   Zhu TT, Zhou CH, Kabwe FB, et al. (2019) Exfoliation of montmorillonite and related properties of clay/polymer nanocomposites. Applied Clay Science 169:48–66. https://doi.org/10.1016/j.clay.2018.12.006

43.   Wang Y, Zhao X, Duan L, et al. (2015) Structure, luminescence and photocatalytic activity of Mg-doped ZnO nanoparticles prepared by auto combustion method. Materials Science in Semiconductor Processing 29:372–379. https://doi.org/10.1016/j.mssp.2014.07.034

44.   Deng Z, Chen M, Gu A, Wu L (2008) A facile method to fabricate ZnO hollow spheres and their photocatalytic property. Journal of Physical Chemistry B 112:16–22. https://doi.org/10.1021/jp077662w

45.   Rezapour M, Talebian N (2011) Comparison of structural, optical properties and photocatalytic activity of ZnO with different morphologies: Effect of synthesis methods and reaction media. Materials Chemistry and Physics 129:249–255. https://doi.org/10.1016/j.matchemphys.2011.04.012

46.   Akkari M, Aranda P, ben Rhaiem H, et al. (2016) ZnO/clay nanoarchitectures: Synthesis, characterization and evaluation as photocatalysts. Applied Clay Science 131:131–139. https://doi.org/10.1016/j.clay.2015.12.013

47.   Yang SJ, Park CR (2008) Facile preparation of monodisperse ZnO quantum dots with high quality photoluminescence characteristics. Nanotechnology 19:1-4. https://doi.org/10.1088/0957-4484/19/03/035609

48.   Talebian N, Amininezhad SM, Doudi M (2013) Controllable synthesis of ZnO nanoparticles and their morphology-dependent antibacterial and optical properties. Journal of Photochemistry and Photobiology B: Biology 120:66–73. https://doi.org/10.1016/j.jphotobiol.2013.01.004

49. Yamamoto O (2001) Influence of particle size on the antibacterial activity of zinc oxide. International Journal of Inorganic Materials 3:643–646. https://doi.org/10.1016/S1466-6049(01)00197-0

50. Raghupathi KR, Koodali RT, Manna AC (2011) Size-dependent bacterial growth inhibition and mechanism of antibacterial activity of zinc oxide nanoparticles. Langmuir 27:4020–4028. https://doi.org/10.1021/la104825u

51. Zarrindokht Emami-Karvani (2012) Antibacterial activity of ZnO nanoparticle on Gram-positive and Gram-negative bacteria. African Journal of Microbiology Research 5:1368-1373. https://doi.org/10.5897/AJMR10.159

52. Sirelkhatim A, Mahmud S, Seeni A, et al. (2015) Review on zinc oxide nanoparticles: Antibacterial activity and toxicity mechanism. Nano-Micro Letters 7:219–242. https://doi.org/10.1007/s40820-015-0040-x

53. Upadhyaya L, Singh J, Agarwal V, et al. (2014) In situ grafted nanostructured ZnO/carboxymethyl cellulose nanocomposites for efficient delivery of curcumin to cancer. Journal of Polymer Research 21:1-9. https://doi.org/10.1007/s10965-014-0550-0

54. Upadhyaya L, Singh J, Agarwal V, et al. (2015) Efficient water soluble nanostructured ZnO grafted O-carboxymethyl chitosan/curcumin-nanocomposite for cancer therapy. Process Biochemistry 50:678–688. https://doi.org/10.1016/j.procbio.2014.12.029

55. Dimapilis EAS, Hsu C-S, Mendoza RMO, Lu M-C (2018) Zinc oxide nanoparticles for water disinfection. Sustainable Environment Research 28:47–56. https://doi.org/10.1016/J.SERJ.2017.10.001

56. Ong CB, Ng LY, Mohammad AW (2018) A review of ZnO nanoparticles as solar photocatalysts: Synthesis, mechanisms and applications. Renewable and Sustainable Energy Reviews 81:536–551. https://doi.org/10.1016/J.RSER.2017.08.020

57.   Kumar JP, Ramacharyulu PVRK, Prasad GK, Singh B (2015) Montmorillonites supported with metal oxide nanoparticles for decontamination of sulfur mustard. Applied Clay Science 116–117:263–272. https://doi.org/10.1016/j.clay.2015.04.007

58.   Sani HA, Ahmad MB, Hussein MZ, et al. (2017) Nanocomposite of ZnO with montmorillonite for removal of lead and copper ions from aqueous solutions. Process Safety and Environmental Protection 109:97–105. https://doi.org/10.1016/j.psep.2017.03.024

59.   Bel Hadjltaief H, ben Ameur S, da Costa P, et al. (2018) Photocatalytic decolorization of cationic and anionic dyes over ZnO nanoparticle immobilized on natural Tunisian clay. Applied Clay Science 152:148–157. https://doi.org/10.1016/j.clay.2017.11.008

60.   Akkari M, Aranda P, Belver C, et al. (2018) ZnO/sepiolite heterostructured materials for solar photocatalytic degradation of pharmaceuticals in wastewater. Applied Clay Science 156:104–109. https://doi.org/10.1016/j.clay.2018.01.021

61.   Unuabonah EI, Taubert A (2014) Clay–polymer nanocomposites (CPNs): Adsorbents of the future for water treatment. Applied Clay Science 99:83–92. https://doi.org/10.1016/J.CLAY.2014.06.016

62.   Gupta SS, Bhattacharyya KG (2012) Adsorption of heavy metals on kaolinite and montmorillonite: a review. Physical Chemistry Chemical Physics 14:6698. https://doi.org/10.1039/c2cp40093f

63.   Uddin MK (2017) A review on the adsorption of heavy metals by clay minerals, with special focus on the past decade. Chemical Engineering Journal 308:438–462. https://doi.org/10.1016/j.cej.2016.09.029

64.   Nataraj SK, Yang KS, Aminabhavi TM (2012) Polyacrylonitrile-based nanofibers - A state-of-the-art review. Progress in Polymer Science (Oxford) 37:487–513

65.   Zhao X, Li Y, Hua T, et al. (2017) Low-Resistance Dual-Purpose Air Filter Releasing Negative Ions and Effectively Capturing PM2.5. ACS Applied Materials and Interfaces 9:12054-12063. https://doi.org/10.1021/acsami.7b00351

66. Li D, Babel A, Jenekhe SA, Xia Y (2004) Nanofibers of conjugated polymers prepared by electrospinning with a two-capillary spinneret. Advanced Materials 16:2062-2066. https://doi.org/10.1002/adma.200400606

67. Yang C (2012) Aerosol filtration application using fibrous media - An industrial perspective. Chinese Journal of Chemical Engineering 20:1–9. https://doi.org/10.1016/S1004-9541(12)60356-5

68. Ramskill EA, Anderson WL (1951) The inertial mechanism in the mechanical filtration of aerosols. Journal of Colloid Science 6:416-428. https://doi.org/10.1016/0095-8522(51)90013-X

69. Friedlander SK (1958) Theory of Aerosol Filtration. Industrial & Engineering Chemistry 50:1161-1164. https://doi.org/10.1021/ie50584a036

70. Ramarao B v., Tien C, Mohan S (1994) Calculation of single fiber efficiencies for interception and impaction with superposed brownian motion. Journal of Aerosol Science 25:295-313. https://doi.org/10.1016/0021-8502(94)90081-7

71. Wang C sen (2001) Electrostatic forces in fibrous filters - A review. Powder Technology 118:166-170. https://doi.org/10.1016/S0032-5910(01)00307-2

72. Sahay R, Kumar PS, Sridhar R, et al. (2012) Electrospun composite nanofibers and their multifaceted applications. Journal of Materials Chemistry 22:12953-12971. https://doi.org/10.1039/c2jm30966a

73. Balgis R, Kartikowati CW, Ogi T, et al. (2015) Synthesis and evaluation of straight and bead-free nanofibers for improved aerosol filtration. Chemical Engineering Science 137:947–954. https://doi.org/10.1016/j.ces.2015.07.038

74. Yun KM, Suryamas AB, Iskandar F, et al. (2010) Morphology optimization of polymer nanofiber for applications in aerosol particle filtration. Separation and Purification Technology 75:340-345. https://doi.org/10.1016/j.seppur.2010.09.002

75. Li XW, Kong HY, He JH (2015) Study on highly filtration efficiency of electrospun polyvinyl alcohol micro-porous webs. Indian Journal of Physics 89:175-179. https://doi.org/10.1007/s12648-014-0542-2

76. Wang Z, Zhao C, Pan Z (2015) Porous bead-on-string poly(lactic acid) fibrous membranes for air filtration. Journal of Colloid and Interface Science 441:121-129. https://doi.org/10.1016/j.jcis.2014.11.041

77. Hung CH, Leung WWF (2011) Filtration of nano-aerosol using nanofiber filter under low Peclet number and transitional flow regime. Separation and Purification Technology 79:34–42. https://doi.org/10.1016/j.seppur.2011.03.008

78. Leung WWF, Hung CH, Yuen PT (2010) Effect of face velocity, nanofiber packing density and thickness on filtration performance of filters with nanofibers coated on a substrate. Separation and Purification Technology 71:30-37. https://doi.org/10.1016/j.seppur.2009.10.017

79. Zhang S, Shim WS, Kim J (2009) Design of ultra-fine nonwovens via electrospinning of Nylon 6: Spinning parameters and filtration efficiency. Materials and Design 30:3659-3666. https://doi.org/10.1016/j.matdes.2009.02.017

80. Maze B, Vahedi Tafreshi H, Wang Q, Pourdeyhimi B (2007) A simulation of unsteady-state filtration via nanofiber media at reduced operating pressures. Journal of Aerosol Science 38:550-571. https://doi.org/10.1016/j.jaerosci.2007.03.008

81. Hajra MG, Mehta K, Chase GG (2003) Effects of humidity, temperature, and nanofibers on drop coalescence in glass fiber media. Separation and Purification Technology 30:79-88. https://doi.org/10.1016/S1383-5866(02)00134-X

82. Kadam V V, Wang L, Padhye R (2018) Electrospun nanofibre materials to filter air pollutants – A review. Journal of Industrial Textiles 47:2253-2280. https://doi.org/10.1177%2F1528083716676812

83. Wang N, Si Y, Wang N, et al. (2014) Multilevel structured polyacrylonitrile/silica nanofibrous membranes for high-performance air filtration. Separation and Purification Technology 126:44–51. https://doi.org/10.1016/j.seppur.2014.02.017

84. Li K, Li C, Tian H, et al. (2020) Multifunctional and Efficient Air Filtration: A Natural Nanofilter Prepared with Zein and Polyvinyl Alcohol. Macromolecular Materials and Engineering 305:1-8. https://doi.org/10.1002/mame.202000239

85. Gopal R, Kaur S, Feng CY, et al. (2007) Electrospun nanofibrous polysulfone membranes as pre-filters: Particulate removal. Journal of Membrane Science 289:210-219. https://doi.org/10.1016/j.memsci.2006.11.056

86. Matulevicius J, Kliucininkas L, Prasauskas T, et al. (2016) The comparative study of aerosol filtration by electrospun polyamide, polyvinyl acetate, polyacrylonitrile and cellulose acetate nanofiber media. Journal of Aerosol Science 92:27-37. https://doi.org/10.1016/j.jaerosci.2015.10.006

87. Chang CY, Chang FC (2016) Development of Electrospun Lignin-based Fibrous Materials for Filtration Applications. BioResources 11:2202-2213. https://doi.org/10.15376/BIORES.11.1.2202-2213

88. Li Y, Yin X, Yu J, Ding B (2019) Electrospun nanofibers for high-performance air filtration. Composites Communications 15:6-19. https://doi.org/10.1016/j.coco.2019.06.003

89. Zhu M, Xiong R, Huang C (2019) Bio-based and photocrosslinked electrospun antibacterial nanofibrous membranes for air filtration. Carbohydrate Polymers 205:55–62. https://doi.org/10.1016/j.carbpol.2018.09.075

90. Huang JJ, Tian Y, Wang R, et al. (2020) Fabrication of bead-on-string polyacrylonitrile nanofibrous air filters with superior filtration efficiency and ultralow pressure drop. Separation and Purification Technology 237:1-11. https://doi.org/10.1016/j.seppur.2019.116377

91. Zhu M, Hua D, Pan H, et al. (2018) Green electrospun and crosslinked poly(vinyl alcohol)/poly(acrylic acid) composite membranes for antibacterial effective air filtration. Journal of Colloid and Interface Science 511:411-423. https://doi.org/10.1016/j.jcis.2017.09.101

92. Choi J, Yang BJ, Bae GN, Jung JH (2015) Herbal Extract Incorporated Nanofiber Fabricated by an Electrospinning Technique and its Application to Antimicrobial Air Filtration. ACS Applied Materials and Interfaces 7:25313–25320. https://doi.org/10.1021/acsami.5b07441

93. Al-Attabi R, Dumée LF, Kong L, et al. (2018) High Efficiency Poly(acrylonitrile) Electrospun Nanofiber Membranes for Airborne Nanomaterials Filtration. Advanced Engineering Materials 20:1–10. https://doi.org/10.1002/adem.201700572

94. Liu H, Huang J, Mao J, et al. (2019) Transparent Antibacterial Nanofiber Air Filters with Highly Efficient Moisture Resistance for Sustainable Particulate Matter Capture. iScience 19:214–223. https://doi.org/10.1016/j.isci.2019.07.020

95. Zhang L, Li L, Wang L, et al. (2020) Multilayer electrospun nanofibrous membranes with antibacterial property for air filtration. Applied Surface Science 515:1-10. https://doi.org/10.1016/j.apsusc.2020.145962

96. Purwar R, Goutham KS, Srivastava CM (2016) Electrospun Sericin/PVA/Clay Nanofibrous Mats for Antimicrobial Air Filtration Mask. Fibers and Polymers 17:1206–1216. https://doi.org/10.1007/s12221-016-6345-7

97. Wang N, Raza A, Si Y, et al. (2013) Tortuously structured polyvinyl chloride/polyurethane fibrous membranes for high-efficiency fine particulate filtration. Journal of Colloid and Interface Science 398:240–246. https://doi.org/10.1016/j.jcis.2013.02.019

98. Wan H, Wang N, Yang J, et al. (2014) Hierarchically structured polysulfone/titania fibrous membranes with enhanced air filtration performance. Journal of Colloid and Interface Science 417:18-26. https://doi.org/10.1016/j.jcis.2013.11.009

99. Li X, Wang N, Fan G, et al. (2015) Electreted polyetherimide-silica fibrous membranes for enhanced filtration of fine particles. Journal of Colloid and Interface Science 439:12-20. https://doi.org/10.1016/j.jcis.2014.10.014

100. Yang Y, Zhang S, Zhao X, et al. (2015) Sandwich structured polyamide-6/polyacrylonitrile nanonets/bead-on-string composite membrane for effective air filtration. Separation and Purification Technology 152:14-22. https://doi.org/10.1016/j.seppur.2015.08.005

101. Wang Z, Pan Z (2015) Preparation of hierarchical structured nano-sized/porous poly(lactic acid) composite fibrous membranes for air filtration. Applied Surface Science 356:1168-1179. https://doi.org/10.1016/j.apsusc.2015.08.211

102. Zhang H, Xie Y, Song Y, Qin X (2021) Preparation of high-temperature resistant poly (m-phenylene isophthalamide)/polyacrylonitrile composite nanofibers membrane for air filtration. Colloids and Surfaces A: Physicochemical and Engineering Aspects 624:1-9. https://doi.org/10.1016/j.colsurfa.2021.126831

103. Zhang L, Luo J, Menkhaus TJ, et al. (2011) Antimicrobial nano-fibrous membranes developed from electrospun polyacrylonitrile nanofibers. Journal of Membrane Science 369:499–505. https://doi.org/10.1016/j.memsci.2010.12.032

104. Chaudhary A, Gupta A, Mathur RB, Dhakate SR (2014) Effective antimicrobial filter from electrospun polyacrylonitrile-silver composite nanofibers membrane for conducive environment. Advanced Materials Letters 5:562–568. https://doi.org/10.5185/amlett.2014.572

105. Castro-Mayorga JL, Fabra MJ, Cabedo L, Lagaron JM (2017) c. Nanomaterials 7:4. https://doi.org/10.3390/nano7010004

106. Kalwar K, Sun WX, Li DL, et al. (2016) Coaxial electrospinning of polycaprolactone@chitosan: Characterization and silver nanoparticles incorporation for antibacterial activity. Reactive and Functional Polymers 107:87-92. https://doi.org/10.1016/j.reactfunctpolym.2016.08.010

107. Sumitha MS, Shalumon KT, Sreeja VN, et al. (2012) Biocompatible and antibacterial nanofibrous poly(ε-caprolactone)- nanosilver composite scaffolds for tissue engineering applications. Journal of Macromolecular Science, Part A: Pure and Applied Chemistry 49:131–138. https://doi.org/10.1080/10601325.2012.642208

108. Lin S, Wang RZ, Yi Y, et al. (2014) Facile and green fabrication of electrospun poly(vinyl alcohol) nanofibrous mats doped with narrowly dispersed silver nanoparticles. International Journal of Nanomedicine 9:3937-3947. https://doi.org/10.2147/IJN.S64985

109. Rath G, Hussain T, Chauhan G, et al. (2016) Collagen nanofiber containing silver nanoparticles for improved wound-healing applications. Journal of Drug Targeting 24:520-529. https://doi.org/10.3109/1061186X.2015.1095922

110. Woranuch S, Pangon A, Puagsuntia K, et al. (2017) Starch-based and multi-purpose nanofibrous membrane for high efficiency nanofiltration. RSC Advances 7:35368-35375. https://doi.org/10.1039/c7ra07484k

111. Lee K, Lee S (2012) Multifunctionality of poly(vinyl alcohol) nanofiber webs containing titanium dioxide. Journal of Applied Polymer Science 124:4038-4046. https://doi.org/10.1002/app.34929

112. Aigbe UO, Osibote OA (2020) A review of hexavalent chromium removal from aqueous solutions by sorption technique using nanomaterials. Journal of Environmental Chemical Engineering 8:104503. https://doi.org/10.1016/j.jece.2020.104503

113. Liu W, Zhang J, Zhang C, Ren L (2012) Preparation and evaluation of activated carbon-based iron-containing adsorbents for enhanced Cr(VI) removal: Mechanism study. Chemical Engineering Journal 189–190:295-302. https://doi.org/10.1016/j.cej.2012.02.082

114. Zhao Y, Qi W, Chen G, et al. (2015) Behavior of Cr(VI) removal from wastewater by adsorption onto HCl activated Akadama clay. Journal of the Taiwan Institute of Chemical Engineers 50:190–197. https://doi.org/10.1016/j.jtice.2014.12.016

115. Kummer G, Schonhart C, Fernandes MG, et al. (2018) Development of Nanofibers Composed of Chitosan/Nylon 6 and Tannin/Nylon 6 for Effective Adsorption of Cr(VI). Journal of Polymers and the Environment 26:4073–4084. https://doi.org/10.1007/s10924-018-1281-9

116. Rosales-Landeros C, Barrera-Díaz CE, Bilyeu B, et al. (2013) A Review on Cr(VI) Adsorption Using Inorganic Materials. American Journal of Analytical Chemistry 04:1-9. https://doi.org/10.4236/ajac.2013.47a002

117. Pereao OK, Bode-Aluko C, Ndayambaje G, et al. (2017) Electrospinning: Polymer Nanofibre Adsorbent Applications for Metal Ion Removal. Journal of Polymers and the Environment 25:1175-1189. https://doi.org/10.1007/s10924-016-0896-y

118. Suja PS, Reshmi CR, Sagitha P, Sujith A (2017) Electrospun Nanofibrous Membranes for Water Purification. Polymer Reviews 57:467-504. https://doi.org/10.1080/15583724.2017.1309664

119. Jiang J, Zhu L, Zhu L, et al. (2013) Antifouling and antimicrobial polymer membranes based on bioinspired polydopamine and strong hydrogen-bonded poly(n -vinyl pyrrolidone). ACS Applied Materials and Interfaces 5:12895-12904. https://doi.org/10.1021/am403405c

120. Vazquez-Velez E, Lopez-Zarate L, Martinez-Valencia H (2020) Electrospinning of polyacrylonitrile nanofibers embedded with zerovalent iron and cerium oxide nanoparticles, as Cr(VI) adsorbents for water treatment. Journal of Applied Polymer Science 137:1-10. https://doi.org/10.1002/app.48663

121. Li L, Li Y, Cao L, Yang C (2015) Enhanced chromium (VI) adsorption using nanosized chitosan fibers tailored by electrospinning. Carbohydrate Polymers 125:206–213. https://doi.org/10.1016/j.carbpol.2015.02.037

122. Chaúque EFC, Dlamini LN, Adelodun AA, et al. (2016) Modification of electrospun polyacrylonitrile nanofibers with EDTA for the removal of Cd and Cr ions from water effluents. Applied Surface Science 369:19-28. https://doi.org/10.1016/j.apsusc.2016.02.018

123. Chen J, Hong X, Xie Q, et al. (2014) Highly efficient removal of chromium(VI) from aqueous solution using polyaniline/sepiolite nanofibers. Water Science and Technology 70:1236-1243. https://doi.org/10.2166/wst.2014.361

124. Yang R, Aubrecht KB, Ma H, et al. (2014) Thiol-modified cellulose nanofibrous composite membranes for chromium (VI) and lead (II) adsorption. Polymer 55:1167-1176. https://doi.org/10.1016/j.polymer.2014.01.043

125. Jia B bin, Wang JN, Wu J, Li CJ (2014) "Flower-Like" PA6@Mg(OH)2 electrospun nanofibers with Cr (VI)-removal capacity. Chemical Engineering Journal 254:98-105. https://doi.org/10.1016/j.cej.2014.05.005

126. Xu GR, Wang JN, Li CJ (2012) Preparation of hierarchically nanofibrous membrane and its high adaptability in hexavalent chromium removal from water. Chemical Engineering Journal 198–199:310-317. https://doi.org/10.1016/j.cej.2012.05.104

127. Mahapatra A, Mishra BG, Hota G (2013) Studies on electrospun alumina nanofibers for the removal of chromium(vi) and fluoride toxic ions from an aqueous system. Industrial and Engineering Chemistry Research 52:1554-1561. https://doi.org/10.1021/ie301586j

128. Beheshti H, Irani M, Hosseini L, et al. (2016) Removal of Cr (VI) from aqueous solutions using chitosan/MWCNT/Fe$_3$O$_4$ composite nanofibers-batch and column studies. Chemical Engineering Journal 284:557-564. https://doi.org/10.1016/j.cej.2015.08.158

129. Taha AA, Wu Y na, Wang H, Li F (2012) Preparation and application of functionalized cellulose acetate/silica composite nanofibrous membrane via electrospinning for Cr(VI) ion removal from aqueous solution. Journal of Environmental Management 112:10-16. https://doi.org/10.1016/j.jenvman.2012.05.031

130. Hadi Najafabadi H, Irani M, Roshanfekr Rad L, et al. (2015) Removal of Cu^{2+}, Pb^{2+} and Cr^{6+} from aqueous solutions using a chitosan/graphene oxide composite nanofibrous adsorbent. RSC Advances 5:16532-16539. https://doi.org/10.1039/c5ra01500f

131. Bhaumik M, Maity A, Srinivasu V V, Onyango MS (2012) Removal of hexavalent chromium from aqueous solution using polypyrrole-polyaniline nanofibers. Chemical Engineering Journal 181–182:323-333. https://doi.org/10.1016/j.cej.2011.11.088

132. Bhaumik M, Choi HJ, McCrindle RI, Maity A (2014) Composite nanofibers prepared from metallic iron nanoparticles and polyaniline: High performance for water treatment applications. Journal of Colloid and Interface Science 425:75-82. https://doi.org/10.1016/j.jcis.2014.03.031

133. Mohammad N, Atassi Y (2021) Enhancement of removal efficiency of heavy metal ions by polyaniline deposition on electrospun polyacrylonitrile membranes. Water Science and Engineering 14:129-138. https://doi.org/10.1016/j.wse.2021.06.004

134. Li Z, Li T, An L, et al. (2016) Highly efficient chromium(VI) adsorption with nanofibrous filter paper prepared through electrospinning chitosan/polymethylmethacrylate composite. Carbohydrate Polymers 137:119-126. https://doi.org/10.1016/j.carbpol.2015.10.059

135. Shahram Forouz F, Hosseini Ravandi SA, Allafchian AR (2016) Removal of Ag and Cr Heavy Metals Using Nanofiber Membranes Functionalized with Aminopropyltriethoxysilane (APTES). Current Nanoscience 12:266-274. https://doi.org/10.2174/1573413712999151216162920

136. Uddin F (2018) Montmorillonite: An Introduction to Properties and Utilization. In: Current Topics in the Utilization of Clay in Industrial and Medical Applications

137. Bhattacharyya KG, Gupta SS (2008) Adsorption of a few heavy metals on natural and modified kaolinite and montmorillonite: A review. Advances in Colloid and Interface Science 140:114-131. https://doi.org/10.1016/j.cis.2007.12.008

138. Shaba EY, Jacob JO, Tijani JO, Suleiman MAT (2021) A critical review of synthesis parameters affecting the properties of zinc oxide nanoparticle and its application in wastewater treatment. Applied Water Science 11:1-41. https://doi.org/10.1007/s13201-021-01370-z

139. Mahdavi S, Jalali M, Afkhami A (2014) Removal of heavy metals from aqueous solutions using Fe3O4, ZnO, and CuO nanoparticles. In: Nanotechnology for Sustainable Development, First Edition

140. Samad A, Din MI, Ahmed M, Ahmad S (2021) Synthesis of zinc oxide nanoparticles reinforced clay and their applications for removal of Pb (II) ions from aqueous media. Chinese Journal of Chemical Engineering 32:454-461. https://doi.org/10.1016/j.cjche.2020.09.043

141. Buruga K, Song H, Shang J, et al. (2019) A review on functional polymer-clay based nanocomposite membranes for treatment of water. Journal of Hazardous Materials 379:1-27. https://doi.org/10.1016/j.jhazmat.2019.04.067

142. Bhattacharyya KG, Gupta SS (2006) Adsorption of chromium(VI) from water by clays. Industrial and Engineering Chemistry Research 45:7232–7240. https://doi.org/10.1021/ie060586j

143. Gładysz-Płaska A, Majdan M, Pikus S, Sternik D (2012) Simultaneous adsorption of chromium(VI) and phenol on natural red clay modified by HDTMA. Chemical Engineering Journal 179:140-150. https://doi.org/10.1016/j.cej.2011.10.071

144. Weng CH, Sharma YC, Chu SH (2008) Adsorption of Cr(VI) from aqueous solutions by spent activated clay. Journal of Hazardous Materials 155:65-75. https://doi.org/10.1016/j.jhazmat.2007.11.029

145. Liu Q, Yang B, Zhang L, Huang R (2015) Adsorptive removal of Cr(VI) from aqueous solutions by cross-linked chitosan/bentonite composite. Korean Journal of Chemical Engineering 32:1314-1322. https://doi.org/10.1007/s11814-014-0339-1

146. Huang F, Xu Y, Liao S, et al. (2013) Preparation of amidoxime polyacrylonitrile chelating nanofibers and their application for adsorption of metal ions. Materials 6:969–980. https://doi.org/10.3390/ma6030969

147. Hu Y, Wu XY, He X, Xing D (2019) Phosphorylated polyacrylonitrile-based electrospun nanofibers for removal of heavy metal ions from aqueous solution. Polymers for Advanced Technologies 30:545-551 https://doi.org/10.1002/pat.4490

148. Feng ZQ, Yuan X, Wang T (2019) Porous polyacrylonitrile/graphene oxide nanofibers designed for high efficient adsorption of chromium ions (VI) in aqueous solution. Chemical Engineering Journal 392:123730 https://doi.org/10.1016/j.cej.2019.123730

149. Bode-Aluko CA, Pereao O, Ndayambaje G, Petrik L (2017) Adsorption of Toxic Metals on Modified Polyacrylonitrile Nanofibres: A Review. Water, Air, & Soil Pollution 228:35. https://doi.org/10.1007/s11270-016-3222-3

150. Neghlani PK, Rafizadeh M, Taromi FA (2011) Preparation of aminated-polyacrylonitrile nanofiber membranes for the adsorption of metal ions: Comparison with microfibers. Journal of Hazardous Materials 186:182–189. https://doi.org/10.1016/j.jhazmat.2010.10.121

151. Parlayıcı Ş, Yar A, Pehlivan E, Avcı A (2019) ZnO-TiO$_2$ doped polyacrylonitrile nano fiber-Mat for elimination of Cr (VI) from polluted water. Journal of Analytical Science and Technology 10:0–11. https://doi.org/10.1186/s40543-019-0183-3

152. Shakiba M, Nabavi SR, Emadi H, Faraji M (2021) Development of a superhydrophilic nanofiber membrane for oil/water emulsion separation via modification of polyacrylonitrile/polyaniline composite. Polymers for Advanced Technologies 32:1301-1316. https://doi.org/10.1002/pat.5178

153. Faraji M, Nabavi SR, Salimi-Kenari H (2020) Fabrication of a PAN-PA6/PANI membrane using dual spinneret electrospinning followed by: In situ polymerization for separation of oil-in-water emulsions. New Journal of Chemistry 44:13488-13500. https://doi.org/10.1039/d0nj03231j

154. Liu J, Jin C, Wang C (2020) Hyperbranched thiourea-grafted electrospun polyacrylonitrile fibers for efficient and selective gold recovery. Journal of Colloid and Interface Science 561:449–458. https://doi.org/10.1016/j.jcis.2019.11.016

155. Karki HP, Kafle L, Ojha DP, et al. (2019) Cellulose/polyacrylonitrile electrospun composite fiber for effective separation of the surfactant-free oil-in-water mixture under a versatile condition. Separation and Purification Technology 210:913–919. https://doi.org/10.1016/j.seppur.2018.08.053

156. Lou T, Yan X, Wang X (2019) Chitosan coated polyacrylonitrile nanofibrous mat for dye adsorption. International Journal of Biological Macromolecules 135:919–925. https://doi.org/10.1016/j.ijbiomac.2019.06.008

157. Gao X, Li ZK, Xue J, et al. (2019) Titanium carbide Ti3C2Tx (MXene) enhanced PAN nanofiber membrane for air purification. Journal of Membrane Science 586:162–169. https://doi.org/10.1016/j.memsci.2019.05.058

158. Chen C, Li F, Guo Z, et al. (2019) Preparation and performance of aminated polyacrylonitrile nanofibers for highly efficient copper ion removal. Colloids and Surfaces A: Physicochemical and Engineering Aspects 568:334–344. https://doi.org/10.1016/j.colsurfa.2019.02.020

159. Farzin L, Sadjadi S, Shamsipur M, et al. (2019) Employing AgNPs doped amidoxime-modified polyacrylonitrile (PAN-oxime) nanofibers for target induced strand displacement-based electrochemical aptasensing of CA125 in ovarian cancer patients. Materials Science and Engineering C 97:679–687. https://doi.org/10.1016/j.msec.2018.12.108

160. Jatoi AW, Gianchandani PK, Kim IS, Ni QQ (2019) Sonication induced effective approach for coloration of compact polyacrylonitrile (PAN) nanofibers. Ultrasonics Sonochemistry 51:399–405. https://doi.org/10.1016/j.ultsonch.2018.07.035

161. Chen L, Bromberg L, Hatton TA, Rutledge GC (2007) Catalytic hydrolysis of p-nitrophenyl acetate by electrospun polyacrylamidoxime nanofibers. Polymer 48:4675–4682. https://doi.org/10.1016/j.polymer.2007.05.084

162. Peng M, Li D, Shen L, et al. (2006) Nanoporous structured submicrometer carbon fibers prepared via solution electrospinning of polymer blends. Langmuir 22:9368–9374. https://doi.org/10.1021/la061154g

163. Wan LS, Ke BB, Wu J, Xu ZK (2007) Catalase immobilization on electrospun nanofibers: Effects of porphyrin pendants and carbon nanotubes. Journal of Physical Chemistry C 111:14091–14097. https://doi.org/10.1021/jp070983n

164. Wang S, Yang Q, Du J, et al. (2007) Variety of photoluminescence intensity of fluorescent whitening agents introduced into polyacrylonitrile nanofibers. Journal of Applied Polymer Science 103:2382–2386. https://doi.org/10.1002/app.25342

165. Doshi J, Reneker DH (1995) Electrospinning process and applications of electrospun fibers. Journal of Electrostatics 35:151–160. https://doi.org/10.1109/ias.1993.299067

166. Ryšánek P, Benada O, Tokarský J, et al. (2019) Specific structure, morphology, and properties of polyacrylonitrile (PAN) membranes prepared by needleless electrospinning; Forming hollow fibers. Materials Science and Engineering C 105:1-7. https://doi.org/10.1016/j.msec.2019.110151

167. Zussman E, Theron A, Yarin AL (2003) Formation of nanofiber crossbars in electrospinning. Applied Physics Letters 82:973–975. https://doi.org/10.1063/1.1544060

168. Karimiyan H, Uheida A, Hadjmohammadi M, et al. (2019) Polyacrylonitrile / graphene oxide nanofibers for packed sorbent microextraction of drugs and their metabolites from human plasma samples. Talanta 201:474–479. https://doi.org/10.1016/j.talanta.2019.04.027

169. Mohamed A, Ghobara MM, Abdelmaksoud MK, Mohamed GG (2019) A novel and highly efficient photocatalytic degradation of malachite green dye via surface modified polyacrylonitrile nanofibers/biogenic silica composite nanofibers. Separation and Purification Technology 210:935–942. https://doi.org/10.1016/j.seppur.2018.09.014

170. Wilkanowicz SI, Hollingsworth NR, Saud K, et al. (2020) Immobilization of calcium oxide onto polyacrylonitrile (PAN) fibers as a heterogeneous catalyst for biodiesel production. Fuel Processing Technology 197:1-12. https://doi.org/10.1016/j.fuproc.2019.106214

171. Abdel-Mottaleb MM, Khalil A, Karim SA, et al. (2019) High performance of PAN/GO-ZnO composite nanofibers for photocatalytic degradation under visible irradiation. Journal of the Mechanical Behavior of Biomedical Materials 96:118–124. https://doi.org/10.1016/j.jmbbm.2019.04.040

172. Yu ZM, Shen LF, Li DS, et al. (2019) Differentiation of photon generation depended on electrospun configuration in Eu^{3+}/Tb^{3+} doped polyacrylonitrile nanofibers. Journal of Alloys and Compounds 786:1040–1050. https://doi.org/10.1016/j.jallcom.2019.02.012

173. Karki HP, Kafle L, Kim HJ (2019) Modification of 3D polyacrylonitrile composite fiber for potential oil-water mixture separation. Separation and Purification Technology 229:1-8. https://doi.org/10.1016/j.seppur.2019.115840

174. Mogolodi Dimpe K, Nomngongo PN (2019) Application of activated carbon-decorated polyacrylonitrile nanofibers as an adsorbent in dispersive solid-phase extraction of fluoroquinolones from wastewater. Journal of Pharmaceutical Analysis 9:117–126. https://doi.org/10.1016/j.jpha.2019.01.003

175. Wang L, Fu Q, Yu J, et al. (2019) Nanoparticle-doped polystyrene/polyacrylonitrile nanofiber membrane with hierarchical structure as promising protein hydrophobic interaction chromatography media. Composites Communications 16:33–40. https://doi.org/10.1016/j.coco.2019.08.008

176. Ismar E, Sarac AS (2019) Electrospun polyacrylonitrile–lauric acid composite nanofiber webs as a thermal energy storage material. Journal of Engineered Fibers and Fabrics 14:1-6. https://doi.org/10.1177/1558925018824890

177. Huang C, Liu Y, Li Z, et al. (2019) N-halamine antibacterial nanofibrous mats based on polyacrylonitrile and N-halamine for protective face masks. Journal of Engineered Fibers and Fabrics 14:1-8. https://doi.org/10.1177/1558925019843222

178. Abd-Elhamid AI, El-Aassar MR, el Fawal GF, Soliman HMA (2019) Fabrication of polyacrylonitrile/β-cyclodextrin/graphene oxide nanofibers composite as an efficient adsorbent for cationic dye. Environmental Nanotechnology, Monitoring and Management 11. https://doi.org/10.1016/j.enmm.2018.100207

179. Asadi M, Shahabuddin S, Mollahosseini A, et al. (2019) Electrospun Magnetic Zeolite/Polyacrylonitrile Nanofibers for Extraction of PAHs from Waste Water: Optimized with Central Composite Design. Journal of Inorganic and Organometallic Polymers and Materials 29:1057–1066. https://doi.org/10.1007/s10904-018-1027-0

180. Bahrami H, Rezaei B, Jafari MT (2019) Coupling of a novel electrospun polyacrylonitrile/amino-Zr-MOF nanofiber as a thin film for microextraction-corona discharge-ion mobility spectrometry for the analysis of chlorpyrifos in water samples. Analytical Methods 11:1073–1079. https://doi.org/10.1039/c8ay02518e

181. Xiao Y, Cao Y, Liu Y, et al. (2019) Electrospun natural cellulose/polyacrylonitrile nanofiber: simulation and experimental study. Textile Research Journal 89:1748–1758. https://doi.org/10.1177/0040517518779256

182. Almasian A, Olya ME, Mahmoodi NM, Zarinabadi E (2019) Grafting of polyamidoamine dendrimer on polyacrylonitrile nanofiber surface: synthesis and optimization of anionic dye removal process by response surface methodology method. Desalination and Water Treatment 147:343–361. https://doi.org/10.5004/dwt.2019.23676

183. Mooste M, Kibena-Põldsepp E, Vassiljeva V, et al. (2019) Electrocatalysts for oxygen reduction reaction based on electrospun polyacrylonitrile, styrene–acrylonitrile copolymer and carbon nanotube composite fibres. Journal of Materials Science 54:11618-11634. https://doi.org/10.1007/s10853-019-03725-z

184. Nthunya LN, Gutierrez L, Derese S, et al. (2019) Adsorption of phenolic compounds by polyacrylonitrile nanofibre membranes: A pretreatment for the removal of hydrophobic bearing compounds from water. Journal of Environmental Chemical Engineering 7:1-13. https://doi.org/10.1016/j.jece.2019.103254

185. Phan DN, Dorjjugder N, Saito Y, et al. (2019) The synthesis of silver-nanoparticle-anchored electrospun polyacrylonitrile nanofibers and a comparison with as-spun silver/polyacrylonitrile nanocomposite membranes upon antibacterial activity. Polymer Bulletin 77:4197-4212. https://doi.org/10.1007/s00289-019-02969-8

186. Tao R, Yang S, Shao C, et al. (2019) Reusable and Flexible g-C 3 N 4 /Ag 3 PO 4 /Polyacrylonitrile Heterojunction Nanofibers for Photocatalytic Dye Degradation and Oxygen Evolution. ACS Applied Nano Materials 2:3081–3090. https://doi.org/10.1021/acsanm.9b00428

187. Wang X, Pan S, Zhang M, et al. (2019) Modified hydrous zirconium oxide/PAN nanofibers for efficient defluoridation from groundwater. Science of the Total Environment 685:401–409. https://doi.org/10.1016/j.scitotenv.2019.05.380

188. Wang CH, Hu LM, Wang ZF, Zhang M (2019) Electrospun and in situ self-polymerization of polyacrylonitrile containing gadolinium nanofibers for thermal neutron protection. Rare Metals 38:252–258. https://doi.org/10.1007/s12598-018-1042-x

189. Wang J, Cai C, Zhang Z, et al. (2020) Electrospun metal-organic frameworks with polyacrylonitrile as precursors to hierarchical porous carbon and composite nanofibers for adsorption and catalysis. Chemosphere 239:1-10. https://doi.org/10.1016/j.chemosphere.2019.124833

190. Weng YC, Wang ZN, Wu SY (2019) Palladium modified carbonized electrospun polyacrylonitrile nanofiber for sulfur dioxide determination. Ionics 25:2865–2872. https://doi.org/10.1007/s11581-018-2790-1

191. Sangeetha G, Rajeshwari S, Venckatesh R (2011) Green synthesis of zinc oxide nanoparticles by aloe barbadensis miller leaf extract: Structure and optical properties. Materials Research Bulletin 46:2560–2566. https://doi.org/10.1016/j.materresbull.2011.07.046

192. Srivastava CM, Purwar R (2016) Fabrication of robust Antheraea assama fibroin nanofibrous mat using ionic liquid for skin tissue engineering. Materials Science and Engineering C 68:276–290. https://doi.org/10.1016/j.msec.2016.05.020

193. Purwar R, Mishra P, Joshi M (2008) Antibacterial Finishing of Cotton Textiles using Neem Extract. AATCC Review 8:36–43

194. Rasli NI, Basri H, Harun Z (2020) Zinc oxide from aloe vera extract: two-level factorial screening of biosynthesis parameters. Heliyon 6:. https://doi.org/10.1016/j.heliyon.2020.e03156

195. Litchfield DW, Baird DG, Litchfield DW, Baird DG (2006) the Rheology of High Aspect Ratio Nano- Particle Filled Liquids. Rheology Reviews 1–60

196. Ahmadzadeh S, Nasirpour A, Keramat J, Desobry S (2015) Effect of surface-modified montmorillonite on viscosity and gelation behavior of cellulose/NaOH solution. Cellulose 22:1829–1839. https://doi.org/10.1007/s10570-015-0597-z

197. Brown JM, Curliss D, Vaia RA (2000) Thermoset-layered silicate nanocomposites. Quaternary ammonium montmorillonite with primary diamine cured epoxies. Chemistry of Materials 12:3376–3384. https://doi.org/10.1021/cm000477+

198. Kader MA, Lyu MY, Nah C (2006) A study on melt processing and thermal properties of fluoroelastomer nanocomposites. Composites Science and Technology 66:1431–1443. https://doi.org/10.1016/j.compscitech.2005.09.001

199. Mousavi MR, Rafizadeh M, Sharif F (2016) Effect of electrospinning on the ionic conductivity of polyacrylonitrile/polymethyl methacrylate nanofibrous membranes: optimization based on the response surface method. Iranian Polymer Journal (English Edition) 25:525–537. https://doi.org/10.1007/s13726-016-0444-6

200. Li Q, Gao D, Wei Q, et al. (2010) Thermal Stability and Crystalline of Electrospun Polyamide 6/Organo-Montmorillonite Nanofibers Qi. Journal of Applied Polymer Science 117:1572–1577. https://doi.org/https://doi.org/10.1002/app.32017

201. Almuhamed S, Bonne M, Khenoussi N, et al. (2016) Electrospinning composite nanofibers of polyacrylonitrile/synthetic Na-montmorillonite. Journal of Industrial and Engineering Chemistry 35:146–152. https://doi.org/10.1016/j.jiec.2015.12.024

202. Deitzel JM, Kleinmeyer J, Harris D, Beck Tan NC (2001) The effect of processing variables on the morphology of electrospun nanofibers and textiles. Polymer 42:261–272. https://doi.org/https://doi.org/10.1016/S0032-3861(00)00250-0

203. Hong JH, Jeong EH, Lee HS, et al. (2005) Electrospinning of polyurethane/organically modified montmorillonite nanocomposites. Journal of Polymer Science, Part B: Polymer Physics 43:3171–3177. https://doi.org/10.1002/polb.20610

204. Son WK, Youk JH, Lee TS, Park WH (2004) The effects of solution properties and polyelectrolyte on electrospinning of ultrafine poly(ethylene oxide) fibers. Polymer 45:2959–2966. https://doi.org/10.1016/j.polymer.2004.03.006

205. Ouyang Q, Cheng L, Wang H, Li K (2008) Mechanism and kinetics of the stabilization reactions of itaconic acid-modified polyacrylonitrile. Polymer Degradation and Stability 93:1415–1421. https://doi.org/10.1016/j.polymdegrad stab.2008.05.021

206. Al-Attabi R, Morsi Y, Kujawski W, et al. (2019) Wrinkled silica doped electrospun nano-fiber membranes with engineered roughness for advanced aerosol air filtration. Separation and Purification Technology 215:500–507. https://doi.org/10.1016/j.seppur.2019.01.049

207. Fotiadou S, Karageorgaki C, Chrissopoulou K, et al. (2013) Structure and dynamics of hyperbranched polymer/layered silicate nanocomposites. Macromolecules 46:2842–2855. https://doi.org/10.1021/ma302405q

208. Philippe C, Claire B (2010) Thomas S, Stephen R (eds) Rubber nanocomposites: preparations, properties and applications. Wiley, Chichester

209. Sikkanthar S, Karthikeyan S, Selvasekarapandian S, et al. (2015) Electrical conductivity characterization of polyacrylonitrile-ammonium bromide polymer electrolyte system. Journal of Solid State Electrochemistry 19:987–999. https://doi.org/10.1007/s10008-014-2697-3

210. Haroosh HJ, Chaudhary DS, Dong Y (2012) Electrospun PLA/PCL Fibers with Tubular Nanoclay: Morphological and Structural Analysis. Journal of Applied Polymer Science 124:3930–3939. https://doi.org/10.1002/app.35448

211. Hou X, Yang X, Zhang L, et al. (2010) Stretching-induced crystallinity and orientation to improve the mechanical properties of electrospun PAN nanocomposites. Materials and Design 31:1726–1730. https://doi.org/10.1016/j.matdes.2009.01.051

212. Jalili R, Morshed M, Ravandi SAH (2006) Fundamental parameters affecting electrospinning of PAN nanofibers as uniaxially aligned fibers. Journal of Applied Polymer Science 101:4350–4357. https://doi.org/10.1002/app.24290

213. Fennessey SF, Farris RJ (2004) Fabrication of aligned and molecularly oriented electrospun polyacrylonitrile nanofibers and the mechanical behavior of their twisted yarns. Polymer 45:4217–4225. https://doi.org/10.1016/j.polymer.2004.04.001

214. Wang ZM (2010) Nanoporous materials. Elsevier Ltd.

215. Stevens K, Fuller M (2015) Thermoregulation and clothing comfort. Elsevier Ltd

216. Sheng J, Zhang M, Xu Y, et al. (2016) Tailoring Water-Resistant and Breathable Performance of Polyacrylonitrile Nanofibrous Membranes Modified by Polydimethylsiloxane. ACS Applied Materials and Interfaces 8:27218–27226. https://doi.org/10.1021/acsami.6b09392

217. Roche R, Yalcinkaya F (2019) Electrospun Polyacrylonitrile Nanofibrous Membranes for Point-of-Use Water and Air Cleaning. ChemistryOpen 8:97–103. https://doi.org/10.1002/open.201800267

218. Oliveira AE, Aguiar ML, Guerra VG (2021) Theoretical Analysis of Air Filtration Phenomena for a Micro-fibrous Filter Medium Enhanced with Electrospun Nanofibers. Aerosol Science and Engineering 5:. https://doi.org/10.1007/s41810-020-00086-y

219. Zhang R, Liu B, Yang A, et al. (2018) In Situ Investigation on the Nanoscale Capture and Evolution of Aerosols on Nanofibers. Nano Letters 18:1130–1138. https://doi.org/10.1021/acs.nanolett.7b04673

220. Liu H, Huang J, Mao J, et al. (2019) Transparent Antibacterial Nanofiber Air Filters with Highly Efficient Moisture Resistance for Sustainable Particulate Matter Capture. iScience 19:214–223. https://doi.org/10.1016/j.isci.2019.07.020

221. Dinari M, Haghighi A (2018) Ultrasound-assisted synthesis of nanocomposites based on aromatic polyamide and modified ZnO nanoparticle for removal of toxic Cr(VI) from water. Ultrasonics sonochemistry 41:75–84. https://doi.org/10.1016/j.ultsonch.2017.09.023

222. Mao J, Tang Y, Wang Y, et al. (2019) Particulate Matter Capturing via Naturally Dried ZIF-8/Graphene Aerogels under Harsh Conditions. iScience 16:133–144. https://doi.org/10.1016/j.isci.2019.05.024

223. Yin X, Yu J, Ding B (2020) Electrospun Fibers for Filtration. Handbook of Fibrous Materials 175–206. https://doi.org/10.1002/9783527342587.CH7

224. Wang S, Zhao X, Yin X, et al. (2016) Electret Polyvinylidene Fluoride Nanofibers Hybridized by Polytetrafluoroethylene Nanoparticles for High-Efficiency Air Filtration. ACS Applied Materials and Interfaces 8:23985-23994. https://doi.org/10.1021/acsami.6b08262

225. Webster TJ, Seil I (2012) Antimicrobial applications of nanotechnology: methods and literature. International Journal of Nanomedicine 7:2767-2781. https://doi.org/10.2147/IJN.S24805

226. Ann LC, Mahmud S, Bakhori SKM, et al. (2014) Effect of surface modification and UVA photoactivation on antibacterial bioactivity of zinc oxide powder. Applied Surface Science 292:405–412. https://doi.org/10.1016/j.apsusc.2013.11.152

227. Jones N, Ray B, Ranjit KT, Manna AC (2008) Antibacterial activity of ZnO nanoparticle suspensions on a broad spectrum of microorganisms. FEMS Microbiology Letters 279:71–76. https://doi.org/10.1111/j.1574-6968.2007.01012.x

228. Li M, Zhu L, Lin D (2011) Toxicity of ZnO nanoparticles to escherichia Coli: Mechanism and the influence of medium components. Environmental Science and Technology 45:1977–1983. https://doi.org/10.1021/es102624t

229. Jalal R, Goharshadi EK, Abareshi M, et al. (2010) ZnO nanofluids: Green synthesis, characterization, and antibacterial activity. Materials Chemistry and Physics 121:198–201. https://doi.org/10.1016/j.matchemphys.2010.01.020

230. Shalumon KT, Anulekha KH, Nair S v., et al. (2011) Sodium alginate/poly(vinyl alcohol)/nano ZnO composite nanofibers for antibacterial wound dressings. International Journal of Biological Macromolecules 49:247–254. https://doi.org/10.1016/j.ijbiomac.2011.04.005

231. Şölener M, Tunali S, Özcan AS, et al. (2008) Adsorption characteristics of lead(II) ions onto the clay/poly(methoxyethyl)acrylamide (PMEA) composite from aqueous solutions. Desalination 223:308–322. https://doi.org/10.1016/J.DESAL.2007.01.221

232. Tangaromsuk J, Pokethitiyook P, Kruatrachue M, Upatham ES (2002) Cadmium biosorption by Sphingomonas paucimobilis biomass. Bioresource Technology 85:103–105. https://doi.org/10.1016/S0960-8524(02)00066-4

233. Khan TA, Nazir M, Ali I, Kumar A (2017) Removal of Chromium(VI) from aqueous solution using guar gum–nano zinc oxide biocomposite adsorbent. Arabian Journal of Chemistry 10:S2388–S2398. https://doi.org/10.1016/J.ARABJC.2013.08.019

234. Singh S, Barick KC, Bahadur D (2013) Functional oxide nanomaterials and nanocomposites for the removal of heavy metals and dyes. Nanomaterials and Nanotechnology 3:1–19. https://doi.org/10.5772/57237

235. Anirudhan TS, Ramachandran M (2008) Synthesis and Characterization of Amidoximated Polyacrylonitrile/Organobentonite Composite for Cu(II), Zn(II), and Cd(II) Adsorption from Aqueous Solutions and Industry Wastewaters. Industrial & Engineering Chemistry Research 47:6175–6184. https://doi.org/10.1021/ie070735d

236. Akar ST, Yetimoglu Y, Gedikbey T (2009) Removal of chromium (VI) ions from aqueous solutions by using Turkish montmorillonite clay: effect of activation and modification. Desalination 244:97–108. https://doi.org/10.1016/j.desal.2008.04.040

237. Recillas S, Colón J, Casals E, et al. (2010) Chromium VI adsorption on cerium oxide nanoparticles and morphology changes during the process. Journal of Hazardous Materials 184:425–431. https://doi.org/10.1016/j.jhazmat.2010.08.052

LIST OF PUBLICATIONS

Publications from Thesis

1. **Priya Bansal** and Roli Purwar, Polyacrylonitrile/clay nanofibrous nanocomposites for efficient adsorption of Cr (VI) ions, **Journal of Polymer Research**, 28 (1), 1-19, 2021.

2. **Priya Bansal** and Roli Purwar, Development of efficient antimicrobial zinc oxide modified montmorillonite incorporated polyacrylonitrile nanofibers for particulate matter filtration, **Fibers and Polymers**, 1-12, 2021, https://doi.org/10.1007/s12221-021-0914-0.

3. **Priya Bansal**, Radhika Batra, Reetu Yadav and Roli Purwar, Electrospun polyacrylonitrile nanofibrous membranes supported with montmorillonite for efficient PM2.5 filtration and adsorption of Cu (II) ions, **Journal of Applied Polymer Science**, 51582, 2022. https://doi.org/10.1002/app.51582

Book Chapter

1. **Priya Bansal** and Roli Purwar, Nanofibers utility for rejuvenation of highly contaminated environment In Nanobiotechnology for Bioremediation: Fundamentals and Mechanisms, Elsevier.

Conference Publications

1. Priya Bansal and Roli Purwar, Fabrication and Characterization of Zinc oxide (ZnO) modified bioactive nanoclay, Clean and Green Energy: The Chemical & Environmental Aspect 2017, February 16-17 Bhaskaracharya College of Applied Sciences, University of Delhi.

2. Priya Bansal, Archna Gangwar and Roli Purwar, Development of breathable and waterproof fabrics by deposition of electrospun polyurethane and nanosilica on cotton and polyester fabric, Asian Polymer Association's International conference 2017, November 23-25 Delhi.

3. Priya Bansal and Roli Purwar, Zinc oxide nanoparticle modified montmorillonite for decontamination of wastewater, International Conference on Advanced Materials (ICAM) 2019, March 6-7 Jamia Millia Islamia, Delhi.

4. Priya Bansal and Roli Purwar, Polyacrylonitrile/zinc oxide modified montmorillonite nanofibrous nanocomposites for the efficient adsorption of Cr (VI), International E-Conference Recent Trends in Textiles 2020, September 18-19.

CURRICULUM VITAE

Priya Bansal
Research Scholar
Department of Applied Chemistry
Delhi Technological University

Area of Research Interest

Electrospun nanofibrous membranes for filtration of PM2.5 present in atmosphere and removal of heavy metal ions from wastewater

Academic Qualifications

PhD (Applied Chemistry), 2106-present, Delhi Technological University
M. Sc. (Chemistry), 2013-2015, Indian Institute of Technology Delhi
B. Sc. (Chemistry), 2010-2013, Daulat Ram College, Delhi University

Research Experience

Junior Research Fellow, Science and engineering Research Board, Department of Science and Technology, Govt. of India sponsored project titled "Design and development of 2D/3D self-assembled antibacterial nanofibrous structures from regenerated non-mulberry silk fibroins and its blends for medical textiles application" at Department of Applied Chemistry, Delhi Technological University, (2018-2021).

Publications

Papers published in SCI/SCIE indexed journals-04
Conference Abstract-04